UNIVERSITY OF
LIVERPOOL

Maximum Power Point Tracking Control of the Permanent Magnet Synchronous Generator based Wind Turbine

Mengqi Zhang

Supervisor: Dr L. Jiang
Co-supervisor: Professor Q.H. Wu

Electrical Engineering and Electronics Department
2012

Abstract

Wind power generation is a promising renewable energy source. The reduced cost of electricity supplied from wind power plants may be attributed to good control strategies such as maximum power point tracking. The control algorithm for maximum power generation is analysed in this thesis. The control algorithm is proposed by regulating the d-q axis voltages of electrical machines in order to control machine torque and rotational speed that allows wind turbines to always extract maximum power from the wind energy source.

A conventional way to control the electrical machine is by using vector control together with PI controllers to regulate voltages. This control method is mature and robust enough for electrical machine control. However, vector control may have difficulties in handling system interconnected nonlinearity and time varying wind power input variables. To improve the control strategy and provide controllers with a wider range of applicability, feedback linearization and nonlinear adaptive control algorithms are investigated. Feedback linearization control cancels out all the nonlinearities of q-axis items to expand operational range and develop interaction between the d-axis and q-axis dynamics for machine torque. For nonlinear adaptive control, the original nonlinear multi-input multi-output system is divided into inter-related subsystems and the system nonlinear items and uncertainties are estimated in order to cancel out the existing nonlinearities. Wind power generation maximum power point tracking is accomplished by using conventional vector control, feedback linearization control and nonlinear adaptive control.

Practically, due to the small range of control capability, the gain-scheduled conventional control strategy requires a set of control parameters in order to match the different input wind speed. And a mapping technique which relies on the wind speed and current sensors is essential for this control strategy. The feedback linearization control strategy proposed in the report gives global trajectory tracking, so only one set of controller parameter is able to handle all the different wind speed inputs. However, the feedback linearization control still requires some of the machine operational parameters such as rotor speed, stator winding current, etc. Therefore, the nonlinear adaptive control strategy is proposed which uses the estimated machine operational parameters instead of actual parameters. This would further

improve the controller capability and robustness. The simulation in this thesis have shown that the proposed nonlinear control strategies are also able to conduct wind turbine maximum power point tracking compare to conventional gain-scheduled control strategy. In the real case, if the proposed nonlinear control strategies can be successfully implemented for wind turbine, it will reduce the number of sensors and the corresponding devices used and thus reduce the cost and enhance the wind turbine robustness.

A magnetic equivalent circuit model of the permanent magnet synchronous machine is developed to analyse the electrical machine performance consider magnetic saturation. This model is usually used for electrical machine design and optimization purpose. It has a significant advantage in computational speed compared to another popular tool, finite element method. The magnetic equivalent circuit model may be used to calculate electrical machine properties such as electromotive force and flux linkages for machine control. The flux worked out by using this model is compared with finite element method analysis and the result shows that this model is five times faster in calculations and gives the percentage error less than ten. Currently, due to the uncertainties of magnetic saturated machines, the electrical machine controller only handles the linear region of machine power speed curve. If the proposed model has the calculation speed fast enough to give real time machine operational parameters, the uncertain parameters can be obtained even when the machine encounters magnetic saturation. It has to be emphasized that the nonlinearities in the magnetic equivalent circuit model is due to the magnetic material, while the nonlinearities in machine controller are due to the summation or product of multiple state variables, they are essentially different.

Table of Contents

List of Figures

List of Tables

Chapter 1 Introduction

1.1 Background

Wind power has been utilised for at least 3000 years and the earliest time recorded people living in the Afghan highlands used wind power to grind grain during the seventh century BC. In the early 20th century wind power was used to provide mechanical power to pump water. The first wind turbine for electricity generation was invented by James Blyth in Scotland in 1887[1], where it was used as a battery charging machine. Since the 1970s, technology has improved rapidly, and by the end of the 1990s, wind energy had become one of the most important sustainable energy resources.

The world's primary energy demand almost doubled between 1971 and 2003 and is expected to increase by another 40 percent by 2020[1]. A large amount of carbon dioxide emission every year has already affected the environment by contributing to global warming. The increasing concerns over global warming have led world governments to discuss ways of slowing down the increase in carbon dioxide emissions. International climate change negotiations are proceeding under the auspices of the United Nations, and at a key meeting at Kyoto in December 1997, an overall target for global reduction of greenhouse gas emission by 5 percent was agreed up to 2020. The European Union has undertaken to reduce emissions by 8 percent and has agreed a share-out of targets among its members. The United Kingdom is committed to a 12.5 percent reduction by 2020 [2].

In 2003, renewable energy contributed 13.5 percent of the world's total primary energy. For electricity generation, hydro contributed 15.9 percent and geothermal, solar, wind

and combustible renewable contributed 1.9 percent. The capacity of the world's hydro plants is over 800 GW and wind energy, which is developing very rapidly, accounted for about 60 GW by the end of 2005 [3].

Wind power is today the largest source of environment-friendly energy production. It gains the most power conversion efficiency in comparison to other renewable energy sources such as tidal, waves and solar. Modern power systems are characterized by massive incorporation of electricity production wind turbines. Due to the large demand to reduce pollution and to improve the environment, the development of wind power has gained successful research efforts. Electricity generation wind turbine is a promising but still partly unknown technology with regards to their impact on the operation and stability of the power grids they feed [1].

The approximate cost of a new offshore wind farm is £50/MWh in 2007 in UK. About 75% of the cost of electricity is the capital cost of construction, and of that about half is the cost of the turbine . The remaining main elements are the tower and the electrical infrastructure [4]. This project will only be concerned with the cost of the turbine. The pie chart in Figure 1.1 indicates the cost of each part of a wind farm.
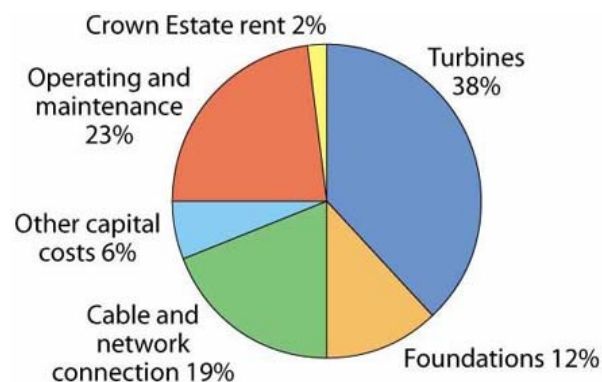
Figure 1.1 Cost of wind farm pie chart[4]

1.1.1 Types of Wind Turbine

Wind turbines can be divided into horizontal axis wind turbine (HAWT) and vertical

axis wind turbine (VAWT) according to the ways of rotation. The horizontal axis wind turbine is more commonly utilized in the wind power industry, and these turbines are either upwind machines or downwind machines as seen in Figure 1.2. The blades of upwind wind turbines face the wind, so the wind meets the blades first then the tower, which is the most commonly used type of wind turbine. The upwind wind turbine has no wind-shadow effect, due to the tower. It generates more power than the downwind type wind turbine though it requires somewhat more complicated yaw control to keep the turbine in the correct position with respect to the varying wind direction [5].

Downwind wind turbines do not require yaw control as the wind automatically turns the nacelle and blades into the right position with respect to the wind direction. The downwind wind turbine is influenced by wind-shadow effect. This can be explained as: when the blade swings past the tower it experiences reduced wind speed. It causes the blade to flex and eventually causes fatigue failure of the blades. As a result it reduces the output power and increases the audible noise.

Vertical type wind turbines are not widely used for large wind farms, and these wind turbines absorb wind power from any direction. The only wind turbine that had any commercial success is called "Darrieus Rotor", which was first developed in the 1920s. These vertical type wind turbines do not need yaw control. Some heavy machinery such as generator, and gear box can be installed on the ground level making it easy to mount and maintain. There is no flex subject to the blades, so they can be lighter in weight and cheaper. The tower does not need to be as strong as a horizontal type wind turbine because the weight of the blades is balanced on the tower, or sometimes can be eliminated if the wind turbine is mounted on the ground.
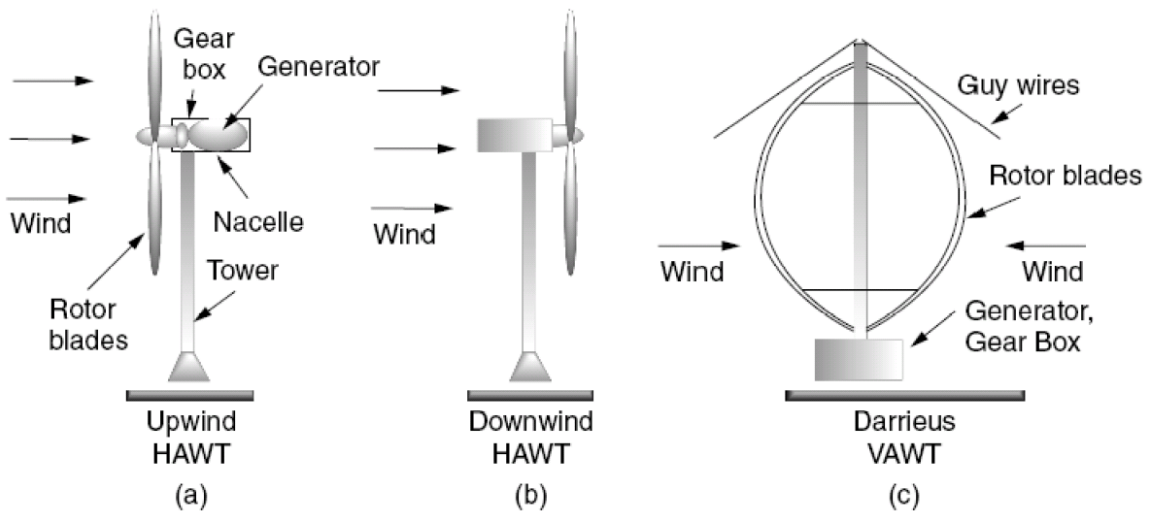
Figure 1.2 Common wind turbine types[5]

1.1.2 Types of Generator

Electric generator is by far the key component in wind turbines; a variety of generators i.e., DC generators, permanent magnet synchronous generator (PMSG), and induction generator (IG) are used in wind power generation. The DC generators are not suitable for large scale wind turbine due to the significant disadvantages of large size and high maintenance cost. The DC generator usually needs a brush to alternate the current direction and this is easily damaged, and also the configuration of DC generator acquires large room to place its devices [6].   to Nevertheless, they are sometimes more suitable in small scale wind turbines especially for battery charging. Induction generator and permanent magnet generator are commonly used in large scale wind power generation. They both operate as variable speed electric generators. The typical configuration of wind turbines coupled with these two types of generator are illustrated in Figures 1.3 and 1.4.

Wind turbines using PMSG usually connect to the power grid through a full scale power converter, while wind turbines using IG usually connect to the grid with a partial scale twin converter, and the IG exciter and stator are controlled separately by

13

the two converters. It is a so-called doubly fed induction generator (DFIG) wind turbine. The PMSG can be driven directly without a gear box, thus it has fewer components than the DFIG turbine. The DFIG turbine has more components but with smaller dimensions and masses, which makes it more convenient to transport and assemble. It is connected to the grid with a partial size power converter, typically 30% of generated power.

For an induction generator wind turbine, both squirrel-cage induction generator and wound-rotor induction generator are compatible. Squirrel-cage generator is simpler and more robust and it provides higher reliability and has lower maintenance costs. Wound-rotor generator has a more complex structure which requires more maintenance and thus is more costly. Nevertheless, the wound rotor electric generator has higher power efficiency than the squirrel-cage IG in wind power generation, but the squirrel-cage generator generates smoother torque.
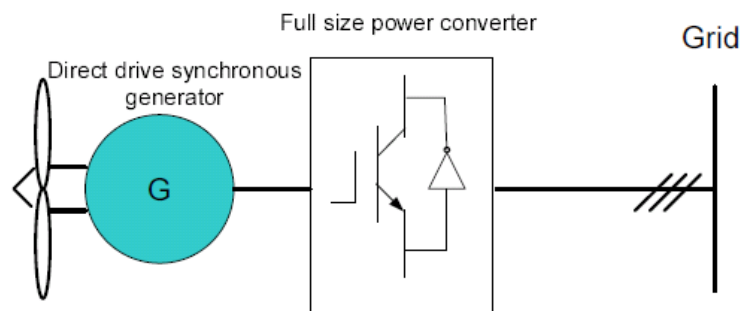
Figure 1.3 PMSG wind turbine configuration

14
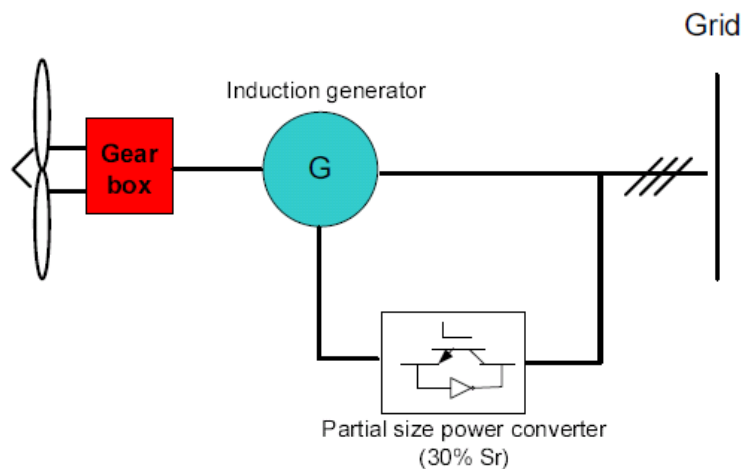
Figure 1.4 DFIG wind turbine configuration

Permanent magnet synchronous generator is the synchronous generator with its dc excitation field winding replaced by a permanent magnet. The advantages of using a permanent magnet include improved machine robustness and minimised winding copper losses. In general, PMSG has higher efficiency and power rating than induction machines. Also, the elimination of dc excitation gives a simpler structure and reduces machine weight and size. In wind power generation, PMSG has better performance and higher flexibility in transportation and assembly. The disadvantage is that the majority of permanent magnets are made from rare-earth material which is more expensive. The choice of permanent magnet for a generator is determined by machine design factors such as weight, size, efficiency, as well as economic reasons regarding the material and production [7].

Three types of commonly used permanent magnet synchronous generator configurations are shown in Figures 1.5-1.7. They are permanent magnet synchronous machines with surface mount type magnet, inset-type magnet, and interior-type magnet, respectively. Surface mount arrangement is popular for high H_c magnetic materials that are not easily susceptible to demagnetization, but this configuration is not suitable for high speed operation as the surface mount magnet is not as rigid as the other two types. The synchronous d-q axis reactances are practically the same for surface mount PMSG if rare-earth PMs are used. The inset type of PMSG has more solid structure than the surface mount type, but the EMF induced by the PMs is lower. The q-axis synchronous reactance is greater than that in the d-axis for this type of PMSG. Interior-type PMSG is the most rigid one of these three types, where PMs are very well protected in the rotor against centrifugal force. This configuration is suitable for high frequency high speed operation [7].
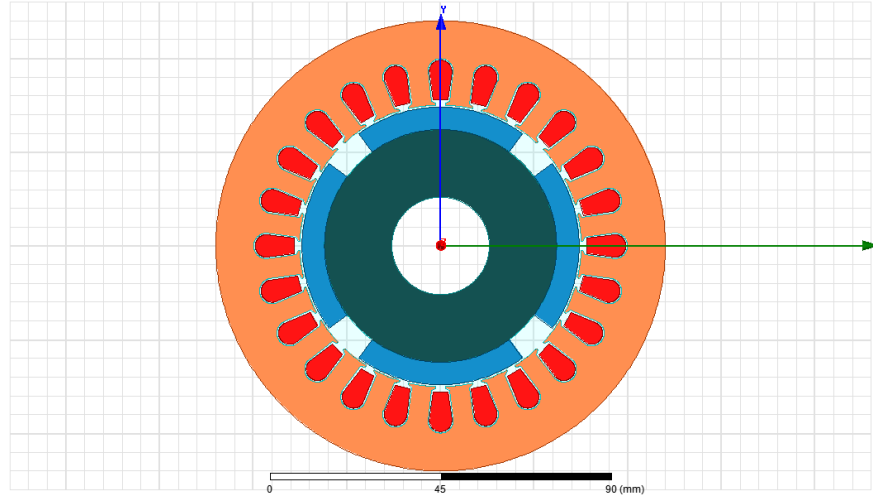
Figure 1.5 Surface mount type permanent magnet synchronous machine
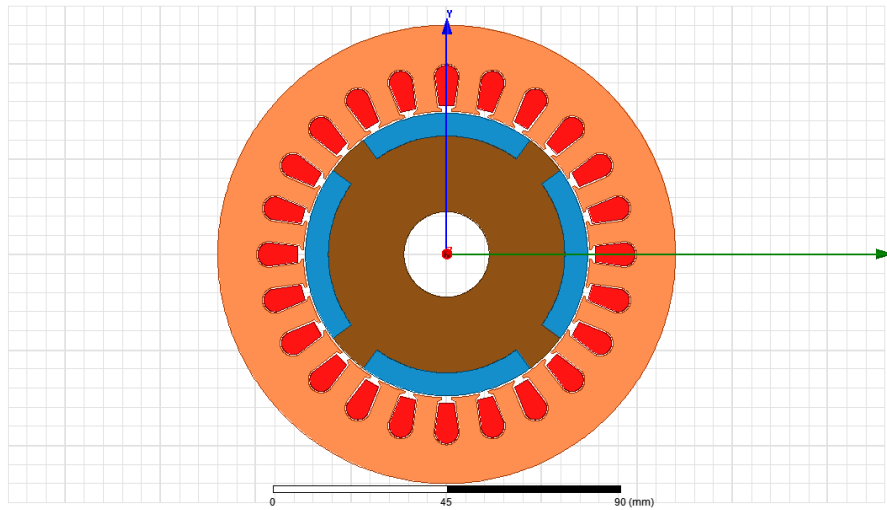
Figure 1.6 Inset-type permanent magnet synchronous machine
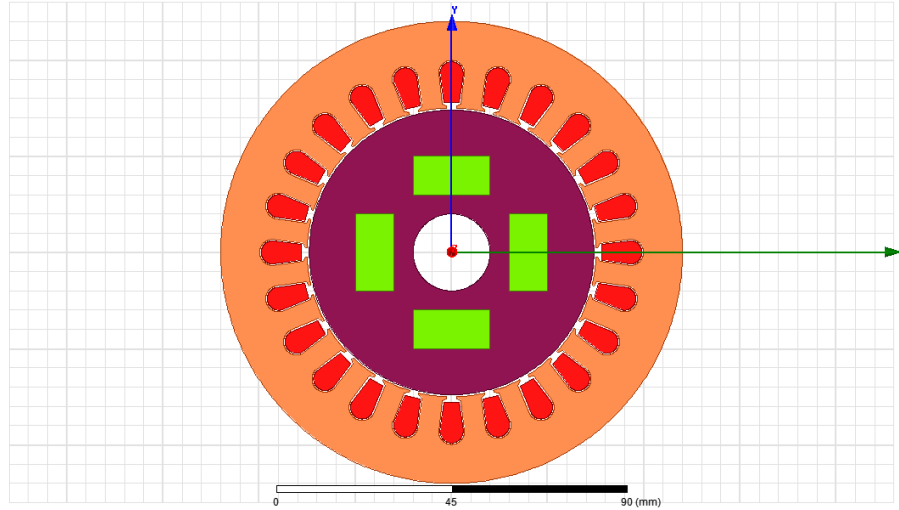
Figure 1.7 Interior-type permanent magnet synchronous machine

1.1.3 Magnetic Material

Mechanical energy does not directly convert into electrical energy in electrical machines; it relies on the magnetic field which acts as the medium to convert energy from mechanical form to electrical form. Therefore the magnetic material in electrical machines has an important position in machine performance. There are two kinds of magnetic material in PMSG; one is the permanent magnet material and the other is ferromagnetic material.

Permanent magnet material acts as the primary source to provide a magnetic field for power generation. Some popular permanent magnet materials on the market include Alnicos, Barium and strontium ferrites, Samarian-cobalt, and Neodymium-iron-boron (NdFeB) materials. Alnicos are alloys of iron with aluminium, nickel, copper, and cobalt. Samarian-cobalt magnets are made from the compounds of iron, nickel, cobalt, and the rare-earth Samarian. NdFeB is made from the compounds of iron, nickel, and neodymium. These materials have different characteristics, and the choice of proper material for an electrical machine is influenced by factors such as service temperature, thermal stability, coercive force, remanence and flux density.

17

Ferromagnetic materials do not produce magnetic field but transduce magnetic field. The characteristics of one type of ferromagnetic material can be derived from its BH curve. The residual magnetism Br is the maximum flux density that the material can conduct, while the coercive force Hc is the magnitude of the field intensity when no flux flows through the material.

Magnetic hysteresis is an important property in ferromagnetic materials. In Figure 1.8, when the field intensity H increases and goes beyond the G point in the negative x-axis, it causes a rapid increase in reverse magnetization until saturation. Hysteresis means the change in flux density B will lag the field intensity H [8].
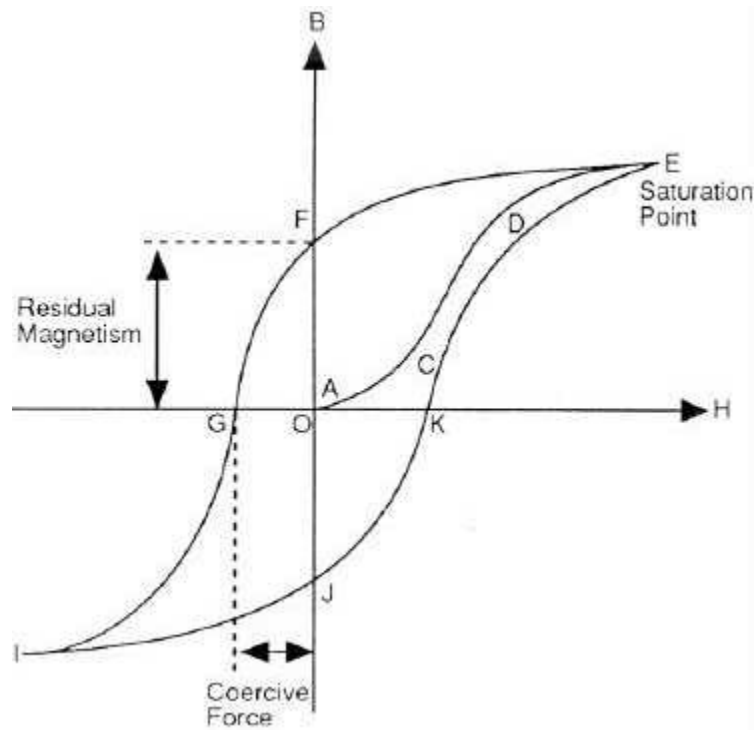
Figure 1.8 B-H curve of ferromagnetic material

1.2 Literature Review

Wind power generation has drawn great attention during the last two decades. In [1], a

systematic introduction for wind power generation can be found, i.e., the structure of wind turbines, different types of power generators, and corresponding power generation; it gives a general idea for young researchers stepping into the renewable energy area. Since permanent magnet synchronous generator has significant advantages in high power density, robustness, and simplicity for control purpose, it is popular in wind power generation. The analysis of this type of wind turbine can be found in [9-11]. In order to improve the power generation efficiency, the wind turbine maximum power point tracking control strategy for PMSM based wind turbines has been studied [11, 12]. A classic electrical machine vector control method is chosen to carry out this control strategy; it is introduced in [13-15].

Nevertheless, this conventional PI control method has limitation in narrow control range since it only controls the object at one operating point. A more comprehensive nonlinear control strategy has been used to enhance the performance of machine controllers and the study of applied nonlinear control is found in [16]. The nonlinear control of permanent magnet machine introduced in [17], wherein a model based control law is developed using the exact linearization control methodology and it is successfully implemented experimentally. This motor is controlled to run at 3000 rpm under unloaded condition based on speed observer and the experimental result show that there is only a slight error between actual speed and reference speed. However this control strategy only considers solely the motor itself, the machine load conditions are not included in the control system. In [18], the nonlinear control strategy of PMSM consider the motor load, moreover it shows a good design of disturbance observers which give good estimation of unknown load torque (1%, 3%, 10% and 100% of nominal torque are used to test disturbance observer) and the states of machine model. With the help of state observers, the mechanical motor speed and position sensors are also removed. More importantly, it presents a good trajectory tracking machine control that is evaluated by simulations. A paper discussed the similar topic in induction machine speed nonlinear control based on perturbation observer is found in [19]. Nevertheless, even the nonlinear control of motors have been widely discussed, there are hardly any can be seen for wind turbine maximum power point tracking control. In

[20], the wind turbine MPPT is conducted by feedback linearization control, the simulation gives a comparison of actual turbine rotational speed and reference turbine speed due to sinusoidal wind change, and it shows good result which with error less than 1%. However the corresponding perturbation observer and detailed controller design is not introduced in this paper. The study of this project will try to propose a nonlinear control strategy for wind turbine MPPT and introduce the corresponding controller design in detail.

The conventional d-q axis permanent magnet synchronous model is not accurate in predicting machine performance when the machine is operating above the linear operation range or faulted conditions, because the parameter of d-q models are rely on the test of real machine experiment during steady state operation [21, 22]. In order to evaluate machine characteristics i.e. inductance, torque, back EMF more accurately, a model based on the magnetic equivalent circuit method is introduced, which includes iron material magnetic nonlinearities. These machine operational parameters may be used to control electrical machine and also the wind turbine during nonlinear operating region and faulted conditions [23, 24]. The magnetic equivalent circuit method is similar to the finite element method but with a significant advantage in fast calculation speed [25-29]. A proper designed MEC model would quickly evaluate machine performance with high degree of accuracy, which may be helpful in electrical machine control if incorporated with conventional d-q model [30, 31]. The design of MEC model can be seen in machine research publications. In [28], an accurate MEC model of a fractional-slot concentrated-winding interior permanent magnet machine is shown. Wherein, a progressive method to develop airgap model is introduced, this increases the number of flux tubes to capture the flux on both radial and circumferential direction. Compared to FEM, the calculation speed of this model is 50 times faster, and gives promising results in airgap flux density, back EMF, phase and d-q axis inductances. A MEC assisting machine control is found in [32], wherein the machine is operated above the nominal operation range by speed controller. The result shows that the machine speed can be controlled more accurately with the model using real-time parameters than the one using d-q parameters.

1.3 Summary of the Thesis

Apart from the background knowledge, wind turbine type, as well as the wind energy development introduced in the first chapter, this thesis also focus on analysing the control strategy of wind turbine maximum power point tracking (MPPT). In order to model wind power generation, the mathematic models corresponding to wind turbine devices, i.e., turbine rotor, drive train, and electrical machine, are introduced in Chapter 2. MPPT allows wind turbine to deliver maximum power to the grid at different wind speeds, and hence improves the power generation efficiency. The conventional way to carry out MPPT control is by the classic vector control, where the electrical machine stator current is transformed into d and q axis current. By setting the d-axis to nil this enables the full capability of q-axis stator current which determines machine torque. This technique has been widely used due to its simplicity and reliability. The MPPT of permanent magnet synchronous generator based wind turbine is given in Chapter 3.

Nevertheless, the PI control method is not perfect; it has small operation range and difficulties in controller tuning. A more comprehensive nonlinear adaptive control method is analysed to conduct maximum power point tracking. This strategy focuses on handling the nonlinear properties in the system, reducing the disturbances and giving the controller higher robustness. However, the nonlinear controller has more complicity in computation and application. It may require more powerful digital signal processor and more sophisticated power converters to carry out the strategy. The relative information about nonlinear control is introduced in Chapter 4.

The magnetic equivalent circuit (MEC) of a permanent magnet synchronous machine is introduced in Chapter 5. This equivalent circuit gives a global insight into electrical machine magnetic flux patterns under loaded or unload conditions. Usually, the conventional vector control technique controls an electrical machine in magnetic unsaturated conditions; it is difficult to handle the magnetic saturated operation because some properties changes such as flux linkage and inductance. The MEC can

be used to calculate machine properties under saturated conditions, and thus broaden the control range.

Future work and prospective results are discussed in Chapter 6, where the conventional and nonlinear adaptive control strategies are expected to be implemented and simulated in hardware in loop environment; further applications of MEC may be carried out and be coupled to online electrical machine control.

Chapter 2 Modelling of Permanent Magnet Synchronous Generator based Wind Turbine

2.1 Introduction

Permanent magnet synchronous generator based wind turbine has its significant advantage in reliability and controllability. The research works relevant to this wind turbine configuration have become very popular in recent decades. To analyse and control the PMSG based wind power conversion system, the corresponding mathematical models are important for accurate modelling. In [11], permanent magnet generator model and vector control algorithm are introduced, and the wind turbine is connected to the power grid through back-to-back IGBT power converter. In [10], PMSG model, pitch-angle controlled wind turbine model, as well as a driven train model, is introduced. Details in wind turbine mechanism at variable speed operation can be found. In [9], performance of grid directly coupled PMSG wind turbine is analyzed, in which an alternative damping system is added to enable the wind turbine to provide greater damping over power angle oscillations.

Operation of a typical wind turbine can be divided into 4 regions, as shown in Figure 2.1. In region 1, wind speed is too low to drive the wind turbine. A wind turbine does not rotate until wind speed reaches the minimum speed that is able to drive the wind turbine to start rotating, and this typical wind speed is so-called cut-in speed. When the wind turbine starts operating, the power output keep increasing as the wind speed increases; when the output power reaches the rated value of an electrical generator, the power output will stop increasing. The

minimum wind speed that enables the wind turbine to constantly deliver its rated power is called rated wind speed V_n. The range between cut-in speed and rated speed is defined as region 2; maximum power point tracking (MPPT) control is applied in this region in order to maximize power output of the wind turbine, and pitch angle is fixed in this region to enable the blades to receive maximum pressure from the air. As output power increases when wind speed increases, the wind turbine will reach its rated power output; pitch angle control is applied to ensure the blades receive the proper pressure that keeps them rotating at rated speed. The wind turbine will be cut out and will brake to protect it being damaged by exceeding the maximum mechanical stress when the wind is from extremely strong and out of the range of pitch angle control. Region 3 is defined between rated wind speed and cut-out speed. When a wind turbine is stopped from generating power, its operation belongs to region 4.
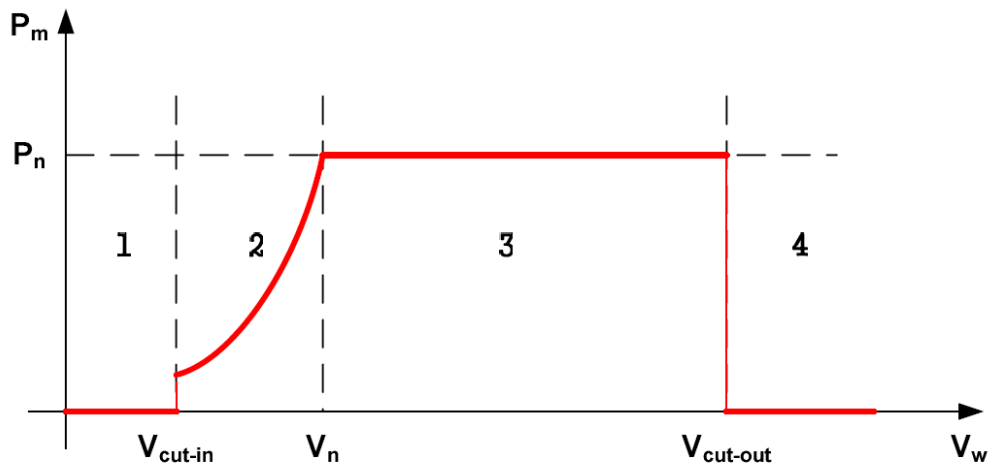
Figure 2.1 Wind turbine operation range

2.2 Power in the Wind

Wind is the flow of air or other gases that compose the atmosphere. Wind turbines are designed to convert wind power to electrical power through the generator, and the generation efficiency is an important parameter for wind turbines. Modern wind

turbines produce electricity for 70-85% of operation time at efficiency of around 30% [33]. The kinetic energy of wind can be calculated by equation 2.1, where v (m/s) is the wind speed, and m is the wind mass (kg).

$$K.E = \frac{1}{2}mv^2 \tag{2.1}$$

The mass of air that passes through an area per unit time can be represented by equation 2.2, where A (m^2) represents the swept area by wind turbine, ρ (kg/m^3) represents the air density, v (m/s) represents the wind speed.

$$m = \rho \cdot A \cdot v \tag{2.2}$$

The areas swept by vertical type wind turbine and horizontal type wind turbine are different. For horizontal wind turbine the swept area can be calculated by equation 2.3. For vertical wind turbine the swept area can be calculated by equation 2.4. D (m) is the blade diameter and breadth in HAWT and Darrieus Rotor respectively. H (m) is the height.

$$A = (\pi/4)D^2 \tag{2.3}$$

$$A \cong (2/3)D \cdot H \tag{2.4}$$

Sine power equals to the work per unit time, power of wind in the swept area is given by equation 2.5. Graphically, the power in the wind per square metre at 15 ^{0}C and 1 atm can be represented by Figure 2.2.

$$P_w = \frac{1}{2}\rho Av^3 \tag{2.5}$$
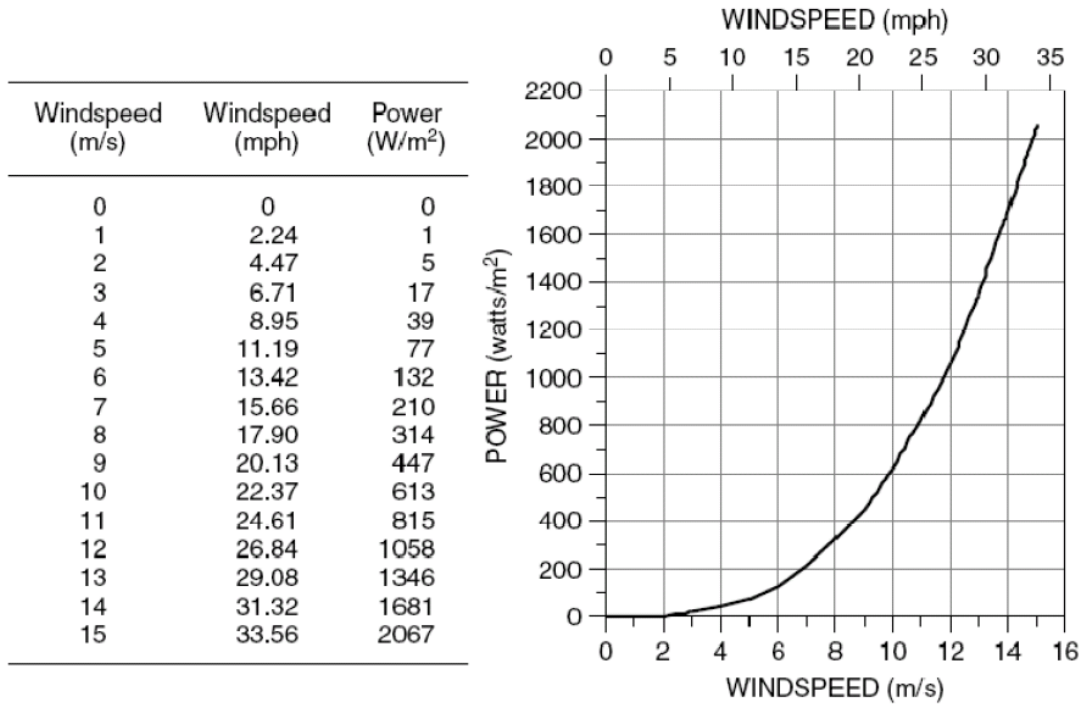
Figure 2.2 Power in wind at 15 ^{0}C and 1 atm per m^2 [33]

The air density is influenced by air temperature and pressure, as the ideal gas law shows in equation 2.6, where n is the mass of air in mol, V (m^3) is the volume of air, P is the pressure in atm, R (m^3.atm.K^{-1}.mol^{-1}) is the ideal gas constant equals to 8.2056x10^{-5}, and T (K) is absolute temperature. The air density is given by equation 2.7, where M is molecular weight of air equals to 0.02897 kg/mol. Hence the air density is proportional to the air pressure P and inversely proportional to absolute temperature K.

$$PV = nRT \Rightarrow (\frac{n}{V}) = \frac{P}{RT} \tag{2.6}$$

$$\rho = \frac{n}{V} \cdot M = \frac{P}{T} \cdot \frac{M}{R} \Rightarrow \rho = 353 \times \frac{P}{T} \tag{2.7}$$

An atmospheric pressure of 1 atm is measured at sites on mean sea level. The pressure decreases at the sites above the mean sea level, which is given by equation 2.8, where h is the height above the mean sea level. Substitute P in equation 2.7 by equation 2.8, and the air density equation at higher altitude and different temperatures is given by equation 2.9.

26

$$P = e^{(\frac{-0.0341}{T}) \cdot h} \qquad (2.8)$$

$$\rho = 353(\frac{P}{T}) = (\frac{353}{T})e^{(\frac{-0.0341}{T}) \cdot h} \qquad (2.9)$$

Since the speed of the wind is influenced by the roughness of the terrain, higher wind speed can be achieved at a certain height above the ground. It is always attempted to place the HAWT at a higher level by increasing the height of the tower in order to generate more power. Sometimes, it is difficult to measure the actual wind speed at high elevations. The approximate empirical formulas can be used to estimate the actual wind speed at high elevations by using lower reference elevation wind speed. This situation is called the impact of tower. In Europe, the impact of tower height can be calculated by equation 2.10, where z is called the roughness length, which value can be found in Table 2.1. While in the USA, the impact of tower is calculated by equation 2.11, where α is called the friction coefficient, which is the empirical value that can be found in Table 2.2. The reference height H_o is usually equal to 10m. The impact of tower causes the power to be different at highest and lowest point of a HAVT; this causes blade flexing in the direction of wind which eventually causes fatigue failure of the blade over a long period and increase maintenance. This phenomenon can be illustrated by Figure 2.3.

$$(\frac{v}{v_o}) = \frac{\ln(\frac{H}{z})}{\ln(\frac{H_o}{z})} \qquad (2.10)$$

$$(\frac{v}{v_o}) = (\frac{H}{H_o})^{\alpha} \qquad (2.11)$$

27

Roughness Class	Description	Roughness Length $z(m)$
0	Water surface	0.0002
1	Open areas with a few windbreaks	0.03
2	Farm land with some windbreaks more than 1 km apart	0.1
3	Urban districts and farm land with many windbreaks	0.4
4	Dense urban or forest	1.6

Table 2.1 The roughness length[34]

Terrain Characteristics	Friction Coefficient α
Smooth hard ground, calm water	0.10
Tall grass on level ground	0.15
High crops, hedges and shrubs	0.20
Wooded countryside, many trees	0.25
Small town with trees and shrubs	0.30
Large city with tall buildings	0.40

Table 2.2 The friction coefficient[34]
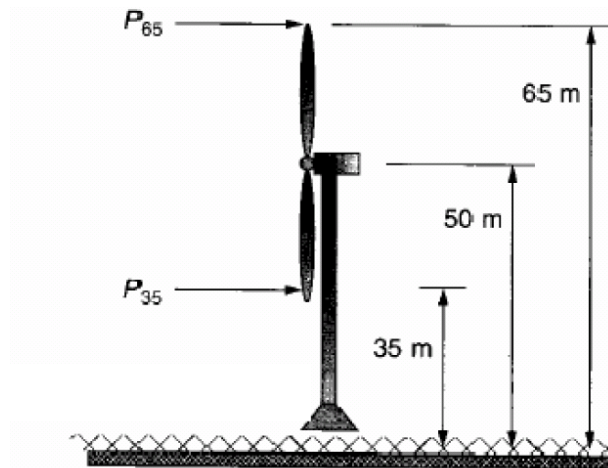
Figure 2.3 Impact of tower phenomena[33]

$$\left(\frac{P}{P_0}\right) = \left(\frac{H}{H_0}\right)^{3\alpha} = \left(\frac{65}{35}\right)^{3*0.25} = 1.59$$

28

The maximum kinetic energy that can be abstracted by a HAWT is 59.3% though it is placed at higher elevations. This theoretically maximum efficiency is called Betz efficiency as it was first proved by German physicist Albert Betz. It happens when the wind turbine reduces the speed of the wind by one third of the input value [33].

Assume v is upwind speed; v_d is downwind speed equal to the product of λ and v; the average wind speed on the blade is $V_b = (1+\lambda)/2$. Then the power absorbed by the wind turbine is equals to the reduction of kinetic energy in the wind, given by equation 2.12. The mass m can be calculated as shown before, and A represents the rotor swap area. Combine equations 2.12, 2.13. The power absorbed by HAWT is given by equation 2.14, where C_p is the power conversion efficiency and P_w is the upwind power. The maximum efficiency can be calculated by using the general method, as given by equation 2.15. By finding the peak value of C_p, the theoretical maximum power extraction ratio is obtain by equation 2.16.

$$P_b = \frac{1}{2}m(v^2 - v_d{}^2) = \frac{1}{2}mv^2(1-\lambda^2) \tag{2.12}$$

$$m = \rho A v_b = \rho A v \frac{1+\lambda}{2} \tag{2.13}$$

$$P_b = [\frac{1}{2}\rho A v^3]\cdot[\frac{1}{2}(1+\lambda)(1-\lambda^2)] = P_w \cdot C_p \tag{2.14}$$

$$\frac{dC_p}{d\lambda} = 0 \Rightarrow \frac{d[\frac{1}{2}(1+\lambda)(1-\lambda^2)]}{d\lambda} = (1+\lambda)(1-3\lambda) = 0 \Rightarrow \lambda = \frac{1}{3} \tag{2.15}$$

$$C_{p.\max} = \frac{1}{2}(1+\frac{1}{3})(1-(\frac{1}{3})^2) = 0.593 = 59.3\% \tag{2.16}$$
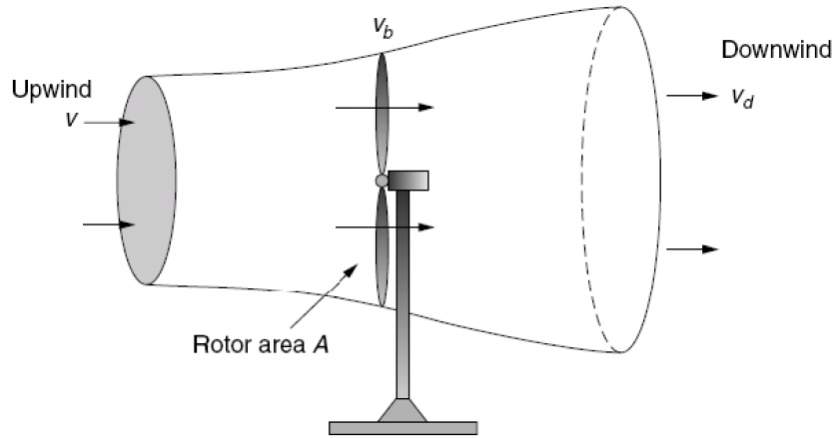
Figure 2.4 The stream tube formed by wind turbine kinetic energy extraction[33]

Wind turbine efficiency is the function of rotating speed. The ideal maximum efficiency is reached when the wind turbine is rotating "very fast". Practically, the ideal rotating speed is not gainable, and some wind will pass through the blade. A practical turbine operates at the efficiency of 45-50%.
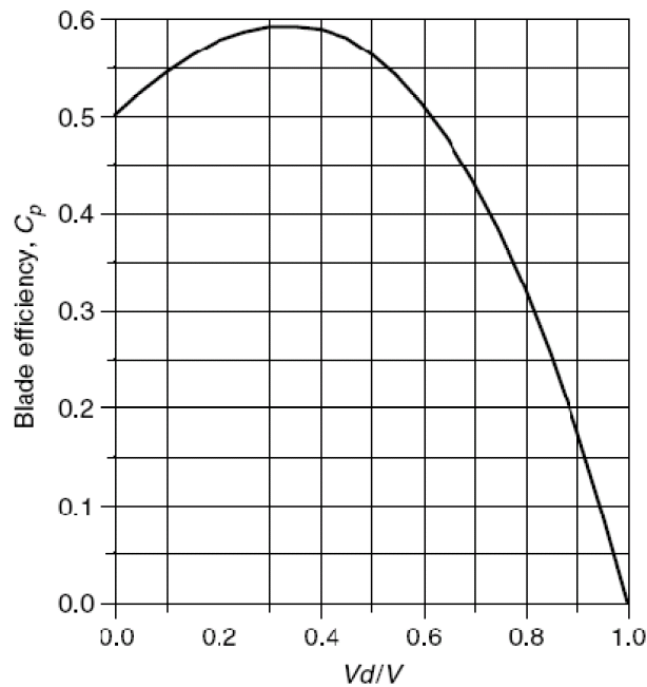
Figure 2.5 General blade efficiency[33]

The wind turbine rotor efficiency is usually presented as Tip Speed Ratio (λ), which

is a function of wind speed and rotating speed. The blade tip is the outermost point of the blade. Figure 2.6 shows the rotor efficiency of some typical rotor types. The three blades rotor reaches maximum efficiency at about TSR equals 4 and the two blades rotor reaches maximum efficiency at about TSR equals 2.17 in Figure 2.6. The American multi-blade rotor efficiency is limited by the turbulence effect, which is the effect of one blade on wind increasingly felt by the following blade.

$$TSP(\lambda) = \frac{Blade\ Tip\ Speed}{Wind\ Speed} \qquad (2.17)$$
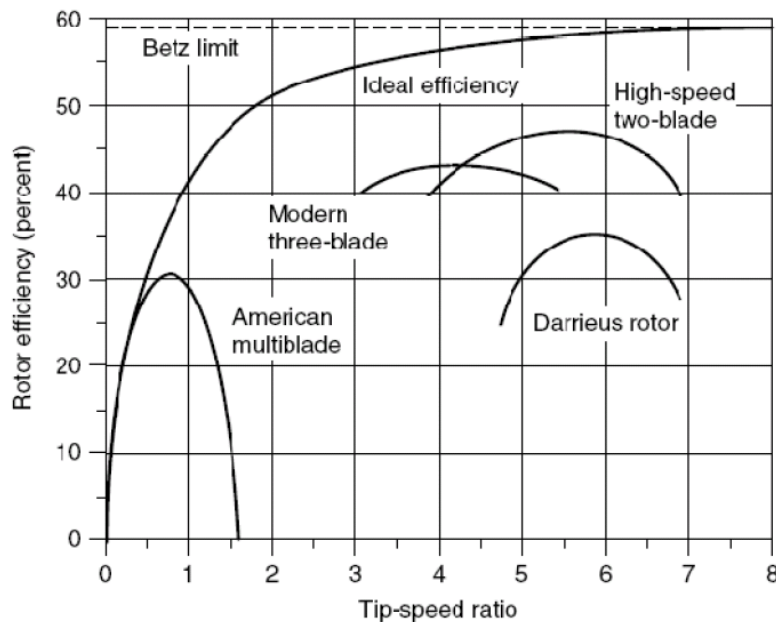
Figure 2.6 Rotor efficiency of some typical rotor types

2.3 Drive Train Model

Drive train couples wind turbine rotor and generator together; it sometimes contain a gear box that speeds up the shaft and drives the electric generator with higher rotating speed. Since the direct driven wind turbine has been developed, the gear box can be eliminated. In the drive train, the corresponding model is simplified for direct driven configuration. For wind turbine system modelling, drive train mode

31

can be either a one-mass or two-mass model.
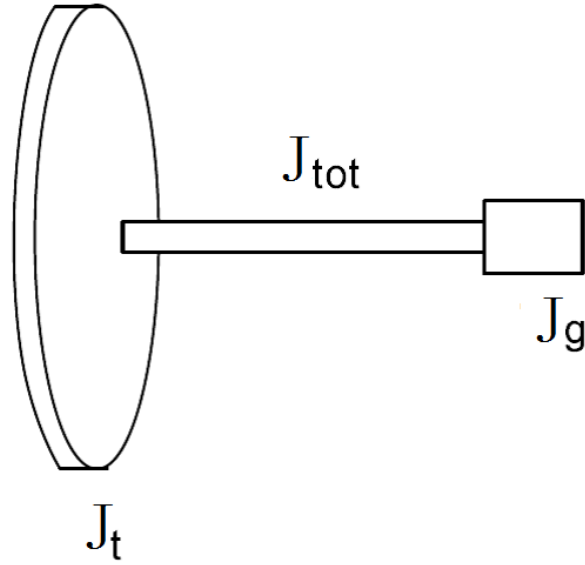
Figure 2.7 Two-mass drive train

For the one-mass model, all the components in the drive train are considered as only one mass. This model is usually used for the direct driven wind turbine which connects by a full scale power converter. The advantage of this type of configuration is that transients from the grid are considered so small that they can be ignored by full scale converter, so the electrical generator is considered decoupled and better protected. The mathematical model of one mass drive train is represented from equations 2.18 to 2.20.

$$J_{tot} \frac{d\omega_t}{dt} = T_e - T_m - B\omega_t \tag{2.18}$$

$$J_{tot} = J_g + J_t \tag{2.19}$$

$$\omega_t = \frac{\omega_e}{p} \tag{2.20}$$

where J_{tot} is the total inertia of the drive train, which is equal to the summation of wind turbine inertia constant and generator inertia. J_t and J_g represent the wind turbine rotor inertia and electrical generator interia, respectively. Constant B is the viscous friction coefficient. The symbols ω_t and ω_e represent the wind turbine speed and electrical machine rotational speed, respectively, and p represents the pole pair.

T_m and T_e represent the mechanical torque of the wind turbine and the electromagnetic torque of the generator, respectively.

The two-mass model is used to represent a drive train with a gear box. It usually connects to the grid with partial scale power converter. This model contains a low speed wind turbine shaft part and a high speed generator shaft coupled with gears. So this drive train configuration is more complex than the one-mass model and the mathematical model is represented from equation 2.21 to 2.23.

$$J_g \frac{d\omega_g}{dt} = T_{aux} - T_{em} + D_{bg}(\omega_b - \omega_g) - D_g \omega_g \tag{2.21}$$

$$\frac{dT_{aux}}{dt} = K_{bg}(\omega_b - \omega_g) \tag{2.22}$$

$$J_b \frac{d\omega_b}{dt} = T_u - T_{aux} - D_{bg}(\omega_b - \omega_g) - D_b \omega_b \tag{2.23}$$

where J_b, J_g represent the inertia constant in low speed wind turbine rotor shaft and high speed generator shaft, respectively. K_{bg} and D_{bg} are the stiffness and damping constants of the flexible coupling, D_b and D_g are the damping constant associated to each mass, T_u is the torque applied from the wind turbine, ω_b and ω_g is the wind turbine rotor speed and generator speed. T_{em} is the electromagnetic transient torque, and T_{aux} is the internal variable of the model [34].

The kinetic power that can be captured from wind by a wind turbine is expressed by the equation 2.24:

$$P_w = \frac{1}{2} \rho \pi R^2 v^3 C_p(\beta, \lambda) \tag{2.24}$$

where ρ is the air density, v is the wind speed, R is the radius of wind turbine rotor, C_p is called power coefficient which is between 0 and 1, and it describes how much power in the wind can be extracted by a wind turbine. The power coefficient C_p is a function of pitch angle β and tip speed ratio λ. The power coefficient C_p can be represented by the following functions 2.25 and 2.26[34]:

$$C_p = c_1(\frac{c_2}{\lambda_i} - c_3\beta - c_4\beta^x - c_5)e^{\frac{-c_6}{\lambda_i}} \tag{2.25}$$

$$\frac{1}{\lambda_i} = \frac{1}{\lambda + 0.08\beta} - \frac{0.035}{\beta^3 + 1} \qquad (2.26)$$

The coefficients x and $c1$ - $c6$ are determined by the rotor type, β is a fixed value for maximum power point tracking. So there is a corresponding optimal tip speed ratio λ_{opt} that determines the maximum power coefficient C_p. For a certain type of wind turbine, the value of λ_{opt} is fixed [34]. If we combine equations 2.25 and 2.26, the relation between wind turbine rotational speed and optimal power output of a typical three blades horizontal wind turbine is observed, as shown in Figure 2.8. Wherein, the coefficient x equals to 3, the pitch angle β equals to 0.0001, and the coefficient c1-c6 equal to 0.5, 116, 0.4, 5, 21, 1e-4, respectively [35].

The maximum power output is determined by wind turbine rotation speed, which can be expressed by equation 2.27:

$$\lambda_{opt} = \frac{\omega_{opt} V}{R} \qquad (2.27)$$

Because the optimal tip speed ratio is determined by wind turbine type, and wind speed V changes all the time while turbine rotor radius is fixed, as a result, the wind turbine is controlled to rotate at its optimal rotational speed ω_{opt} in order to follow the wind speed changes, thus to keep λ_{opt}. When optimal tip speed ratio does not change, maximum power output is always achieved. The method that controls the wind turbine generating maximum power under different wind speeds is called wind turbine maximum power point tracking (MPPT).

34
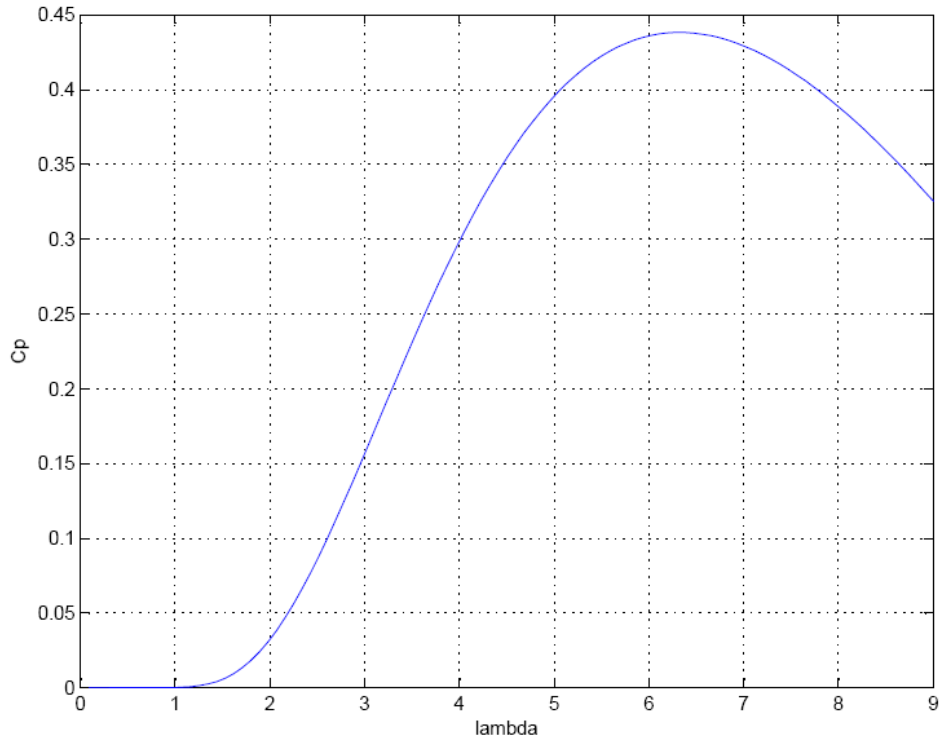
Figure 2.8 Power coefficient changes against tip speed ratio

2.4 Permanent Magnet Synchronous Generator Model

2.4.1 Park's Transformation

Mathematical transformation is a very important tool in power system modelling and analysis. It transforms difficult equations with time-varying coefficients to common stationary reference frame. Park's transformation is a very common three-phase to two-phase transformation tool in analyzing synchronous machines. It is used to transform the stator quantities of a synchronous machine onto a rotor fixed d-q reference frame. The positive d-axis of this frame is aligned with the magnetic axis of the field winding, while the positive q-axis is defined as 90 degrees leading the q-axis in generator motion. The transformation equation is in equations 2.28-2.29 [36].
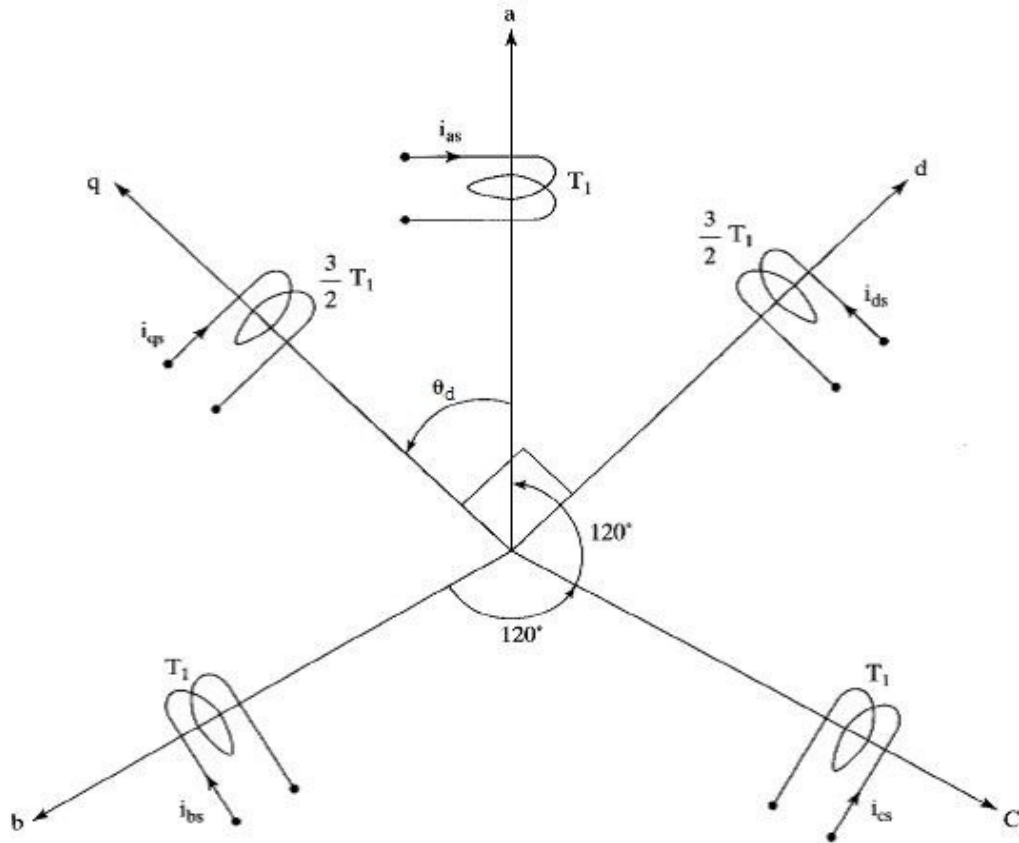
Figure 2.9 Relationships of d-q and abc quantities

$$[f_{dq0}] = [T_{dq0}(\theta_c)][f_{abc}] \qquad (2.28)$$

$$[T_{dq0}] = \frac{2}{3} \begin{bmatrix} \cos\theta_d & \cos(\theta_d - \frac{2\pi}{3}) & \cos(\theta_d + \frac{2\pi}{3}) \\ -\sin\theta_d & -\sin(\theta_d - \frac{2\pi}{3}) & -\sin(\theta_d + \frac{2\pi}{3}) \\ \frac{1}{2} & \frac{1}{2} & \frac{1}{2} \end{bmatrix} \qquad (2.29)$$

The inverse form is given by equation 2.30

$$[T_{dq0}]^{-1} = \begin{bmatrix} \cos\theta_d & -\sin\theta_d & 1 \\ \cos(\theta_d - \dfrac{2\pi}{3}) & -\sin(\theta_d - \dfrac{2\pi}{3}) & 1 \\ \cos(\theta_d + \dfrac{2\pi}{3}) & -\sin(\theta_d + \dfrac{2\pi}{3}) & 1 \end{bmatrix} \qquad (2.30)$$

where θ_d is the angle that defined between two dimension d-q frame and three phase a-b-c which is shown in Figure 2.9.

In some particular applications, fixed d-q frame quantities are required to transform onto another d-q frame which is rotating. Since the three phase variables are already transformed onto the stationary d-q axis frame by equation 2.28, which can be seen as $I_q{}^s$ and $I_d{}^s$, if we observe the stationary frame from a rotating frame at speed ω, the rotating reference frame can be written as equation 2.31 when we take the stator current for example.

$$\begin{bmatrix} i_q \\ i_d \end{bmatrix} = \begin{bmatrix} \cos\theta_c & -\sin\theta_c \\ \sin\theta_c & \cos\theta_c \end{bmatrix} \begin{bmatrix} i_q{}^s \\ i_d{}^s \end{bmatrix} \qquad (2.31)$$

The angle θ_c is the angle between rotating q-axis frame and stationary q-axis frame as illustrated in Figure 2.10. This angle is a function of angular speed, ω_c, of rotating reference frame and the initial angle, which can be represented by equation 2.32.

$$\theta_c(t) = \int_0^t \omega_c(t)dt + \theta(0) \qquad (2.32)$$

Initial angle $\theta(0)$ is the angle measured at time 0. To choose the rotational speed and initial angle is really dependent on the kinds of simplification and the best way to fit with the application at hand [37].
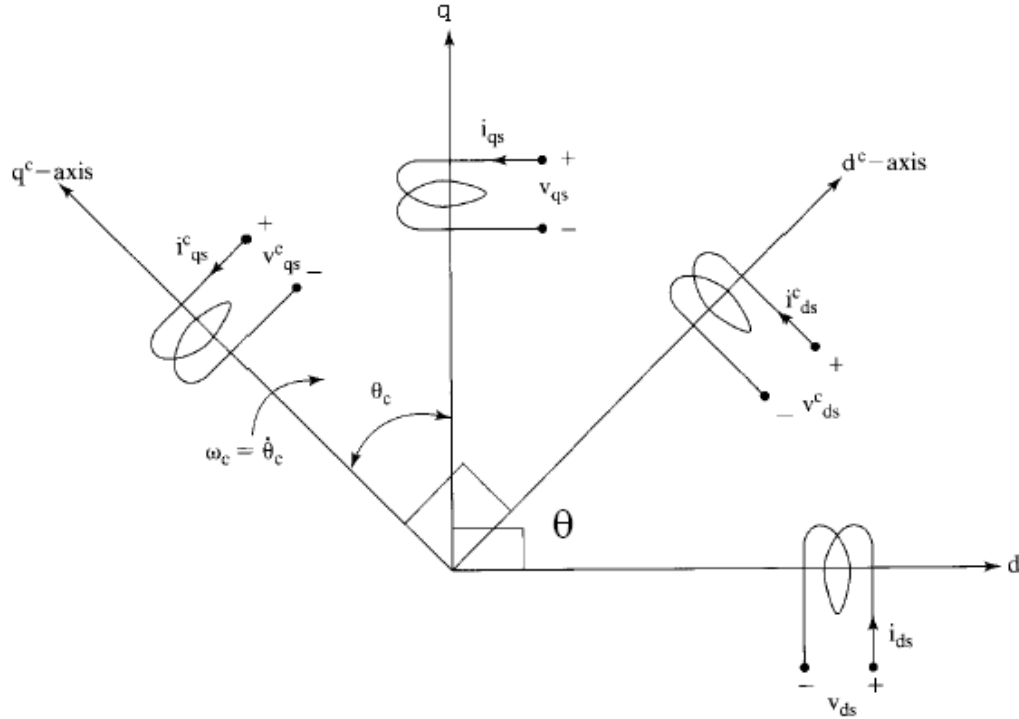
Figure 2.10 Relationship of stationary d-q frame and rotational d-q frame

2.4.2 Mathematical Model

A PM machine single phase equivalent circuit of PMSG is illustrated in Figure 2.11. Permanent magnet generator can be seen as a synchronous generator with constant flux linkage. By introducing Park transformation, machine AC stationary voltage and current are transformed into two DC rotatory d-q reference frames.

$$E = \omega_e \psi_{PM} = 2\pi f_e \psi_{PM} \tag{2.33}$$

$$L_s \frac{di_{sd}}{dt} = u_{sd} - R_s i_{sd} + \omega_e L_s i_{sq} \tag{2.34}$$

$$L_s \frac{di_{sq}}{d_t} = u_{sq} - R_s i_{sq} + \omega_e L_s i_{sd} - \omega_e \psi_{PM} \tag{2.35}$$

where u_{sd} and u_{sq}, i_{sd} and i_{sq} are direct(d) axis and quadrature(q) axis stator voltage and current, respectively. R_s is the stator resistance, and L_s is the stator inductance. ω_e is the generator electrical speed. ψ_{PM} is the permanent magnet flux linkage.

38
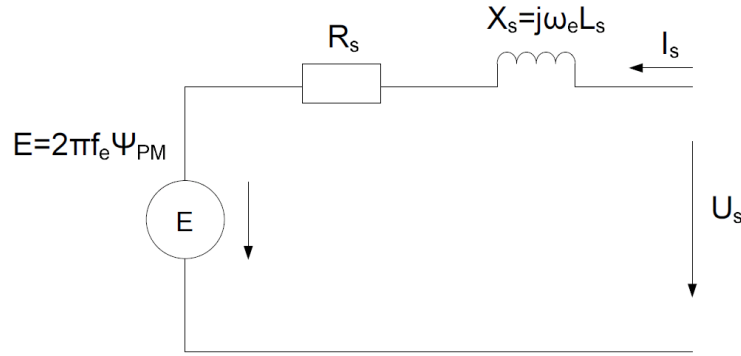
Figure 2.11 Single phase equivalent circuit of PMSG

In the PMSG model, machine torque (T_e) and electromotive force (E) can be calculated by the following equations 2.36 and 2.37. For the electrical machine has saliency, the value of stator d-q axis inductance L_d and L_q has slight difference. For the simplicity of analysis, in this project the difference is neglected and replaced by the same value L_s. Machine EMF depends on the machine rotational speed, which expression is the same as for the DC machine.

$$T_e = \frac{3}{2} pi_{sq} (\psi_{PM} + (L_d - L_q)i_d)$$
(2.36)

$$E = \omega_e \psi_{PM}$$
(2.37)

where p represents the number of poles; ω_e represents the generator electrical speed; ψ_{PM} represents the permanent magnet flux linkage.

2.5 Full Scale Converter

The PMSG wind turbine is interfaced with the power grid by full scale back-to-back converter. It consists of a generator side converter and a grid side converter connected by a DC link capacitor. The generator side converter acts as a rectifier that converts unstable AC voltage to unstable DC voltage, then the DC voltage is stabilized by the DC-link capacitor which is also controllable, and this DC voltage is finally converted to stable AC voltage by the grid side converter.

The full scale back-to-back converter is illustrated in Figure 2.12, where the

DC-link is operated to balance the active power flow through the converters. By defining the direction of currents, the power balance equation can be expressed as [38]:

$$P_{DC} = P_g + P_s \qquad (2.38)$$

$$P_{DC} = u_{DC} \cdot i_{DC} = C \cdot u_{DC} \frac{du_{DC}}{dt} \qquad (2.39)$$

$$P_g = u_{gd}i_{gd} + u_{gq}i_{gq} \qquad (2.40)$$

where C is the capacitance of the DC-link capacitor. P_{DC} represents the calculation of power for the DC-link capacitor, and u_{DC} and i_{DC} are the DC-link voltage and current, respectively. P_g is the grid side power fed by the grid side converter. P_s is the power supplied from the generator. u_{gd} and u_{gq} are the d-q voltages of the grid side converter, and i_{gd} and i_{gq} the d-q currents of the grid side converter.

Since the generator side converter is decoupled with the grid side converter through the DC-link, the two converters can be operated at different frequencies. Hence the d-q and gd-gq frames are applied to generator and grid, respectively. The model of the whole back-to-back converter can be therefore represented as:

$$C \cdot u_{DC} \frac{du_{DC}}{dt} = u_{gd} \cdot i_{gd} + u_{gq} \cdot i_{gq} + u_{sd} \cdot i_{sd} + u_{sq} \cdot i_{sq} \qquad (2.41)$$
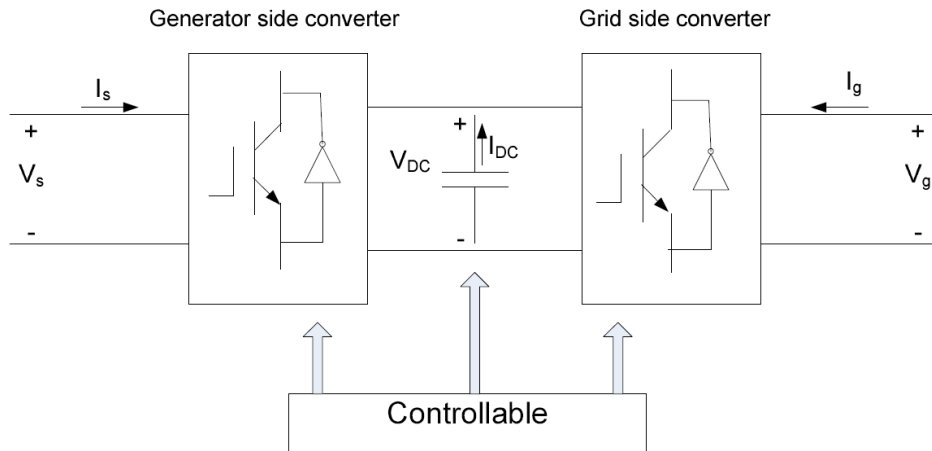
Figure 2.12 Full-scale power converter

40

A wind power generation system is a very comprehensive system. It is a combination of electrical machinery, mechanics, and control system, as well as power transmission. Power electronics play an important role in system control and optimization; in other words, we are able to manipulate the wind power generation system with the help of power electronics and make the system better serve humankind. Though this project does not emphasize analysing power electronics, it is worthy spending some time to understand how it works. Moreover, to understand the operation of power converters it is important to simulate the control system in a hardware-in-loop environment.

2.5.1 DC-DC Converters

The DC-DC converters are widely used in electronic devices. They are commonly used in lower power areas such as mobile phones and laptops; and also in high power areas such as hydro and wind power plants. They always work with a power supply primarily from batteries, converting the dc voltage from a lower level to a higher level by storing the energy temporarily and then releasing that energy at a higher voltage level. The storage could be either by magnetic field storage components such as inductors and, transformers, or electric field storage like capacitors.

Boost converter is a power converter to make the output DC voltage greater than the input DC voltage. The schematic of a boost converter is illustrated in Figure 2.13. There are two switch modes during the operation of this converter. In on-state mode, the voltage across the inductor jumps instantaneously to the source voltage and the current through the inductor increase linearly and stores energy in the inductor. In off-state mode, the energy stored in the inductor is transferred to the capacitor through the diode and the inductor voltage adds to the source voltage to increase the output voltage. When the switch is closed again, the capacitor energy supplies the load voltage and the cycle is repeated.

Another booster converter is called push-pull converter which is a transformer based DC-to-DC converter as shown in Figure 2.14. The transformer's turns ratio is arbitrary but fixed, however in many circuits, implementation of the duty cycle of switching action is used to affect a range of voltage ratios. This type of converter is usually used for high power levels [39].
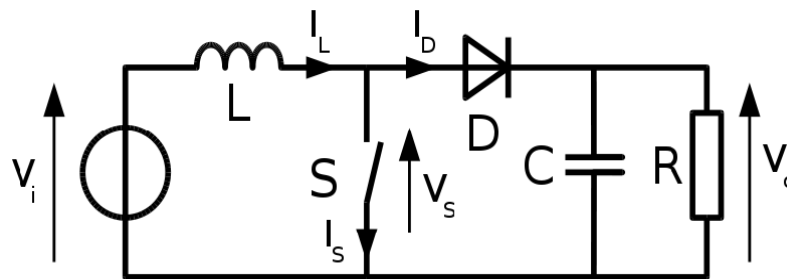
Figure 2.13 Booster converter topology
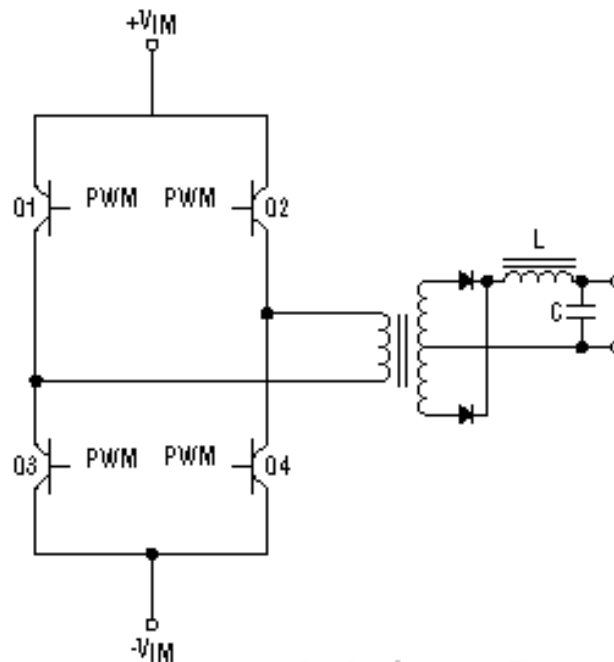
Figure 2.14 Pull-push converter topology

2.5.2 DC-AC Inverter

Inverters are used to change the input dc voltage to ac voltage, which is also known as the dc-to-ac converter. The function of an inverter is to generate the symmetrical ac voltage with desired magnitude and frequency, and both of them could be variable. The variable output voltage can be obtained by varying the input dc voltage, furthermore, if the input dc voltage is fixed the variable output voltage could be achieved by varying the gain of the inverter. The gain of the inverter is defined as the ratio of ac output voltage to dc input voltage. The variable gain of the inverter can be obtained by the pulse-width-modulation (PWM) control. The majority of the inverters we used are voltage source inverters (VSIs), where the input is dc voltage. The other type of inverters is current source inverters (CSIs), where the dc input of the inverter is dc current. This type of inverter is rarely used, now for very high power ac motor drives [39].

In these inverters, the input dc voltage is essentially constant in magnitude. In order to supply desirable output voltages, PWM technique is applied to control the magnitude and frequency of the output voltage in the inverter. The inverter switches are pulse-width modulated in order to shape the output voltage as close to a sine wave as possible. So the inverter has to control the frequency of the output ac voltage. The output voltage has a waveform similar to a square wave. These inverters are called square-wave inverters.

For the case of inverters with single-phase output, it is possible to control the magnitude and the frequency of the inverter output voltage even though the input to the inverter is a constant dc voltage and the inverter switches are not pulse-width modulated. The voltage cancellation technique works only with single-phase inverters.

Single phase inverters are used to supply the single phase load. The most commonly used single phase inverters are half-bridge inverters and full-bridge inverters. Figure 2.15 shows the topology of a half-bridge inverter. Here, two equal capacitors are connected in series across the dc input and their junction is at a

middle-potential, with a voltage equal to half V_s across each capacitor.

In order to generate AC voltage, only one transistor is turned on for a time T/2 . When Q_1 is on, Q_2 is off, the current passes through and we say that the current passing through is in the positive direction. If Q_1 is off, Q_2 is on, and the current will pass in the opposite direction, so we say it is negative. So, without apply the PWM control, the output voltage and current will be like in Figure 2.16. Voltage is acting as a square wave with peak amplitude $V_s/2$ during the period T/2. When the voltage is applied on a resistive load, the current will be like a sine wave, and when it is applied to an inductive load, the current will be like a triangle wave because of the characteristic of inductor itself, where f represents the switching frequency and L represents the load inductance.

A single phase full-bridge inverter circuit is shown in Figure 2.17. This inverter consists of two one-leg (half-bridge) inverters. It is preferred over other arrangements in higher power ratings. With the same dc voltage input, the maximum output voltage of the full-bridge inverter is twice that of the half-bridge inverter. It also implies that for the same amount of power input, the output current and the switch currents are half of those for a half-bridge inverter. At high power levels, this is a distinct advantage, since it requires less paralleling of devices. Figure 2.18 illustrates the output voltage and current of a full-bridge inverter.
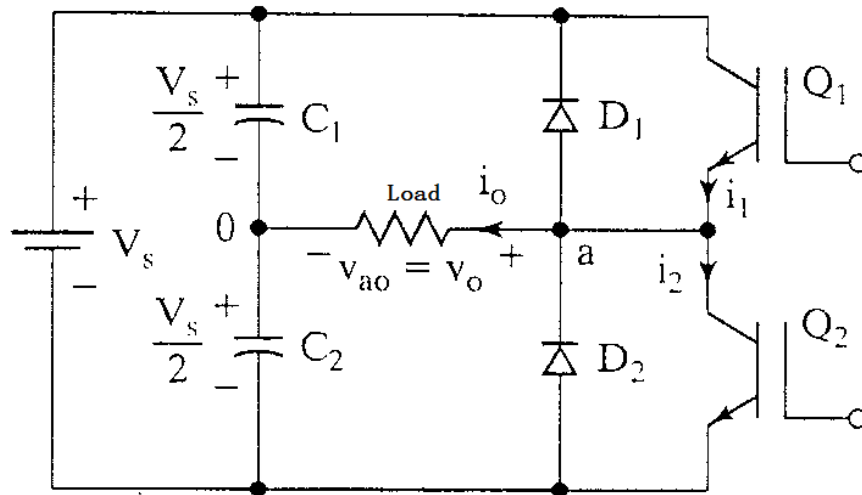
Figure 2.15 Half-bridge inverter
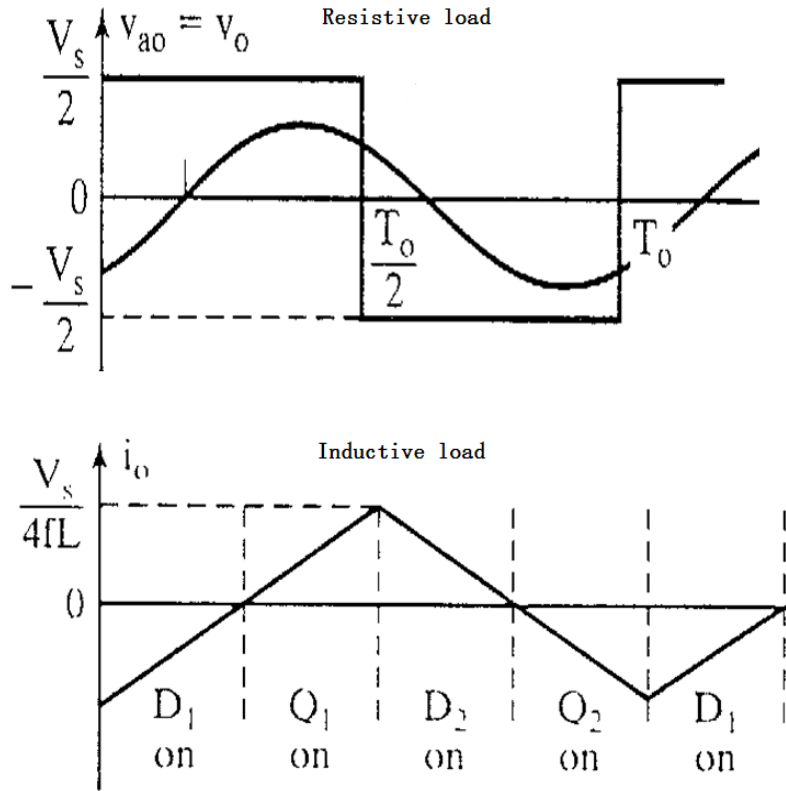
Figure 2.16 Output of a half-bridge inverter
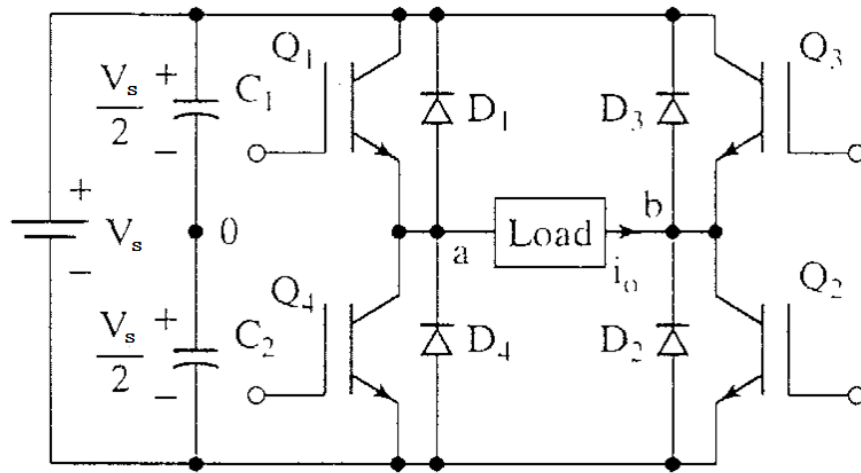
Figure 2.17 Full-bridge inverter
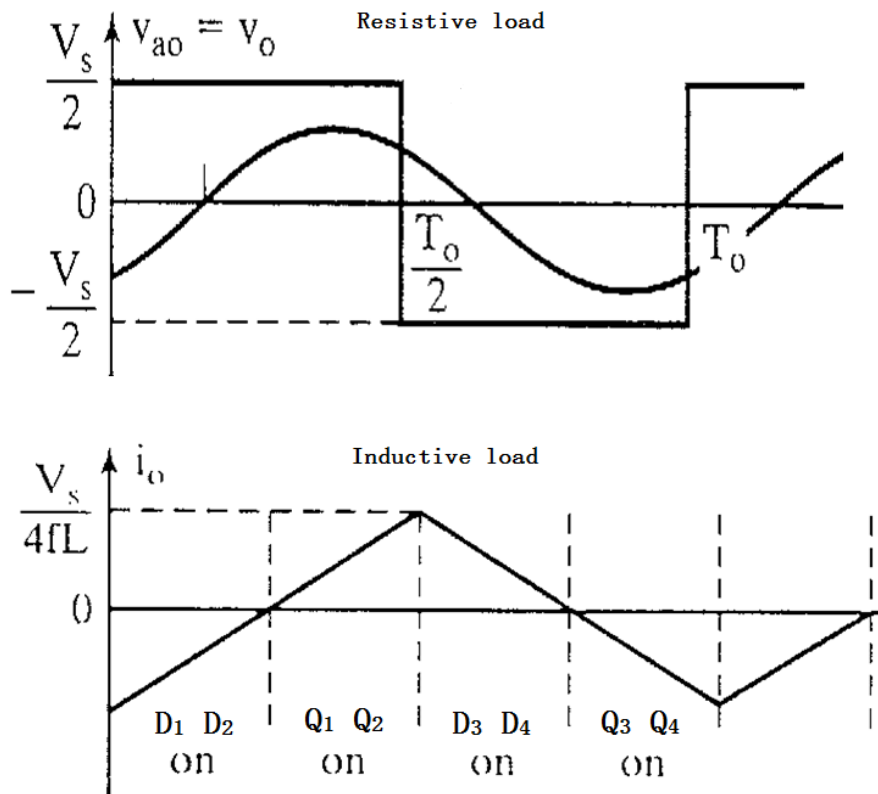
Figure 2.18 Output voltage of a full-bridge inverter

There are various techniques to vary the output voltage and frequency of power converters. The most efficient method to control the output of power converters is

by using pulse-width-modulation (PWM). A brief introduction of three common types of PWM techniques and the PWM control method of a single phase inverter will be included in this section.

Only one pulse is generated per half-cycle and the width of the pulse is varied to control the inverter output voltage. Figure 2.19 shows the technique of single pulse-width-modulation and the output voltage of a full-bridge single phase inverter. The gating signals are generated by comparing a rectangular reference signal of amplitude A_r, with a triangular carrier signal of amplitude A_c. By modulating the amplitude of A_c and A_r, the pulse width σ of the gating signal can be varied from 0° to 180°. The ratio of A_r to A_c is defined as the modulation index M, which is used to control the output voltage of the inverter. The relative functions are:

$$M = \frac{A_r}{A_c} \tag{2.42}$$

$$\sigma = M \times \pi \tag{2.43}$$

$$V_o = V_s \sqrt{(\frac{\sigma}{\pi})} \tag{2.44}$$

where V_0 is the inverter output voltage
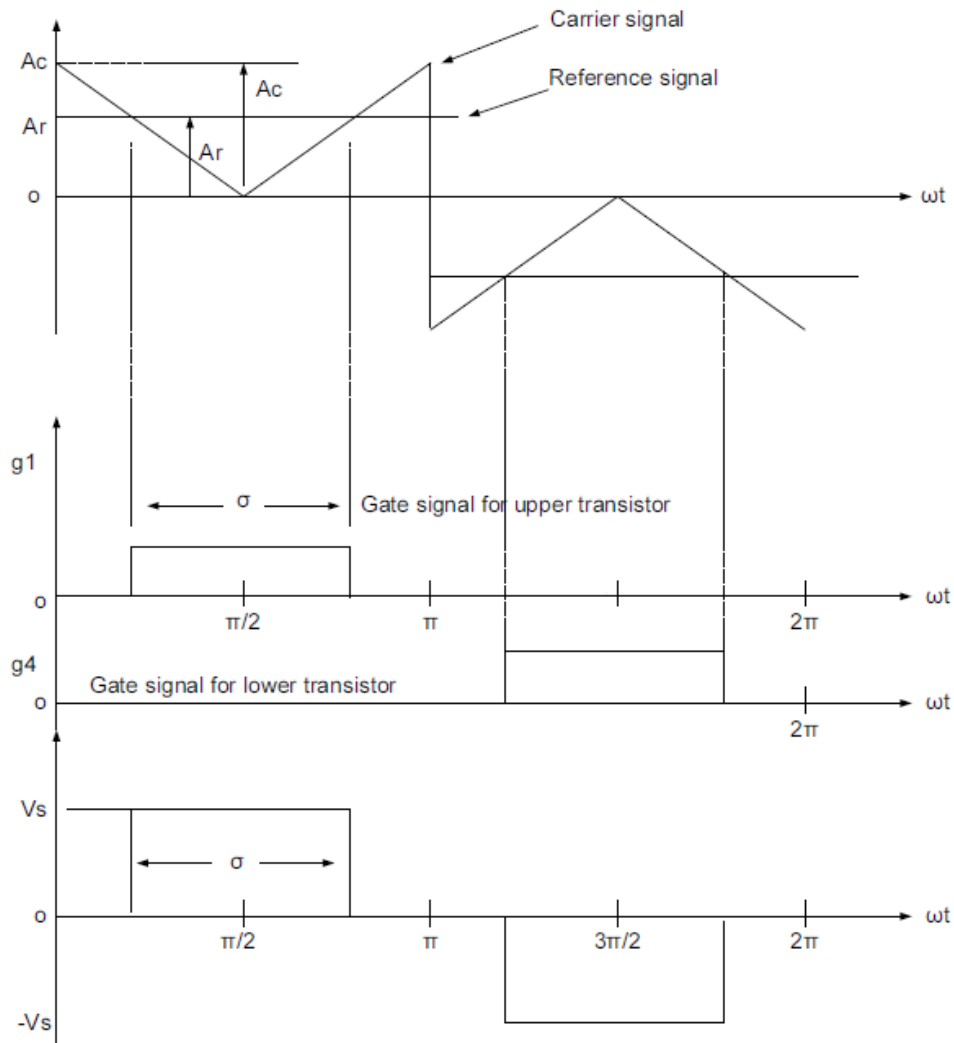
Figure 2.19 Single pulse-width-modulation

Instead of a single pulse per half-cycle of single-pulse-width modulation, multiple pulse-width modulation generates several pulses in each half-cycle of output voltage. Figure 2.20 shows the generated gating signal for turning on and off transistors. The triangle carrier signal compares with the reference signal to generate a certain number of pulses. The number of pulses per half-cycle is found from:

$$p = \frac{f_c}{2f_0} = \frac{m_f}{2} \qquad (2.45)$$

$$m_f = \frac{f_c}{f_0} \qquad (2.46)$$

The term m_f is the frequency modulation ratio which determines the inverter output voltage; f_o is the frequency of reference signal which sets the output frequency of

48

the inverter. The variation of modulation index M from 0 to 1 varies the pulse width from 0 to π/p and the output voltage from 0 to V_s. If σ is the width of each pulse, the rms output voltage can be found from:

$$V_o = V_s \sqrt{\frac{p\sigma}{\pi}}$$ (2.47)

Compared with single-pulse-width modulation, multiple-pulse-width modulation reduces the harmonic contents.
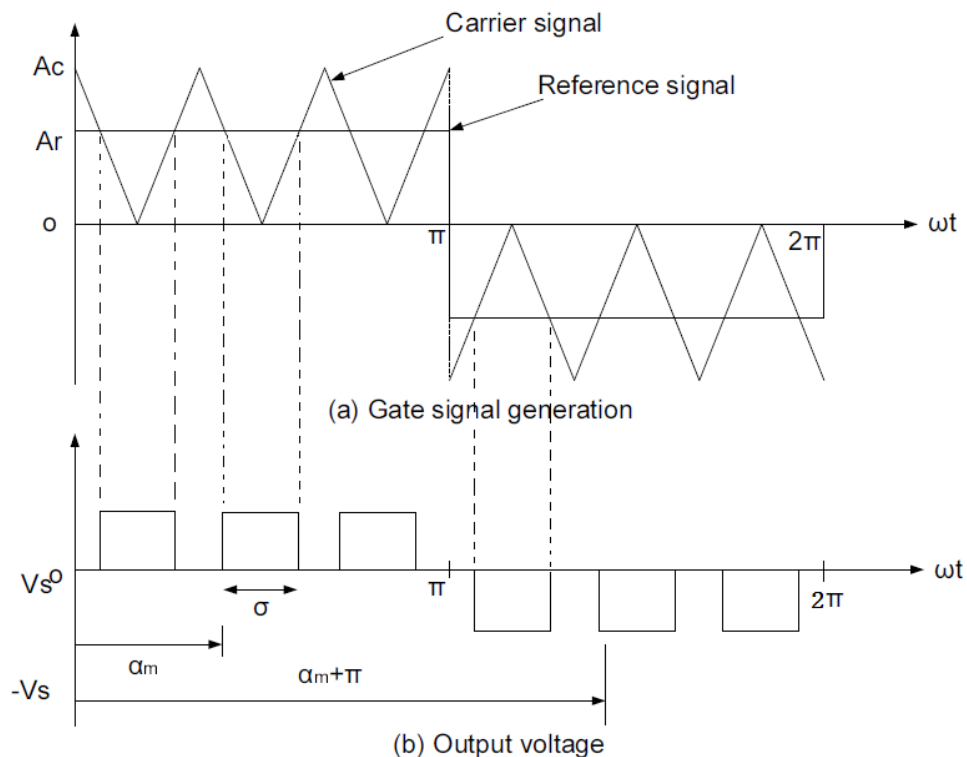
Figure 2.20 Multiple pulse-width-modulation

The most commonly used pulse-width-modulation in industrial applications is sinusoidal pulse-width modulation, because of its significant reduction of distortion factor and lower-order harmonics, which is abbreviated as SPWM. A sinusoidal reference signal with frequency f_r is compared with a triangular carrier signal with frequency f_c to generate a gating signal. The width of each pulse is varied in proportion to the amplitude of a sine wave evaluated at the centre of the same pulse. Inverter output frequency is the same as the frequency of reference signal f_r. The modulation index M is the ratio of the amplitude of reference signal to the

amplitude of carrier signal, which determines the rms of output voltage [38], Vo. If σ_m is the width of m-th pulse, then the rms value of output voltage can be written as:

$$V_o = V_s (\sum_{m=1}^{p} \frac{\sigma_m}{\pi})$$
(2.48)

where p is the number of pulses per half cycle. To vary the output voltage, we could change the peak amplitude of the reference signal A_r to turn the modulation index M as the amplitude of the carrier signal does not change all the time.
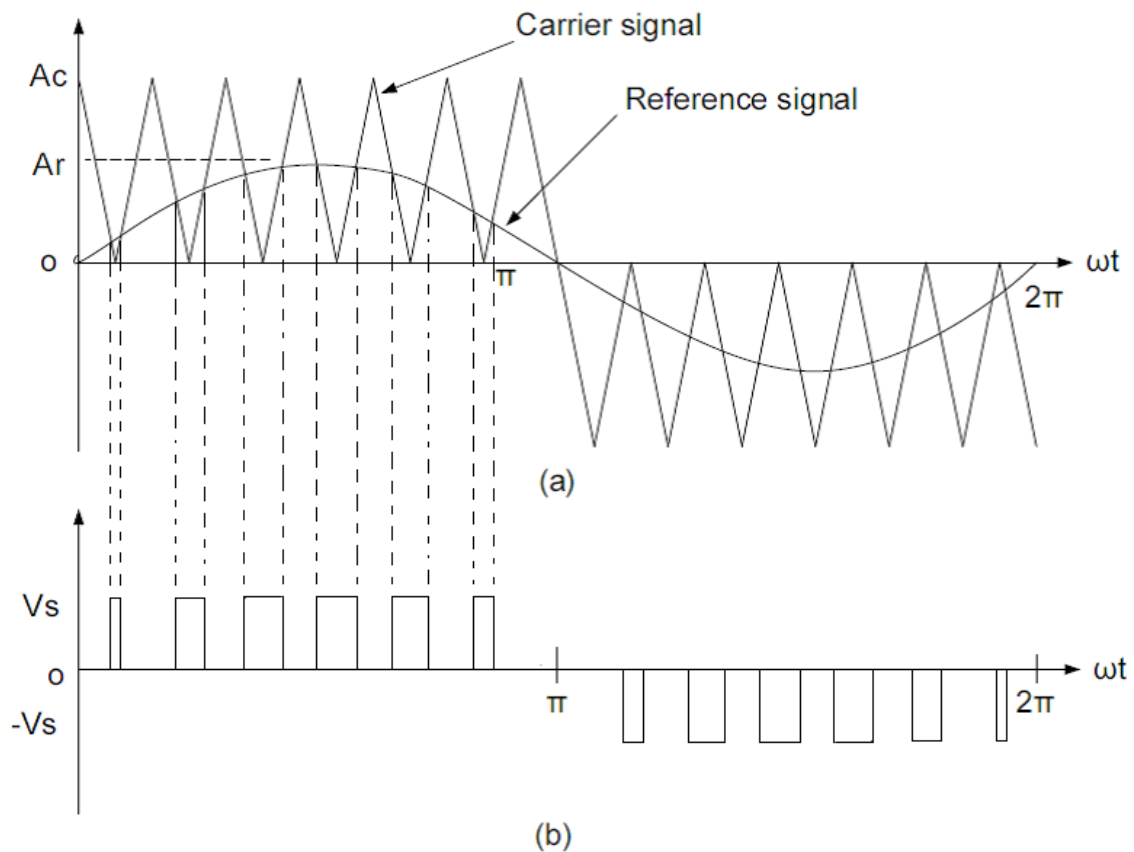
Figure 2.21 Sinusoidal pulse-width-modulation

In order to convert a magnitude and frequency controllable sinusoidal ac voltage, we have to use the pulse-width-modulation technique, where control signal $V_{control}$ (constantly or slowly varying in time) with the desired frequency is compared with a repetitive switching-frequency triangular waveform to generate the switching

signals, as shown in Figure 2.21. The frequency of the triangle waveform establishes the inverter switching frequency and is generally kept constant along with its amplitude.

To modulate the switch duty ratio, we need to define a few new terms; the triangular waveform V_{tri} is at switching frequency f_s; it is also called carrier frequency which is the switch frequency of the devices within the inverter. The control signal $V_{control}$ is used to modulate the switch duty ratio and has a frequency f_1, which is the desired frequency of the inverter voltage output; it is also called modulating frequency. The inverter voltage output will not be a perfect sine wave and will contain voltage components at harmonic frequencies of f_1. The amplitude modulation ratio m_a is defined as [38]:

$$m_a = \frac{V_{control}}{V_{tri}}$$ (2.49)

where $V_{control}$ and V_{tri} are all peak values, ma $\leq$ 1.

The frequency modulation ratio m_f is defined as:

$$m_f = \frac{f_s}{f_1}$$ (2.50)

The switches are controlled based on the comparison of $V_{control}$ and V_{tri}, as shown in Figure 2.22. Since the two switches are never turned off simultaneously, the output voltage V_o fluctuates between $V_d/2$ and $-V_d/2$. The peak amplitude of the output voltage V_o is m_a times the maximum output voltage.

Vcontrol   Vtri

Vo

Vcontrol less
than Vtri
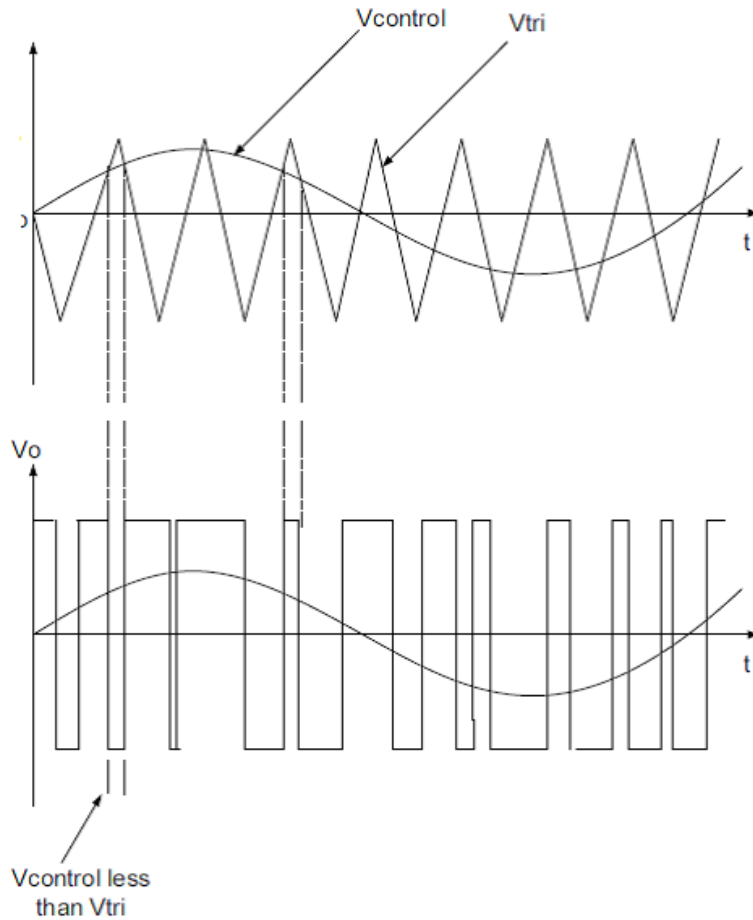
Figure 2.22 Single phase inverter pulse-width-modulation

2.6 Summary

This chapter contains the fundamental models of wind turbine components, and they are the foundations for electrical machine control and modelling. These devices are mechanically coupled to each other, i.e., turbine rotor coupled to drive train at one side and coupled to electrical machine at the other side; and the mathematical expression of each component allows these devices to be modelled as a system. Park's transformation is the revolutionary invention for electrical machine control, where the rotatory three dimensional problems are converted into two dimensions, and hence allows the decoupling of machine torque and flux.

Some studies of power electronics that related to electrical machine control have also been introduced in the chapter. The development of power converters and its application on electrical machines have greatly helped wind power generation. Since the electrical machine speed and torque can be controlled via power electronic, the wind turbine can be controlled to generate as much power as it can.

In the next chapter, the wind turbine system is modelled in the computation software according to these mathematical models. Electrical machine stator current is sensed and decoupled into d-q axis, and then the corresponding vector control strategy is used to control machine speed following the optimal rotation speed.

Chapter 3 Vector Control

3.1 Introduction

Vector control is a very common and powerful method to control brushless ac drives, it is also called field orientated control (FOC). In this section, vector control of the PMSG wind turbine is introduced. A large number of research publications have introduced vector control topics applied to wind power generation. A brief review of different wind turbine topologies and control strategies are compared in [40]. In [11] a sensorless vector control strategy for wind power generation is demonstrated. The elimination of sensors can significantly reduce wind turbine maintenance. The vector control for MPPT and relevant controller design are contained in [14, 15, 41].

3.2 Vector Control

Since the variable speed wind turbine has become the dominant turbine configuration in the wind power industry, it is necessary to control the turbine rotating at the optimal speed under different circumferential conditions in order to generate maximum power. Vector Control (VC) is the most popular method of controlling ac machines and also it is an economical approach to handle variable speed power generation.

In general, VC means to decouple machine flux linkage and torque, hence to produce fast torque response and high energy conversion rates [13]. Machine torque is controlled indirectly by closed loop stator current, as given by equation 3.1-3.3, which is the three phase stator current; by using three phase to d-q transformation, the d-q axis stator current can be represented by equation 3.4-3.6. Figure 3.1 shows the phasor diagram of PMSG in dq reference frame, where δ is the torque angle. i_{qs}^r

is the torque-producing stator current component which is equals to i_T, and i^r_{ds} is the flux-producing stator current component which is equals to i_f. The machine torque can then be computed by equation 3.7 and supplementary flux linkage by equation 3.8, where L_d and L_q are axial value of stator inductance; P represents the number of machine poles; λ_{af} represents fireld flux linkage; L_m represents mutual inductance; and i_{fr} represents the field current.

$$i_{as} = i_s \sin(\omega_r t + \delta) \tag{3.1}$$

$$i_{bs} = i_s \sin(\omega_r t + \delta - \frac{2}{3}\pi) \tag{3.2}$$

$$i_{cs} = i_s \sin(\omega_r t + \delta + \frac{2}{3}\pi) \tag{3.3}$$

$$\begin{bmatrix} i^r_{qs} \\ i^r_{ds} \end{bmatrix} = \frac{2}{3} \begin{bmatrix} \cos(\omega_r t) & \cos(\omega_r t - \frac{2}{3}\pi) & \cos(\omega_r t + \frac{2}{3}\pi) \\ \sin(\omega_r t) & \sin(\omega_r t - \frac{2}{3}\pi) & \sin(\omega_r t + \frac{2}{3}\pi) \end{bmatrix} \begin{bmatrix} i_{as} \\ i_{bs} \\ i_{cs} \end{bmatrix} \tag{3.4}$$

$$i^r_{qs} = i_s \sin\delta \tag{3.5}$$

$$i^r_{ds} = i_s \cos\delta \tag{3.6}$$

$$T_e = \frac{3}{2} \cdot P \left[\frac{1}{2}(L_d - L_q)i^2_s \sin 2\delta + \lambda_{af} i_s \sin\delta \right] \tag{3.7}$$

$$\lambda_{af} = L_m i_{fr} \tag{3.8}$$
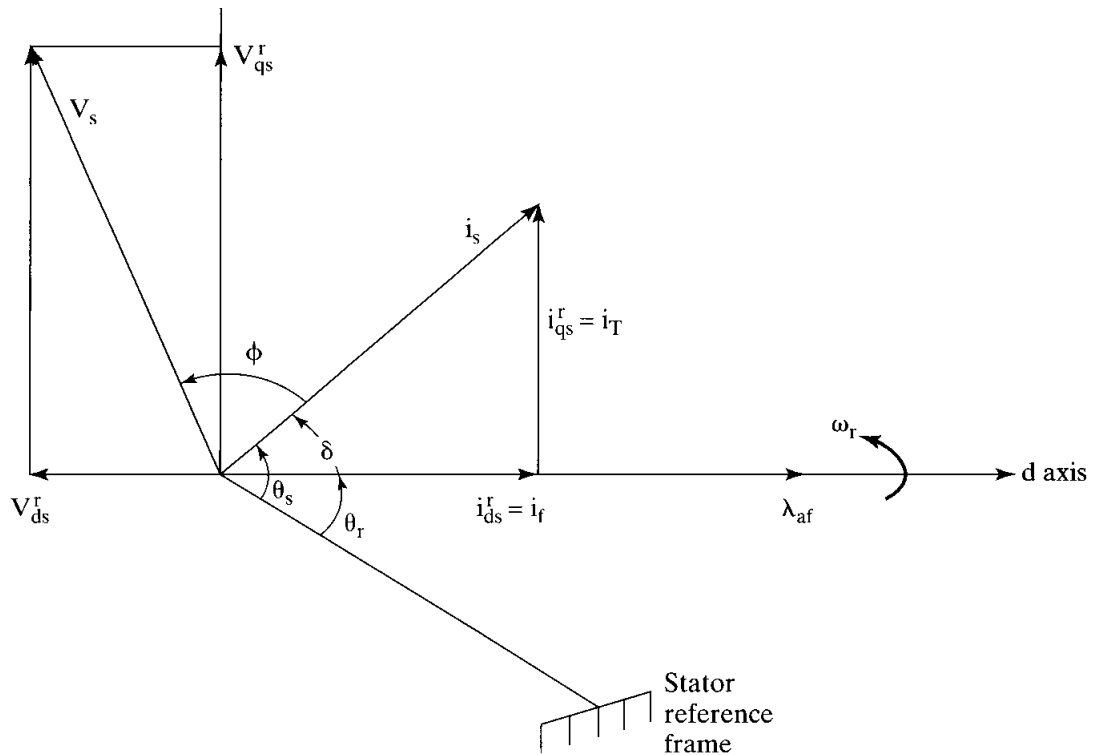
Figure 3.1 Phasor diagram of vector control

There are also some other popular control strategies to control the machine torque, such as:

- Constant torque angle control:
- Unity-Power-Factor control
- Constant mutual air gap flux linkages control
- Optimum toque-per-ampere control
- Flux-weakening operation

In constant torque angle control, the d-axis stator current is set to zero and all the stator current components align with the q-axis. Assuming the electrical machine has non-saliency and thus the general torque equation 3.7 can be written as equation 3.9. Since i_{ds} is equal to zero, the steady state d-q axes voltages are represented by equation 3.10 and 3.11. Then the machine torque is directly proportional to the stator q-axis current since d-axis current is set to zero. This constant torque angle control phasor diagram is shown in Figure 3.2. The power factor equation in constant torque angle control is represented by equation 3.12.

56

$$T_e = \frac{3}{2} P \lambda_{af} i_s \qquad (3.9)$$

$$V^r_{qs} = R_s i_s + \omega_r \lambda_{af} \qquad (3.10)$$

$$V^r_{ds} = -\omega_r L_q i_s \qquad (3.11)$$

$$\cos\phi = \frac{V^r_{qs}}{V_s} = \frac{V^r_{qs}}{\sqrt{(V^r_{qs})^2 + (V^r_{ds})^2}} \qquad (3.12)$$

where T_e represents the machine torque; P represents the number of machine poles; λ_{af} represents the flux linkage; V^r_{qs} represents the q-axis stator voltage align on the rotational reference frame; V^r_{ds} represents the d-axis stator voltage align on the rotational reference frame; R_s is the stator resistance; i_s represents the stator current which has q-axis component only; ω_r is the rotor rotational speed; L_q represents the q-axis inductance.
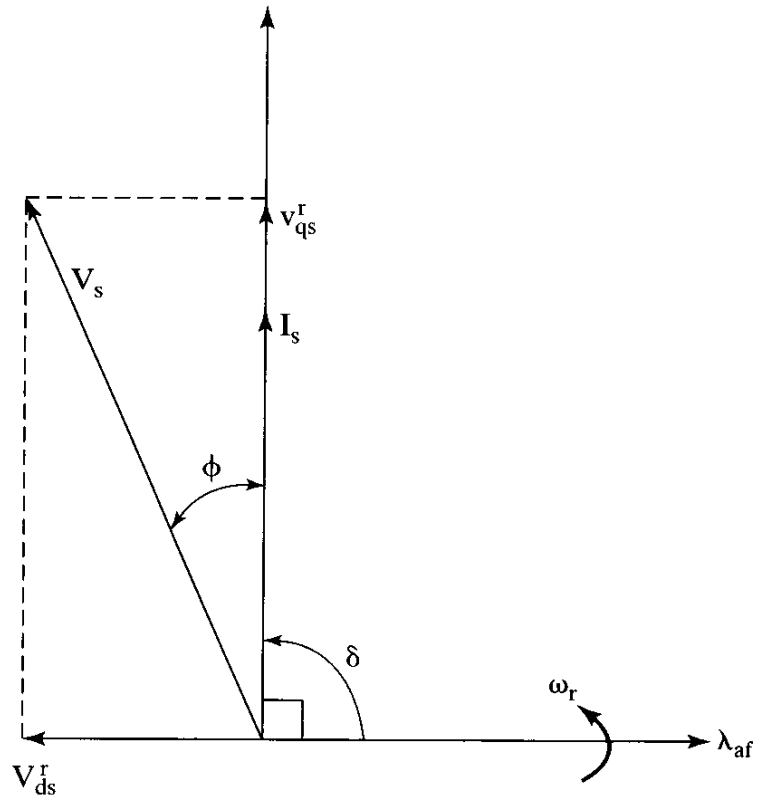
Figure 3.2 Phasor diagram of constant torque angle control

3.3 Maximum Power Point Tracking (MPPT)

Wind power is an unpredictable and intermittent renewable energy source; it changes when the weather changes. This property directly influences the power generation of the wind turbine. Since the rotating speed of the wind turbine determines the rotating speed of the electrical generator, the change of wind speed therefore results in the fluctuation of the output power. Figure 3.3 shows the output power changes of a horizontal type wind turbine under different wind speeds. Each curve represents power output against wind turbine rotating speed at one certain wind speed, and the maximum power point is reached at one specific wind turbine rotational speed. Maximum power point tracking means controlling the wind turbine to follow the maximum power point at different wind speeds during its operation.

The machine torque is controlled by closed loop stator current control through PI controllers, while the torque angle is controlled to constant by setting the d-axis current to zero. The relative control strategy is carried out by a generator side power converter. Since electrical generator toque is controllable, the rotational speed is controlled at different wind speeds, and thus maximum power point tracking can be achieved.
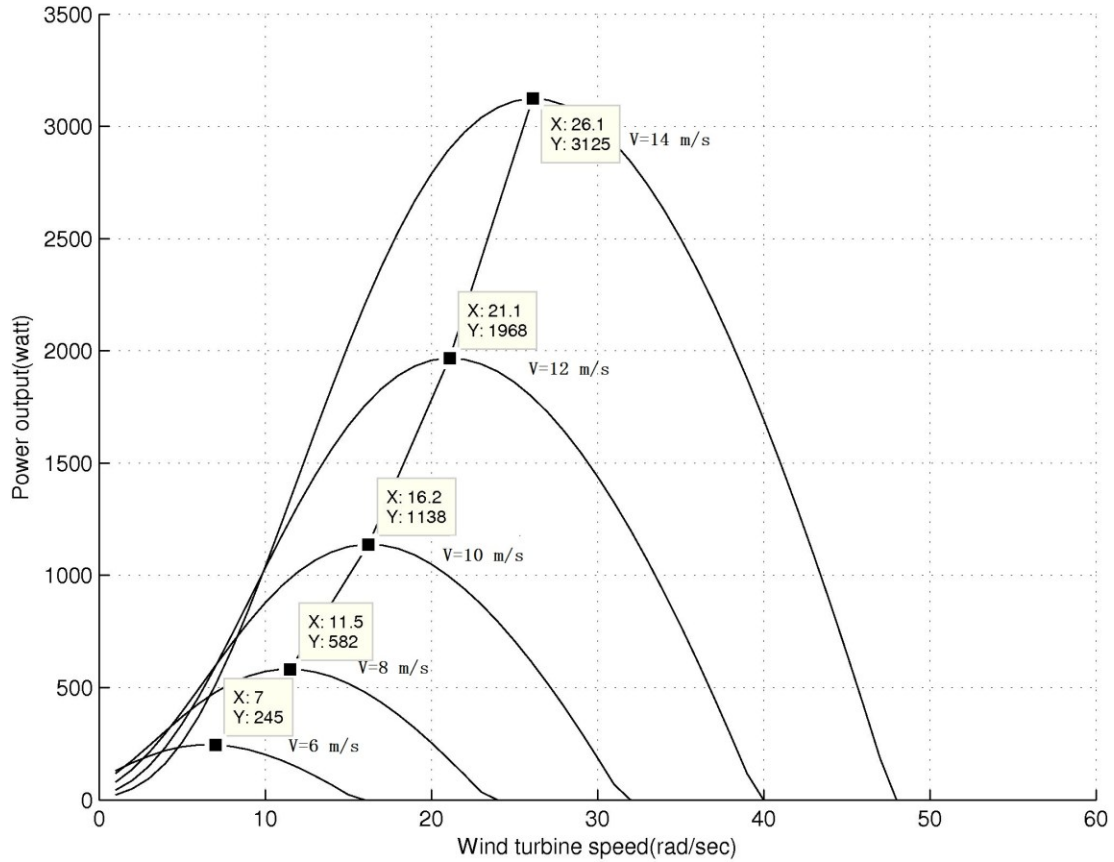
Figure 3.3 Wind turbine output power

The maximum power that wind turbines can extract from wind is determined by power coefficient C_p. which is a function of tip speed ratio λ and pitch angle β. When MPPT control is applied to the wind turbine, pitch angle β is adjusted to zero, hence the blades would provide maximum torque. Thus C_p only changes with one variable λ. The relationship between tip speed ratio and power coefficient is represented by equation 3.13-3.14.

$$P_w = \frac{1}{2}\rho\pi R^2 v^3 C_p(\beta,\lambda) \tag{3.13}$$

$$\lambda = \frac{R\omega_m}{V} \tag{3.14}$$

In order to control the wind turbine rotational speed, permanent magnet synchronous generator torque can be controlled according to equation 3.7. L_d and L_q are axial value of stator inductance; due to the machine saliency L_d and L_q

59

usually have different values in reality. However, for the simplicity of analysis, L_d and L_q are treated as having the same value and the machine torque equation is simplified as

$$T_e = \frac{3}{2} p i_{sq} \psi_{PM} \tag{3.15}$$

In a permanent magnet excited machine, P is the number of poles, i_{sq} is stator q-axis current, ψ_{PM} is equivalent to the terms λ_{af} represents in section 3.2, where λ_{af} is a more general form. Here use different symbol just to emphasize this property in an interior permanent magnet machine, and the value flux linkage ψ_{PM} is looked at as constant in machine modelling, though the value of flux linkage varies in some extreme conditions such as high temperature and machine or grid fault. Therefore, the machine torque is seen as a linear equation in respect to the stator q-axis current, and can be controlled through stator current control.

Possible ways to control the machine torque include unity power factor control and maximum torque per ampere control, as well as maximum torque angle control. Maximum torque angle control is used here to conduct the control purpose of maximum power point tracking. By which the d-axis stator current component is set to zero at 90 degrees with respect to the q-axis, and the stator current vector component has q-axis only to enrich the stator current controllability.
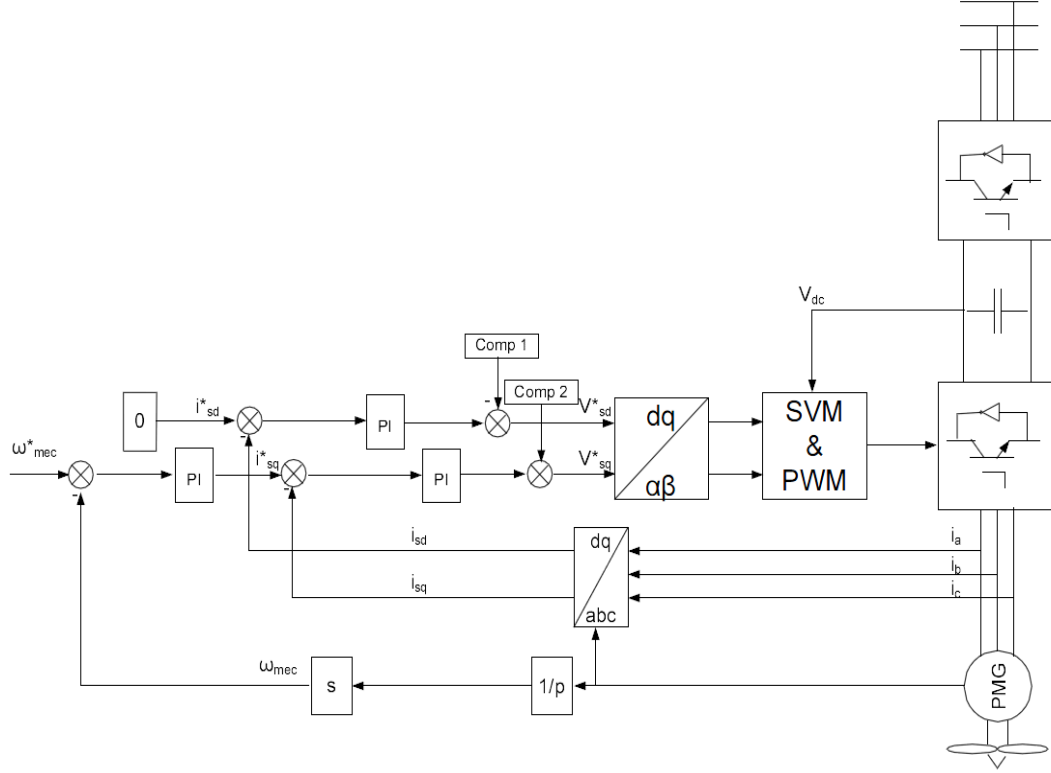
Figure 3.4 Field oriented control algorithm for MPPT

Figure 3.5 shows the control strategy of maximum torque angle control for MPPT. The control algorithm is conducted by generator side power converter through an inner current control loop and an outer speed control loop. The reference mechanical speed is calculated by equation 3.17. By using the PI (Proportional and Integral) controller, the q-axis reference current is derived. Two compensation items Comp-1 and Comp-2, which are represented by equations 3.18 and 3.19, are added to linearize the system and improve the system's dynamic behaviour, as the PI controller controls the linear system only.

$$\omega_{opt}{}^* = \frac{\lambda_{opt} R}{V_W} \tag{3.16}$$

$$Comp-1 = \omega_m (L_d i_{sd} + \psi_{PM}) \tag{3.17}$$

$$Comp-2 = \omega_m L_q i_{sq} \tag{3.18}$$

where $\omega_{opt}{}^*$ is the optimal turbine rotational speed, λ_{opt} is the optimal tip speed ratio, R represents the turbine radius; ω_m is the turbine actual rotational speed;

61

V_w represents the wind speed; the other terms are defined previously.

3.4 Current and Speed Controller

This section introduces the conventional Proportional-Integral (PI) control algorithm. Controller design method and control parameters tuning method are presented. There are three PI controllers are used in this control strategy. This PI control method is based on linear control ideas; any nonlinear items would be neglected in the control loop. The compensation items are added to improve the system dynamic behaviour.
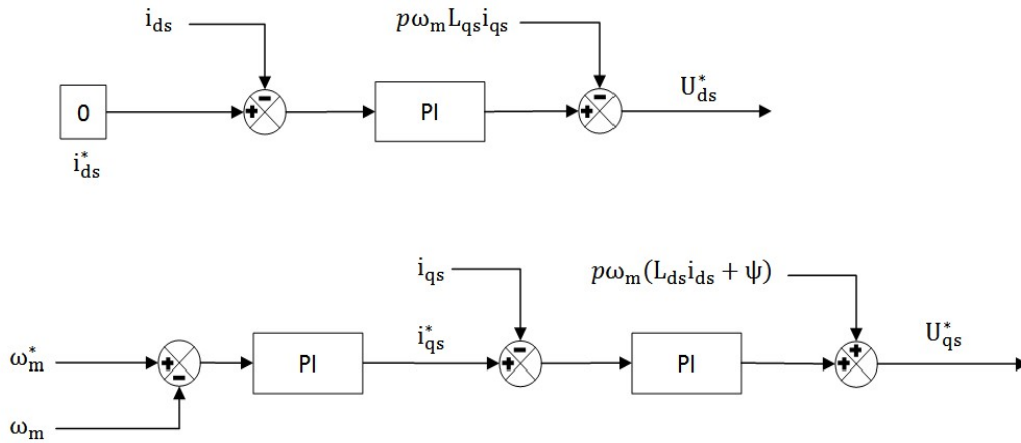
Figure 3.5 PI control scheme for current control

Figure 3.6 show the d-axis control loop, which contains one PI controller which controls the d-axis current by closed loop. The PI controller can be expressed as equation 3.20, and α is the control plant which can be represented by equation 3.21, wherein L_q is the q-axis inductance and R is stator resistance. The open loop transfer function is represented by equation 3.22. The PI controller parameters are determined by the zero-pole cancellation method.

$$PI = \frac{K_p s + K_i}{s} \tag{3.19}$$

$$\alpha = \frac{1}{L_q s + R} \qquad (3.20)$$

$$G(s) = (\frac{K_p s + K_i}{s})(\frac{1}{L_q s + R}) = \frac{K_p s + K_i}{s^2 L_q + sR} \qquad (3.21)$$

3.4.1 Tuning of the PI controller

This section presents the PI controller tuning method for the proposed control strategy. There are three different PI controllers used in the control system where two of them are used in the current (torque) control loop and the third one is used in the d-axis current control loop. The proportional and integral parameters Kp and, Ki have to be tuned properly in order to carry out the expected system response.

There are several methodologies for tuning the PI controllers; one of them is called pole-zero cancellation method. This method is used to tune both current and speed loop controllers.

Firstly, the transfer function of PI controller is given by:

$$C(s) = K_p + \frac{K_i}{s} = \frac{K_p s + K_i}{s}? \qquad (3.22)$$

The transfer function of Plant can be described as:

$$P(s) = \frac{1}{L_q s + R} \qquad (3.23)$$

The open loop transfer function of current control loop is therefore:

$$G(s) = C(s) \times P(s) = \frac{K_p(s + \frac{K_i}{K_p})}{L_q s(s + \frac{R}{L_q})} \qquad (3.24)$$

The transfer function 3.25 reflects that, in this 2nd order system, the poles are s=0 and s=-R/L_q and; zero is-K_i/K_p. The zero pole is now placed to an appropriate location to cancel out the slow pole –R/L_q, so the system's slow dynamic response

63

can be compensated. Equation 3.26 indicates the corresponding compensation item, and the 2nd order system is simplified into a 1st order system as shown in 3.31.

Figure 3.7 describe the block diagram of the control system including the plant (PMSG) α.

$$\frac{K_i}{K_p} = \frac{R}{L_q} \tag{3.25}$$

$$G(s)' = \frac{K_p}{L_q s} \tag{3.26}$$

For the closed loop transfer function, the output current i_{ds} can be represented by equation 3.28. From it, the ratio of d-axis current and reference d-axis current is derived as equation 3.29. For the 1st order system, the time constant is τ, and if the time constant is set to 4ms, then K_p can be calculated as equals 3.5 and K_i as equals to 350.

$$i_{ds} = e(s) \times G(s)' = (i^*_d - i_d) \times \frac{K_p}{L_q s} \tag{3.27}$$

$$\frac{i_d}{i_d^*} = \frac{\dfrac{K_p}{L_q s}}{1 + \dfrac{K_p}{L_q s}} = \frac{\dfrac{K_p}{L_q}}{s + \dfrac{K_p}{L_q}} \tag{3.28}$$

$$\tau = \frac{L_q}{K_p} \tag{3.29}$$

$$T_s = 4\tau = 4 \times \frac{L_q}{K_p} \tag{3.30}$$

$$K_i = \frac{R \times K_p}{L_q} \tag{3.31}$$
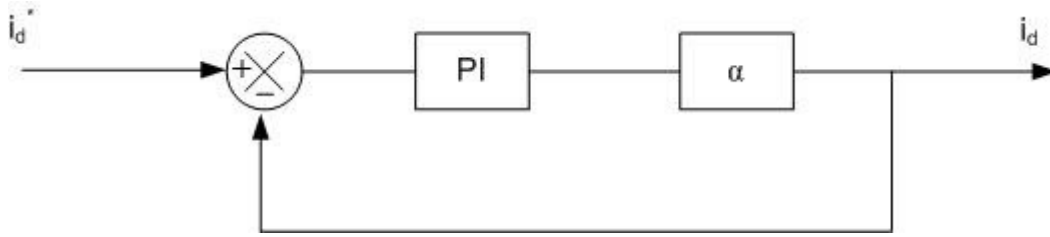
Figure 3.6 d-axis control loop
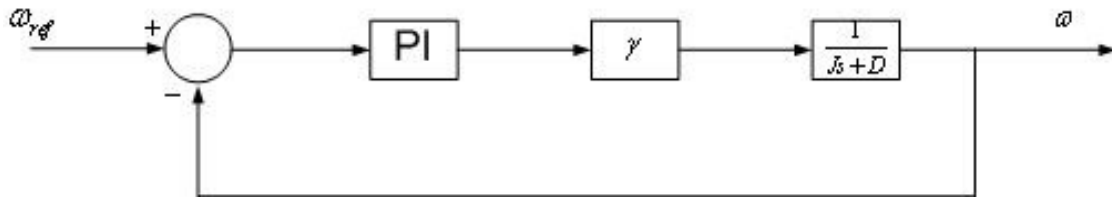
Figure 3.7 Speed control loop

Figure 3.8 illustrates the speed control loop; the open loop transfer function G(s) is represented by equation 3.33. The PI controller configuration is also done by zero-pole cancellation method. Cancelling out the zero-poles results in the new open loop transfer function G(s)'. The actual and reference speed relationship is derived as equation 3.36. In this 1st order system, the time constant is τ, and for the mechanical system we set the time constant to 5 second, then the values of K_p and K_i are derived.

$$G(s) = \frac{K_p s + K_i}{s} \cdot \frac{1}{Js + D} \gamma = \frac{\gamma K_p (s + \frac{K_i}{K_p})}{Js(s + \frac{D}{J})} \qquad (3.32)$$

$$\text{Zero: } s = -\frac{K_i}{K_p} \quad \text{poles: } s = -\frac{D}{J} \quad s = 0$$

$$G(s)' = \frac{\gamma K_p}{Js} \qquad (3.33)$$

Closed loop transfer function:

$$\omega = e(s) \times G(s)' = (\omega_{ref} - \omega) \times \frac{\gamma K_p}{Js} \qquad (3.34)$$

$$\frac{\omega}{\omega_{ref}} = \frac{\dfrac{\gamma K_p}{J}}{s + \dfrac{\gamma K_p}{J}} \qquad (3.35)$$

$$T_s = 4\tau = \frac{4J}{\gamma K_p} \qquad (3.36)$$

where γ is used to represents the inner control loop, J represents the total inertia of the system, D represents the damping ratio of the system.

3.5 Simulation Results

The wind speed is shown in Figure 3.9, where wind speed start from 6 m/s, and experiences two step changes at 2 seconds and 4 seconds, when it jumps to 8 m/s and 10 m/s. The corresponding power in the wind at these three wind speeds is shown in Figure 3.10. The power coefficient in this wind turbine is about 0.43 and the corresponding optimal tip speed ratio λ_{opt} equals to 6.2. With the help of this parameter, the reference wind turbine rotating speed can be calculated and set as seen in Figure 3.11, where the dashed blue line represents the reference wind turbine rotational speed, and the red solid line represents the actual wind turbine rotational speed. It can be shown that the proposed vector control strategy controls the wind turbine rotation following the required reference speed. Even when the circumferential wind speed is subject to critical step change, the wind turbine still rotates at the required speed in order to maintain the maximum power generation.
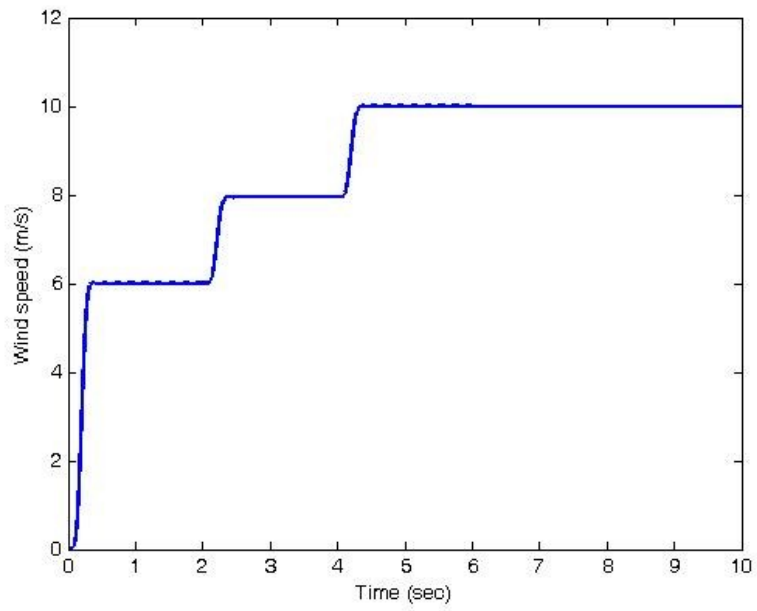
Figure 3.8 Wind speed in MPPT control modelling
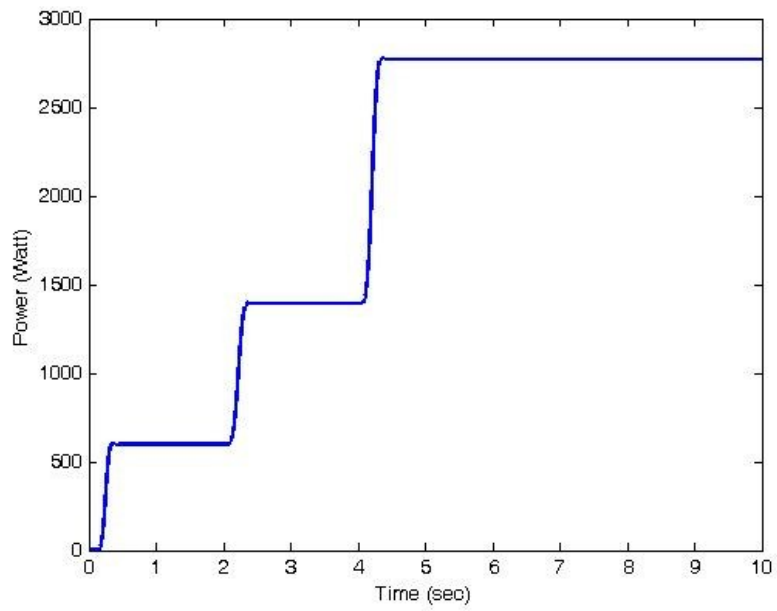
Figure 3.9 Power in the wind at specified wind speed
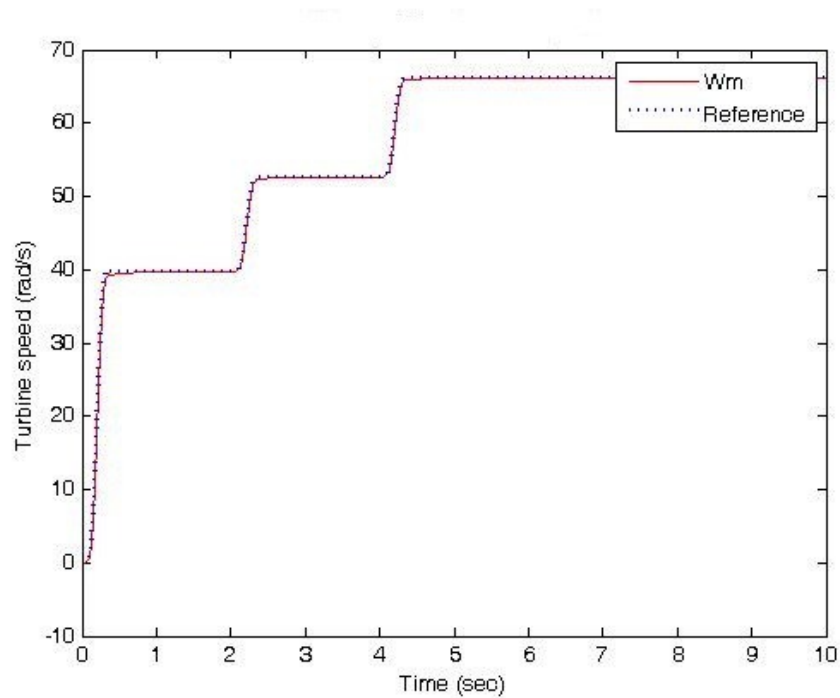
Figure 3.10 Reference and actual wind turbine speed

The reference d-axis current is set to nil to leave the full capability of magnetic flux to generate torque. The real d-axis current is shown in Figure 3.12, where the current fluctuation can be seen, and the magnitude of the fluctuation becomes greater as the wind speed goes higher. However, the scope of this current is in a very small range, i.e., $1e^{-15}$, so the fluctuation is ignorable. It is fairly reasonable to state that the d-axis current is controlled very well. The q-axis current directly determines machine torque and hence the wind turbine rotational speed. Under the different wind speed, it can be seen that the q-axis current also experiences step change which follows wind speed changes, as shown in Figure 3.13.

The real power and reactive power generated from this PMSM coupled wind turbine are shown in Figures 3.14 and 3.15, respectively. It also can be seen that both active and reactive power experiences step change under step change circumferential wind speed. There is a slight overshoot when speed changes. In Figure 3.16, the power coefficient of this wind turbine can be seen kept at the

68

optimal value of 0.42.
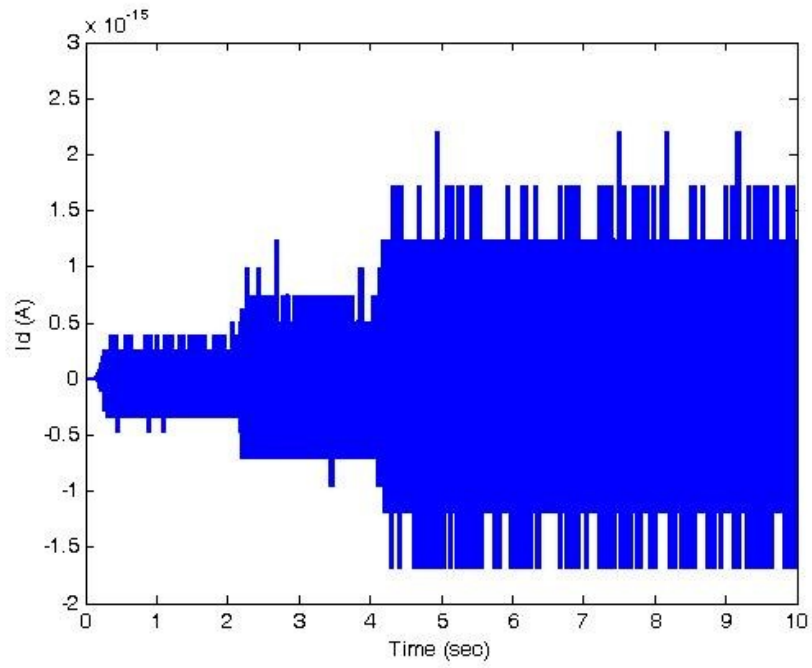
Figure 3.11 Control output d-axis current
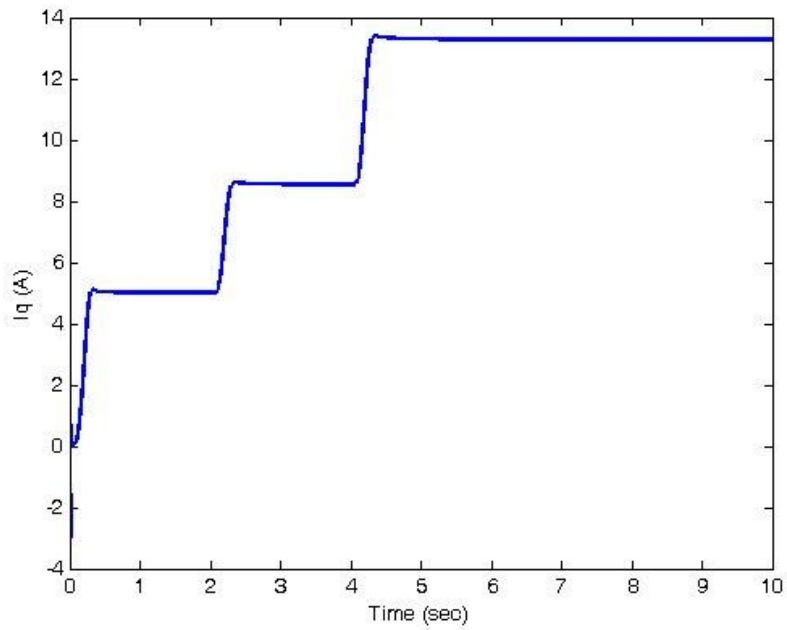
Figure 3.12 Control output q-axis current
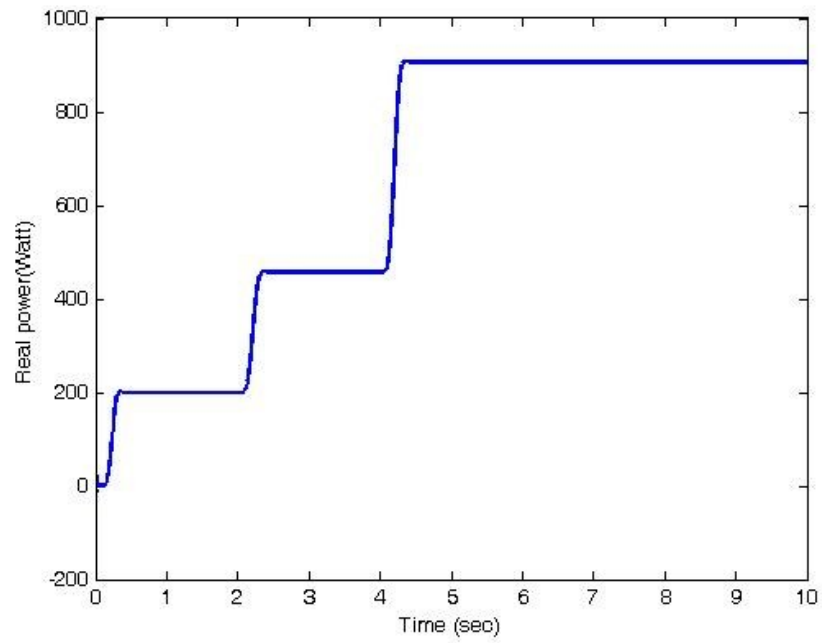
Figure 3.13 Real power of the wind turbine
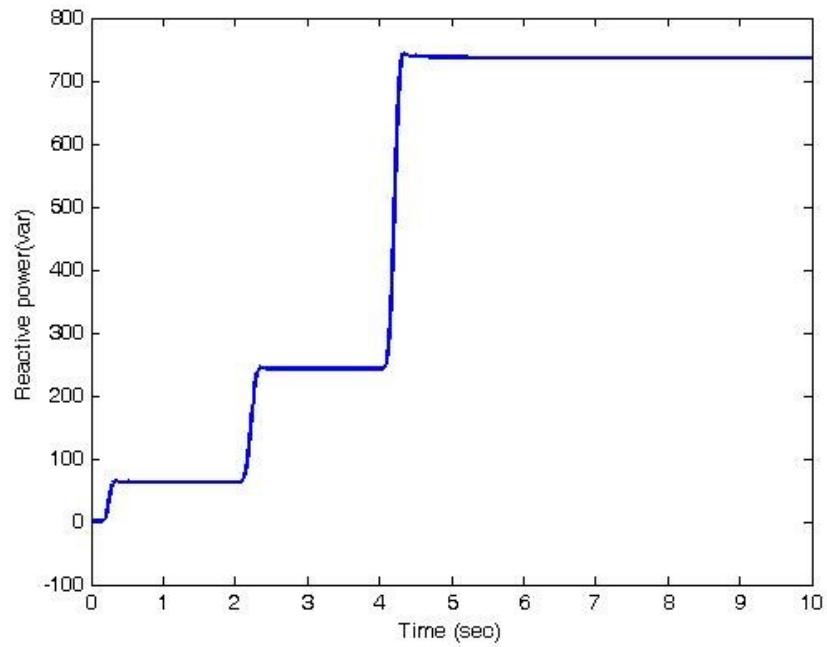
Figure 3.14 Reactive power of the wind turbine

70
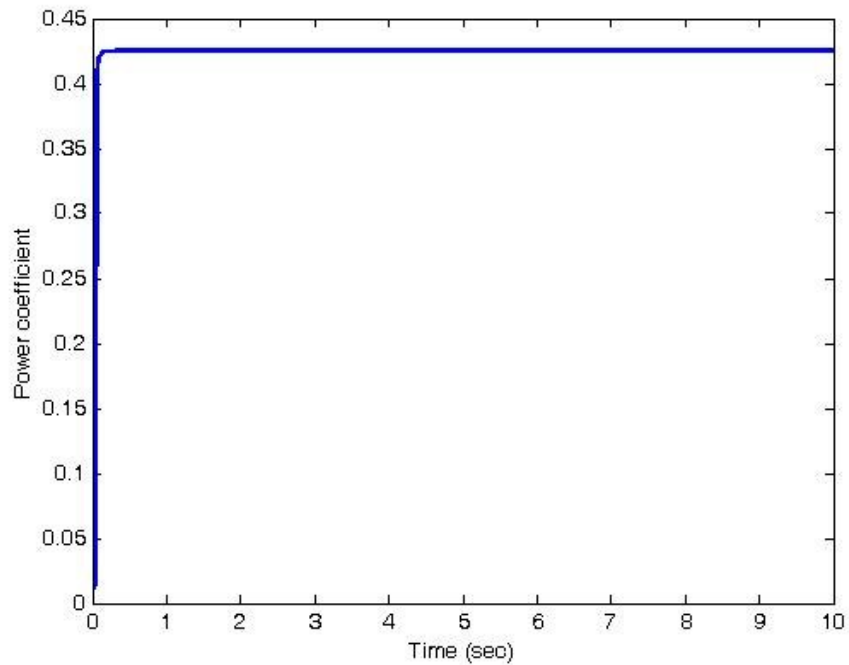
Figure 3.15 Power coefficient under different wind speed

3.6 Summary

The conventional vector control strategy for wind power maximum power point tracking is introduced in this chapter. Since electrical machine three phase ac items are converted into dc items in two dimensional d-q vector, machine torque and flux are hence controlled separately. By setting the d-axis stator current to nil, the full magnetic flux contributed by stator loading current is aligned to the q-axis, hence giving the machine the maximum capability to generate torque.

The PI controller parameters are tuned by the zero-pole cancellation method in order to control the stator d-axis current to nil and the q-axis current to the optimal value, which corresponding to the optimal torque and thus the maximum power. From the simulation result, it has been shown that this control strategy works very well.

Because the PI controllers directly work on the control plant by changing the

71

corresponding current and voltage, any change of system itself will affect the PI controller and it only works on one operation point. Therefore, this conventional PI control strategy has certain limits due to the drawback of narrow control range. But on the other hand, this control method is easy to design and almost suitable for all the control problems. For the presented work, the PI controllers are set to ideal values, and the real power control systems are not able to achieve such wide control range. A set of PI parameters will work together to cover the full range control. So mapping technic based on mechanical sensors and look-up table are essential to control the wind turbine.

In order to expand the control range, one possible approach may be by using the nonlinear control strategy. Different from the PI controllers, nonlinear controller is able to provide full range trajectory tracking. This is due to the inherent methodology and the mathematic transformation of the controller design approach. Moreover, the perturbation observer may also be used for nonlinear control which improves the system robustness. However, this nonlinear controller is more difficult to design and implement. In the next chapter, a feedback linearization controller will be studied first, and then a more sophisticated nonlinear adaptive controller will be designed. The nonlinear control strategy will be studied for the same purpose as conventional control strategy, that to conduct wind turbine maximum power point tracking.

Chapter 4 Nonlinear Control

4.1 Introduction

Nonlinear control strategy focuses on dealing with the nonlinear properties existing in the system. Some nonlinear controllers handle all of the nonlinearities in the system, on the other hand, some only handle part of the nonlinearities in the system. In this chapter, a nonlinear feedback controller and nonlinear adaptive controller for MPPT strategy are introduced. The nonlinear feedback controller design is considered as a quasi-linear control strategy. It is basically using the vector control method and isolating the nonlinear items and eliminating their effect. The nonlinear adaptive control strategy is more robust and is able to handle inaccurate time-varying variables in the system. The details of these two nonlinear control strategies will be introduced. In [17], it introduces the nonlinear feedback control of a permanent magnet synchronous machine. The other nonlinear control strategy is applied to estimate torque disturbance in [18]. The simulation results of conventional PI control and modified nonlinear feedback control, as well as nonlinear adaptive control are compared.

4.2 Nonlinear Feedback Controller

Permanent magnet synchronous generators are highly nonlinear device which are difficult for a single controller to control. The classic method linearizes the system dynamics about one operating point, so the relative control parameter may be effective only at the specific point. A wind turbine system with a permanent magnet synchronous generator constantly accelerating or decelerating, and a gain-scheduled controller, may not guarantee the precise tracking. Hence, nonlinear feedback control is used to provide global trajectory tracking. A side advantage of such a control law is that it is well-suited to self-tuning and adaptive control since it

is model-based [16, 17].

Equations 4.1 and 4.2 describe the electrical dynamics of the machine system which shows nonlinearity since it involves products of state variables. In order to find the linear relations, auxiliary input vector $[v_d \quad v_q]^T$ is introduced to cancel the nonlinearities in the system [18].

$$v_{sd} = \frac{1}{L_d} u_{sd} - \frac{1}{L_d} R_s i_{sd} + \omega_e i_{sq} \frac{L_q}{L_d} \tag{4.1}$$

$$v_{sq} = \frac{1}{L_q} u_{sq} - \frac{1}{L_q} R_s i_{sq} - \frac{L_d}{L_q} \omega_e i_{sd} - \omega_e \frac{1}{L_d} \psi_{PM} \tag{4.2}$$

Substitute equation 4.1 and 4.2 into 4.3 and 4.4 and the new description of the generator system becomes:

$$\frac{di_{sd}}{dt} = v_{sd} \tag{4.3}$$

$$\frac{di_{sq}}{dt} = v_{sq} \tag{4.4}$$

By introducing the auxiliary inputs, the original 4th order nonlinear system has transformed into a 1st order linear system. Linear control laws now can be considered for controller design. However, in order to control wind turbine rotation speed ω_m, control output is still indirect with control input u_q. To derive the relation of control input from output, the output differentiation approach is applied:

$$\frac{di_{sd}}{dt} = (u_{sd} - R_s i_{sd} + \omega_e L_q i_{sq}) \times \frac{1}{L_d} \tag{4.5}$$

$$\frac{di_{sq}}{dt} = (u_{sq} - R_s i_{sq} - \omega_e L_d i_{sd} - \omega_e \psi_{PM}) \times \frac{1}{L_q} \tag{4.6}$$

$$\frac{\omega_m}{dt} = (T_e - T_m - B\omega_m) \times \frac{1}{J} \tag{4.7}$$

$$y = \omega_m \tag{4.8}$$

$$\frac{dy}{dt} = \frac{\omega_m}{dt} \tag{4.9}$$

74

$$\frac{d^2 y}{dt^2} = \frac{1.5 P \psi_{PM}}{L_q J} v_q + f_1 \qquad (4.10)$$

where f_1 contains all nonlinearities in the system that need to be cancelled in the system:

$$f_1 = \frac{3 P \psi_{PM}}{2 L_d J} (i_q R + \omega_m \psi_{PM} + \omega_m i_d L_d) \qquad (4.11)$$

Linear control technique can be used to design a tracking controller for this linear system [16], by choosing the new input v as shown in equation 4.12 and introducing the standard trajectory tracking algorithm shown in equation 4.13 and 4.14:

$$\frac{d^2 y}{dt^2} = v \qquad (4.12)$$

$$v = \frac{d^2 y_d}{dt^2} - k_1 e - k_2 e \qquad (4.13)$$

$$\frac{d^2 e}{dt^2} + k_2 \frac{de}{dt} + k_1 e = 0 \qquad (4.14)$$

where y_d is the reference linear output; e represents the error between real and reference control output, and the two control parameters k_1 and k_2 will be chosen in order to place the poles always at the negative axis in the zero plane, in this case to keep the tracking error e always equal to zero. The scenario can be represented as:

For $e(0) = \dfrac{de(0)}{dt} = 0$, then $e(t) \equiv 0, \forall\ t \geq 0$

4.3 Nonlinear Adaptive Control

Nonlinear adaptive control is a useful tool for analysing systems with uncertainties and/or time varying component. The advantage of this control algorithm is that it sets clearly defined goals: focusing on the known properties of the control plant and

avoiding the unknown items and slow time-varying items. Adaptive control has been most successful for the plant models in which the unknown parameters appear linearly. The systematic theories have been developed for adaptive control of linear systems. The existing adaptive control techniques can also treat important classes of non-linear systems, with measureable states and linearly parameterizable dynamics [30]. Adaptive control of nonlinear plants was analysed for its advance in the differential-geometric theory of non-linear feedback control in the mid 1980s. This control algorithm grew rapidly in the 1990s. In the 2000s, the attempts to apply nonlinear adaptive control to wind power plants have attracted great interests from researchers. This chapter will propose the wind turbine rotational speed control and electrical machine torque control by nonlinear adaptive control strategies to achieve the maximum power point tracking.

4.3.1 Nonlinear Adaptive Control based on Perturbation Observer

In order to apply nonlinear adaptive control, the multi-input multi-output (MIMO) system is converted into interacted subsystems according to input output linearization at first. For each subsystem, a perturbation term is defined which includes all subsystem nonlinearities before linearization. The relation between subsystems and uncertainties is estimated by a perturbation observer. At the end, the estimates of perturbations are used to compensate the real perturbation in order to satisfy an adaptive linearization. Thus the original nonlinear system can be decoupled and controlled.

Input-output Feedback Linearization

A fundamental linearization method is by differentiating the control output until the control input appears. For a single input single output (SISO) system, the procedure is demonstrated as follows:

$$\begin{cases} \dot{x} = f(x) + g(x)u \\ y = h(x) \end{cases} \tag{4.15}$$

where x is the state variables, u is the system control inputs, y is the system output, and f(x) and g(x) are smooth fields of the system, h(x) is a smooth scalar function. By differentiating the output y shows above.

$$\dot{y} = \nabla h(f + gu) = L_f h(x) + L_g h(x)u \tag{4.16}$$

where the Lie derivative is defined as:

$$L_f h = \nabla h f = \frac{\partial h}{\partial x} u \tag{4.17}$$

for $L_g h(x)$ is not equal to zero, the input transform can be derived as:

$$u = \frac{v - L_f h}{L_g h} \tag{4.18}$$

this will lead to a linear relation between input and output,

$$\dot{y} = v \tag{4.19}$$

when $L_g h(x) = 0$ for all x, differentiate equation 4.16 gives:

$$\ddot{y} = L_f^2 h(x) + L_g L_f h(x)u \tag{4.20}$$

when $L_g L_f h(x) = 0$ again, differentiate repeatedly:

$$y^r = L_f^r h(x) + L_g L_f^{r-1} h(x)u \tag{4.21}$$

Until $L_g L_f h(x) \neq 0$, and the times of derivation acquired to obtain this relation is counted by r, also r is called the relative degree of the system. Rewritten equation 4.21, the system input can be represents by:

$$u = \frac{v - L_f^r h}{L_g L_f^{r-1} h} \tag{4.22}$$

Rewritten the nonlinear relations in linear form, it is given by:

$$y^r = v \tag{4.23}$$

The approach above has shown the procedure to linearize the input and output of a SISO nonlinear system. To extend the application of this method, it is better to represent it in a more general way and use it for the MIMO system. Here, we introduce the equation 4.15 again, but give the symbols in it with different meaning:

$$\begin{cases} \dot{x} = f(x) + g(x)u \\ y = h(x) \end{cases} \tag{4.24}$$

For equation 4.24 which is represented a MIMO nonlinear system, the variable x in the above equations is the state variable vector, u is the control input vector, y is the system output vector, and f(x), g(x) and h(x) are smooth vector fields. The linearization approach is the same as SISM by differentiating the output y_i until the control input u_j appears.

If we assume r_i is the smallest integer which, in at least one of the inputs, explicitly appears as $y_i^{(ri)}$, the function can be written as:

$$y_i^{(r_i)} = L_f^{r_i} h_i + \sum_{j=1}^{m} L_{gj} L_f^{r_i-1} h_i u_j \tag{4.25}$$

where $y_i^{(ri)}$ is the ith order derivative of y_i, and $L_{gj} L_f^{r_i-1} h_i(x)$ is not equal to zero for at least one j. Applying the above procedure to each output y_i yields:

$$\begin{bmatrix} y_1^{(r_1)} \\ \vdots \\ y_m^{(r_m)} \end{bmatrix} \begin{bmatrix} L_f^{r_i} h_i \\ \vdots \\ L_f^{r_m} h_m \end{bmatrix} \begin{bmatrix} u_1 \\ \vdots \\ u_m \end{bmatrix} \tag{4.26}$$

$$B(x) = \begin{bmatrix} L_{g1} L_f^{r_1-1} h_1 \cdots & h_1 \\ \vdots & \vdots & \vdots \\ L_{g1} L_f^{r_m-1} h_m \cdots & h_m \end{bmatrix} \tag{4.27}$$

where B(x) is a m × m control gain matrix. If B(x) is invertible, the feedback linearization control of the MIMO nonlinear system can be obtained as:

$$u = B(x)^{-1} \left\{ \begin{bmatrix} -L_f^{r_1} h_1 \\ \vdots \\ -L_f^{r_m} h_m \end{bmatrix} \begin{bmatrix} v_1 \\ \vdots \\ v_m \end{bmatrix} \right\} \tag{4.28}$$

where v_i is the new inputs of the system, and the new relation of input-output is given by:

$$y_i^{(r_i)} = v_i \tag{4.29}$$

At this point, the required dynamics can be imposed on the system by the new system inputs.

Perturbation Observer

The design of perturbation observer is an important step for nonlinear adaptive control. These observers are used to estimate the behaviour of system perturbations and feed it to the nonlinear controller. The usage of observers gives the nonlinear controller higher robustness since it does not rely on the actual machine perturbations [16]. The procedure below shows how to use the high gain method to design the perturbation observer.

Assuming all the nonlinearities in equation 4.26 of the MIMO system are unknown, and define the perturbation terms as:

$$\begin{bmatrix} \psi_1 \\ \vdots \\ \psi_m \end{bmatrix} \begin{bmatrix} L_f^{r_1} h_1 \\ \vdots \\ L_f^{r_m} h_m \end{bmatrix} \qquad \begin{bmatrix} u_1 \\ \vdots \\ u_m \end{bmatrix} \tag{4.30}$$

where ψ_i is the perturbation term, and $B_0 = B(x)|_{x=x(0)}$ is the nominal control gain.

then the system shown is 4.26 can be written by:

$$\begin{bmatrix} y_1^{(r_1)} \\ \vdots \\ y_m^{(r_m)} \end{bmatrix} \begin{bmatrix} \psi_1(x) \\ \vdots \\ \psi_m(x) \end{bmatrix} \qquad \begin{bmatrix} u_1 \\ \vdots \\ u_m \end{bmatrix} \tag{4.31}$$

79

Defining state variables as

$$z_{i1} = y_i$$
$$\vdots$$
$$z_{i(r_i+1)} = y_i^{(ri)}$$

(4.32)

and define a virtual state to represent the perturbation:

$$z_{i(r_i+1)} = \psi_i$$

(4.33)

then the ith subsystem is given:

$$\begin{cases} \dot{z}_{i1} = z_{i2} \\ \vdots \\ \dot{z}_{ir_i} = z_{i(r_i+1)} + B_{0_i}u \\ \dot{z}_{i(r_i+1)} = \dot{\psi}_i \end{cases}$$

(4.34)

where B_{0i} is the ith row of B_0.

When all the states are available, the perturbation is estimated by a second-order perturbation observer which uses the last state $z_{i(ri-1)}$ as measurement. A state and perturbation observer will be designed to obtain the states and perturbation together when only one system state $z_{i1}=y_i$ is available.

When all system states are available and the last state $z_{i(ri)}$ is taken as a measurement, a PO is designed as

$$\begin{cases} \dot{\hat{z}}_{ir_i} = \hat{z}_{i1} + h_{i1}(z_{i1} - \hat{z}_{ir_i}) + B_{0i}u \\ \dot{\hat{z}}_{i(r_i+1)} = h_{i2}(z_{ir_i} - \hat{z}_{ir_i}) \end{cases}$$

(4.35)

where h_{i1} and h_{i2} are gains of the high gain observer. The hat symbol represents estimation of the corresponding term.

By choosing

$$\begin{cases} h_{i1} = \dfrac{\alpha_{i1}}{\varepsilon_i} \\[2mm] h_{i2} = \dfrac{\alpha_{i2}}{\varepsilon_i} \end{cases} \tag{4.36}$$

where ε_i is a positive constant between 0 and 1.

The other positive constant α_{ij} are chosen by allocating the roots of equation 4.37 to the left-half of complex plain.

$$s^2 + \alpha_{i1}s + \alpha_{i2} = 0 \tag{4.37}$$

When only the system output $y_i = z_{i1}$ is available, a (r_i+1)th-order state and perturbation observer can be designed to estimate the system states and perturbation as:

$$\begin{cases} \dot{\hat{z}}_{i1} = \hat{z}_{i2} + h_{i1}(z_{i1} - \hat{z}_{i1}) \\[2mm] \cdots \\[2mm] \dot{\hat{z}}_{ir_i} = \hat{z}_{ir_i} + h_{ir_i}(z_{i1} - \hat{z}_{i1}) + B_{0i}u \\[2mm] \dot{\hat{z}}_{i(r_i+1)} = h_{i(r_i+1)}(z_{i1} - \hat{z}_{i1}) \end{cases} \tag{4.38}$$

where $h_{ij} = \dfrac{\alpha_{ij}}{\varepsilon_i}$, $j = 1, 2, \cdots$ are gains of the high gain observer

ε_i is a positive constant between 0 and 1. The other positive constants α_{ij}, $j = 1, 2, \cdots$ are chosen by allocating the roots of equation 4.39 to the left-half of the complex plane.

$$s^{r_i+1} + \alpha_{i1}s^{ri} + \cdots \qquad \cdot \alpha_{i(r_i+1)} = 0 \tag{4.39}$$

By using the estimate of perturbation $\hat{\Psi}_i = z_{i(r_i+1)}$ to compensate the real system perturbation, the control law of the nonlinear adaptive control can be obtained as

$$u = B_0^{-1} \left\{ \begin{bmatrix} -\hat{\Psi}_1 \\ \vdots \\ -\hat{\Psi}_m \end{bmatrix} \begin{bmatrix} v_1 \\ \vdots \\ v_m \end{bmatrix} \right\} \tag{4.40}$$

where $v_i = -k_i z_i$ is the state feedback control of the ith linear system when a

perturbation observer (PO) is designed, or an output feedback $v_i = -k_i \hat{z}_i$ when a

state and perturbation observer (SPO) is designed. The

parameters $K_i = [k_{i1}, \cdots \quad {}^r$ are the linear feedback controller gains which can be

determined via linear system method.

This part introduces the design of nonlinear adaptive controller. A good explanation of the term 'adaptive' is perhaps by using the perturbation observer. In general, there are two steps to handle a MIMO system.

The first step is to linearize the MIMO system by equation 4.24-4.29. Then after the system is linearized, there will be two situations, one is when all the states are available and the other is when only one system state $z_{i1}=y_i$ is available. For the first situation, the standard approach to design perturbation observer (PO) is used from equation 4.35-4.37, and for the second situation, the standard approach to design states and perturbation observer (SPO) is used which can be done by equation 4.38-4.39. Basically, these POs or SPSs are the estimated system nonlinearities.

The second step is that after the system is linearized, the conventional linear system control method can be used by applying the linear feedback controller explained by equation 4.40. The equations given above represent the general form of the NAC design approach which may not clear. In the next section, this design approach is applied for a two input and two output wind turbine system MPPT control.

4.3.2 Controller Design

Maximum power point tracking is achieved by controlling either wind turbine rotational

speed or electrical machine torque. Both of the control algorithms are demonstrated in this section. The control strategy is carried out by nonlinear adaptive controller.

Wind turbine rotational speed control

For nonlinear adaptive controller design, system is linearized first by using the similar approach introduced in the nonlinear feedback control section. The wind turbine system state space model can be derived from system states equation 4.5-4.7and represented by the following expression:

$$\dot{x} = f(x) + g_1(x)u_1 + g_2(x)u_2 \qquad (4.41)$$

where

$$x = [i_d \quad i_q \quad w_m]^T \qquad (4.42)$$

$$f(x) = \begin{bmatrix} -\dfrac{R_s}{L_d} i_d + \dfrac{w_e L_q}{L_d} i_q \\[2mm] -\dfrac{R_s}{L_q} i_q - \dfrac{1}{L_q} w_e \left(L_d i_d + \psi_{PM} \right) \\[2mm] \dfrac{1}{J} \left(T_m + T_e \right) \end{bmatrix}, \qquad (4.43)$$

$$\begin{cases} g_1(x) = \left[\dfrac{1}{L_d} \quad 0 \quad 0 \right]^T \\[4mm] g_2(x) = \left[0 \quad \dfrac{1}{L_q} \quad 0 \right]^T \end{cases} \qquad (4.44)$$

$$\begin{cases} u_1 = V_d \\ u_2 = V_q \end{cases} \qquad (4.45)$$

This system is regarded as a two-input and two-output nonlinear system which can be linearized by differentiating the system output as introduced by equation 4.25-4.27 .

$$y_1 = i_d \qquad (4.46)$$

$$y_2 = w_m \qquad (4.47)$$

by differentiation , it yields:

$$\dot{y}_1 = L_f h_1 + \left(L_{g1} h_1 \right) u_1 + \left(L_{g2} h_1 \right) u_2 \qquad (4.48)$$

which is equivalent to:

$$\dot{y}_1 = -\frac{R_s}{L_d} i_d + \frac{w_e L_q}{L_d} i_q + \frac{1}{L_d} u_1 \qquad (4.49)$$

83

since the control variable v_q is not appeared, we try the second derivative:

$$\ddot{y}_2 = L_f\left(L_f h_2\right) + L_{g1}(L_f h_2)u_1 + L_{g2}\left(L_f h_2\right)u_2 \tag{4.50}$$

$$\ddot{y}_2 = \frac{p\psi_{PM}}{JL_q}V_q + \frac{1}{J}\frac{dT_m}{dt} - \frac{p\psi_{PM}}{J}(\frac{i_q R_s}{L_q} + w_e i_d + \frac{w_e \psi_{PM}}{L_q}) \tag{4.51}$$

Using the equations derived , the system can be described in the matrix form:

$$\begin{pmatrix} \dot{y}_1 \\ \ddot{y}_2 \end{pmatrix} = \begin{pmatrix} m_1(x) \\ m_2(x) \end{pmatrix} + \begin{pmatrix} \dfrac{1}{L_d} & 0 \\ 0 & \dfrac{p\psi_{PM}}{JL_q} \end{pmatrix}\begin{pmatrix} u_1 \\ u_2 \end{pmatrix} \tag{4.52}$$

or

$$\begin{pmatrix} \dot{y}_1 \\ \ddot{y}_2 \end{pmatrix} = M(x) + B(x)\begin{pmatrix} u_1 \\ u_2 \end{pmatrix} \tag{4.53}$$

where

$$m_1(x) = \frac{1}{L_d}(-i_d R_s + w_e L_q i_q) \tag{4.54}$$

$$m_2(x) = -\frac{p\psi_{PM}}{J}(\frac{i_q R_s}{L_q} + w_e i_d + \frac{w_e \psi_{PM}}{L_q}) + \frac{1}{J}\frac{dT_m}{dt} \tag{4.55}$$

$$B(x) = \begin{pmatrix} \dfrac{1}{L_d} & 0 \\ 0 & \dfrac{p\psi_{PM}}{JL_q} \end{pmatrix} \tag{4.56}$$

Since B(x) is a non-singular matrix, the control law is defined as:

$$\begin{pmatrix} u_1 \\ u_2 \end{pmatrix} = B(x)^{-1}\left(-M(x) + \begin{pmatrix} v_1 \\ v_2 \end{pmatrix}\right) \tag{4.57}$$

where

$$\begin{pmatrix} \dot{y}_1 \\ \ddot{y}_2 \end{pmatrix} = \begin{pmatrix} v_1 \\ v_2 \end{pmatrix}$$

By introducing the reference output $\dot{y}_{1r}$ and $\dot{y}_{2r}$, and define the error between real and reference value, the system control law is written as:

$$\begin{cases} \dot{e}_1 + k_1 e_1 = 0 \\ \ddot{e}_2 + k_2\,\dot{e}_2 + k_3 e_2 = 0 \end{cases} \tag{4.58}$$

where

$$\begin{cases} e_1 = y_{1r} - y_1 \\ e_2 = y_{2r} - y_2 \end{cases}$$

Since the system is linearized, the perturbations ψ_1 and ψ_2 and constant control gains B_{01} and B_{02} for two subsystems q_1 and q_2 are defined according to equations 4.30-4.31 and 4.54-4.56:

$$q_1 : \begin{cases} \psi_1(x) = m_1(x) + (B_{01}(x) - B_{01}) \begin{bmatrix} u_1 \\ u_2 \end{bmatrix} \\ B_{01} = [-\dfrac{1}{L_d} \quad 0] \end{cases} \tag{4.59}$$

$$q_2 : \begin{cases} \psi_2(x) = m_2(x) + (B_{02}(x) - B_{02}) \begin{bmatrix} u_1 \\ u_2 \end{bmatrix} \\ B_{02} = [0 \quad -\dfrac{3p\psi_{PM}}{2JL_q}] \end{cases} \tag{4.60}$$

Defining the state vectors as:

$z_{11} = y_1 = i_d$, $z_{12} = \psi_1$, $z_{21} = y_2 = w_m$, $z_{22} = y_2^{(1)}$, $z_{23} = \psi_2$, $u_1 = v_d$ and $u_2 = v_q$

then the system dynamic equation can be given by:

$$q_1 : \begin{cases} z_{11} = y_1 \\ \dot{z}_{11} = \psi_1(x) + B_{01} \begin{bmatrix} u_1 \\ u_2 \end{bmatrix} \end{cases}$$

$$q_2 : \begin{cases} z_{21} = y_2 \\ \dot{z}_{21} = z_{22} \\ \dot{z}_{22} = \psi_2(x) + B_{02} \begin{bmatrix} u_1 \\ u_2 \end{bmatrix} \end{cases}$$

The second order perturbation observer (PO) is derived to estimate the subsystem q_1 perturbation which is given by:

$$\begin{cases} \dot{\hat{z}}_{11} = \hat{z}_{12} + h_{11}(z_{11} - \hat{z}_{11}) + B_{10}u_2 \\ \dot{\hat{z}}_{12} = h_{12}(z_{11} - \hat{z}_{11}) \end{cases} \tag{4.61}$$

where h_{11} and h_{12} are gains which equal to:

$$\begin{cases} h_{11} = \dfrac{\alpha_{11}}{\varepsilon_1} \\[3mm] h_{12} = \dfrac{\alpha_{12}}{\varepsilon_1^{\,2}} \end{cases} \tag{4.62}$$

q_2 states and perturbation observer (SPO) are estimated by a third order observer, which is given as,

$$\begin{cases} \dot{\hat{z}}_{21} = \hat{z}_{22} + h_{21}(z_{21} - \hat{z}_{21}) \\[3mm] \dot{\hat{z}}_{22} = \hat{z}_{23} + h_{22}(z_{21} - \hat{z}_{21}) + B_{20}u_1 \\[3mm] \dot{\hat{z}}_{23} = h_{23}(z_{21} - \hat{z}_{21}) \end{cases} \tag{4.63}$$

and

$$h_{21} = \dfrac{\alpha_{21}}{\varepsilon_2}, \quad h_{22} = \dfrac{\alpha_{22}}{\varepsilon_2^{\,2}}, \quad h_{23} = \dfrac{\alpha_{23}}{\varepsilon_2^{\,3}}$$

Since all the perturbations are estimated, the subsystems q_1 and q_2 are controlled by feedback loop control

$$q_1 : u_2 = \frac{1}{B_{10}}(-k_1(\hat{z}_{11} - z_{11r}) - (\hat{z}_{12} - \dot{y}_{1r})) \tag{4.64}$$

$$q_2 : u_1 = \frac{1}{B_{20}}(-k_3(\hat{z}_{21} - z_{21r}) - k_2(\dot{\hat{z}}_{21} - \dot{z}_{21r})) - (\hat{z}_{23} - \ddot{y}_{2r}) \tag{4.65}$$

The NAC control parameters are

$$q_1 = \begin{cases} \alpha_{11} = 5.2 \times 10^2 \\ \alpha_{12} = 2.7 \times 10^5 \\ \varepsilon_1 = 0.01 \\ k_{11} = 1.6 \times 10^3 \end{cases}$$

$$q_2 = \begin{cases} \alpha_{21} = 2.7 \times 10^3 \\ \alpha_{22} = 2.43 \times 10^6 \\ \alpha_{23} = 7.29 \times 10^8 \\ \varepsilon_2 = 0.01 \\ k_{21} = 8.5 \times 10^2 \\ k_{22} = 3 \times 10^5 \end{cases}$$

4.4 Simulation Results

The simulation of the wind turbine MPPT control strategies is taken under the assumptions: the input wind speed follows the step change which usually is not realistic but critical to test the controllers; the wind turbine pitch angle is fixed at the maximum angle, and quantitatively reflected by setting wind turbine coefficient c6 to a small value which is 1e-4; the wind turbine drive train is simplified by one mass model; the power generated by this system are all absorbed; The constraints shown above which the real wind turbine system may be encountered are simplified or ignored. The simulation solely is to validate the feedback linearization and nonlinear adaptive control strategies to conduct wind turbine maximum power point tracking control. The control parameters are set to ideal values and the effect of power electronics including harmonics and power rating are not considered.

The dynamic models of wind turbines were put into simulation software. In this section, the corresponding nonlinear controllers were applied to a 1KW PMSG based wind turbine. Parameters of this wind turbine are included in Table 4.1. The modelling of this system was carried out by a very common simulation package Matlab/Simulink. For computation of nonlinear items, Runge-Kutta (RK) method was chosen to solve the differential equations.

Parameters	Value
Generator resistance, Rs (ohm)	0.035
Initial angle, θ_o (radians)	0
PMSG d-axis inductance, L_d (H)	0.0035
PMSG q-axis inductance, L_q (H)	0.0035
PMSG flux linkage, ψ_{pm} (T)	0.0533
Pole pairs, p	9
Drive train inertia constant, J	0.006
Wind turbine radius, r (m)	1.2
c1-c6 coefficients	0.52;116;0.4;5;21;1e-4
Air density, ρ (kg/m^3)	1.225

Table 4.1 Parameters of 1KW PMSG wind turbine[35]

87

4.4.1 Nonlinear Feedback Control

The simulation for nonlinear feedback control was taken under three different speeds, 4 m/s,6 m/s, and 8 m/s as shown in Figure 4.1. Wind speed experienced two step changes at 2 seconds and 4 seconds, respectively. Power in the wind at three different wind speeds was 600, 1500, and 2700 watts, respectively as seen in Figure 4.2. The d-q axis voltage is shown in Figures 4.3 and 4.4. Since turbine speed is controlled by nonlinear feedback controller, q-axis input current is no longer specified and d-axis current is controlled to zero, as seen in Figure 4.5. The actual turbine speed varies as the reference speed under the effect of controllers, as shown in Figure 4.6. Real and reactive power generated by this wind turbine is shown in Figures 4.7 and 4.8, which shows that this turbine would be able to generate the maximum power if we do not consider the mechanical overloading. Maximum power coefficient is kept at 0.42 under different wind speeds as shown in Figure 4.9.
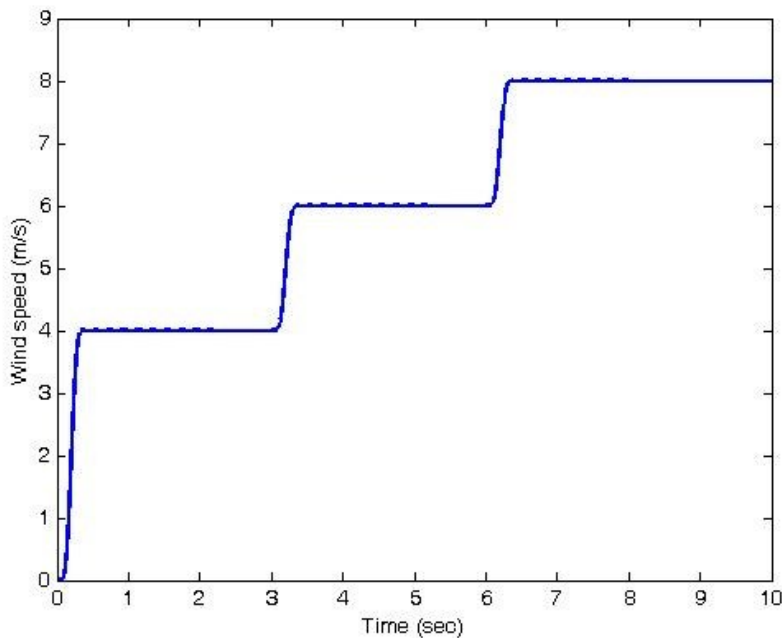
Figure 4.1 Input wind speed for modelling
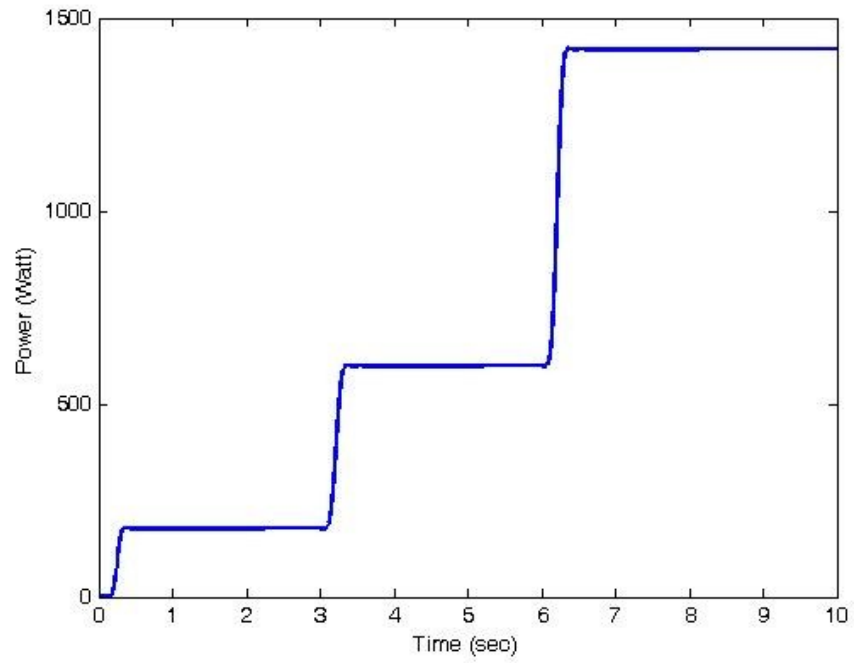
Figure 4.2 Power in the wind
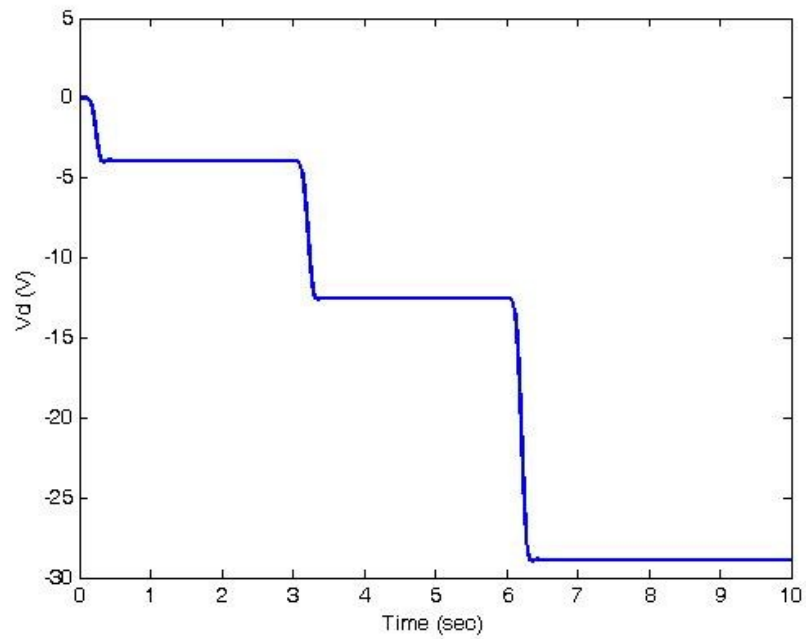
Figure 4.3 d-axis control output voltage
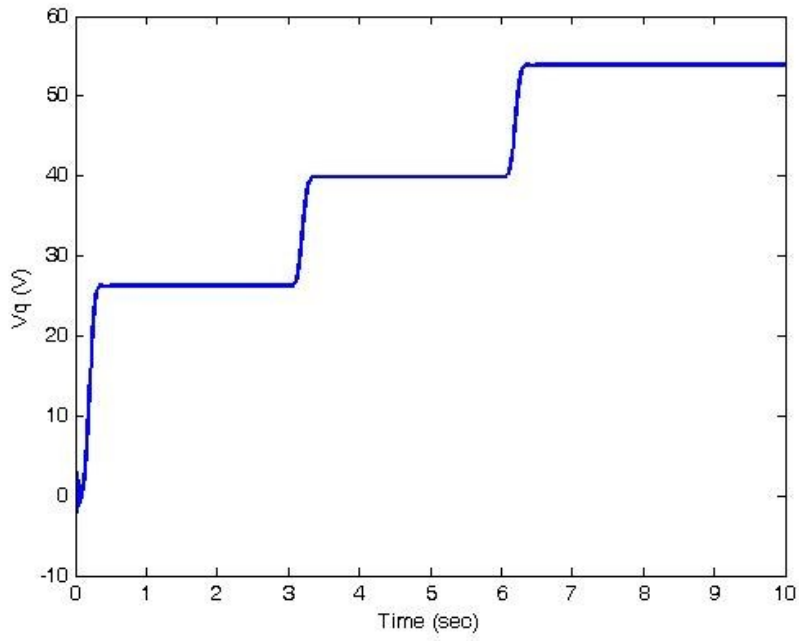
Figure 4.4 q-axis control output voltage
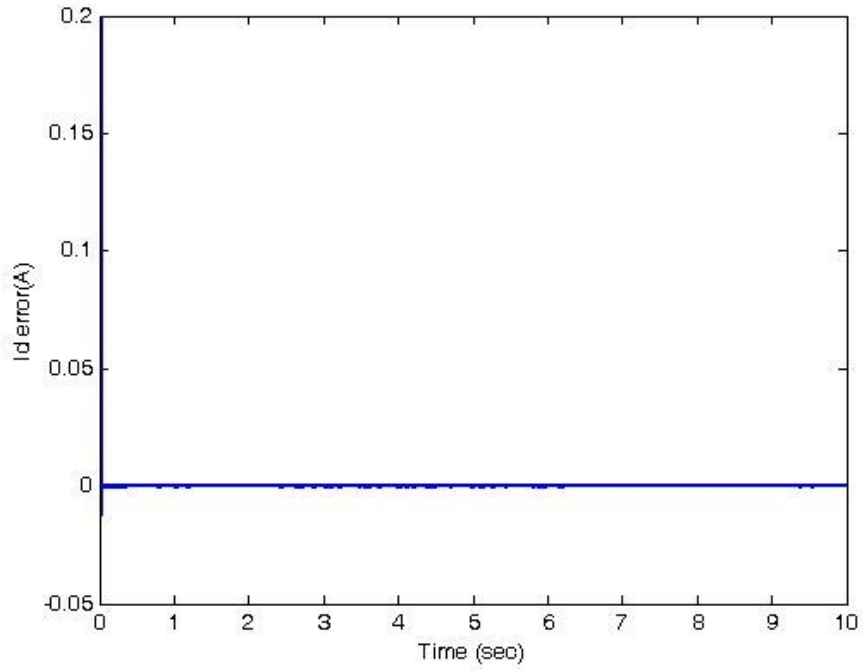
Figure 4.5 d-axis control input current

90
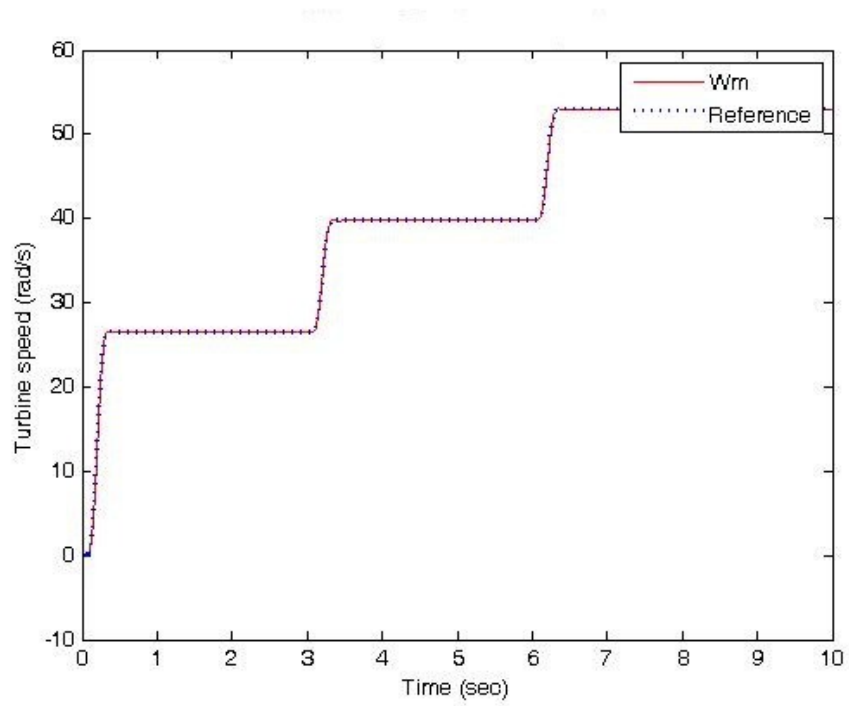
Figure 4.6 Reference and real wind turbine rotational speed
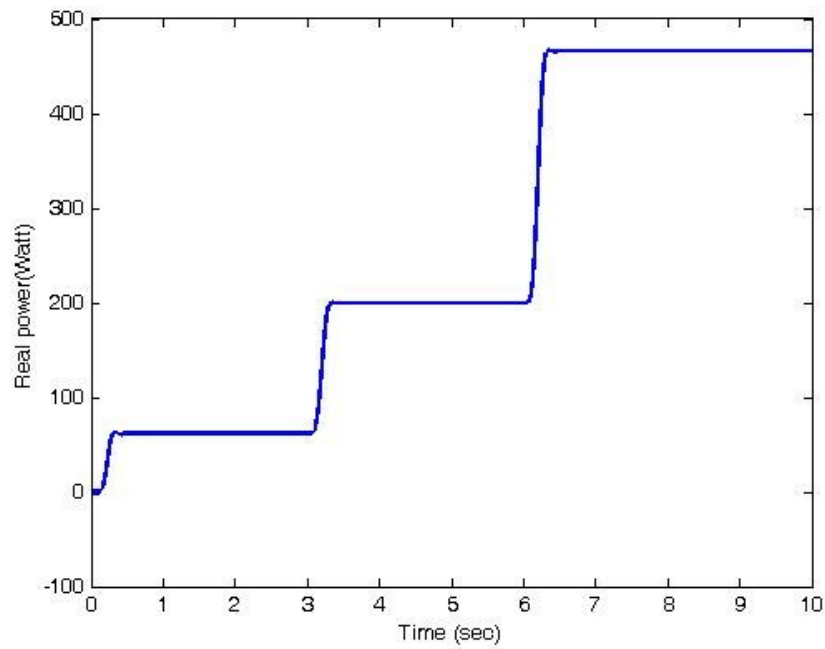
Figure 4.7 Wind turbine real power under MPPT control
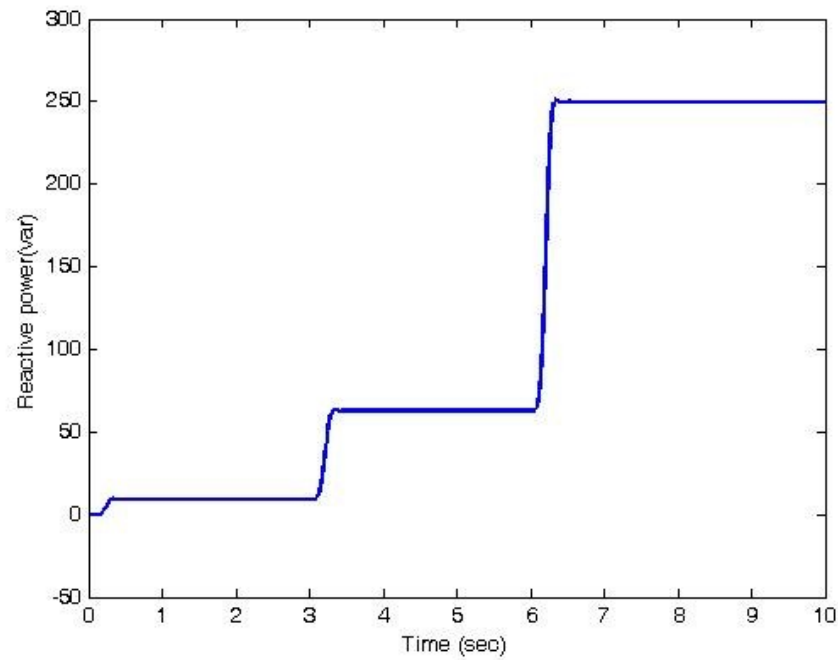
Figure 4.8 Wind turbine reactive power under MPPT control
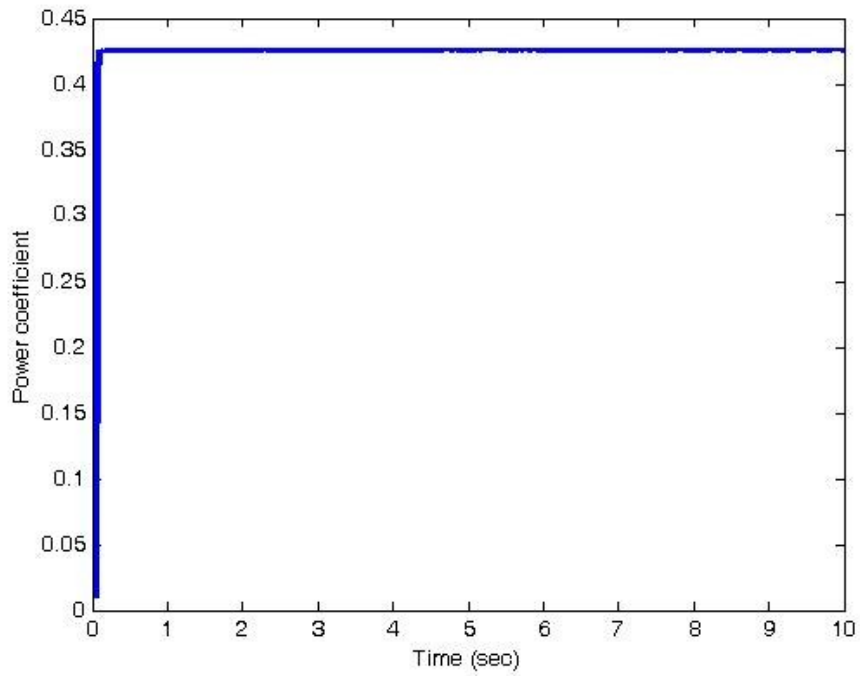
Figure 4.9 Wind turbine power coefficient under different wind speeds

4.4.2 Nonlinear Adaptive Control

The simulation for nonlinear adaptive control is taken under both step change wind speed and random wind speed. A step change from 10 m/s to 12 m/s is shown in Figure 4.10. Figure 4.11 depicts that the actual wind turbine rotational speed follows the reference speed, which indicates that the proposed controller is effective. The perturbation observer and estimated reference perturbation observer are compared in Figure 4.12, which shows that the perturbations also follow the estimation changes. In Figure 4.13, state and perturbation observers also follow the estimated observer changes. Figure 4.14 shows that, during the wind speed changes, the power coefficient had a very short responding time and kept at maximum power coefficient value.

The wind turbine performance under random wind speed change is shown in Figure 4.15 and Figure 4.16. The results show that a nonlinear adaptive controller would control the wind turbine very well, as in the wind step change. Wind turbine rotational speed, perturbation observer and state perturbation observer all follow the references. In Figure 4.17, power coefficient is kept at maximum power and fluctuates at very small range.
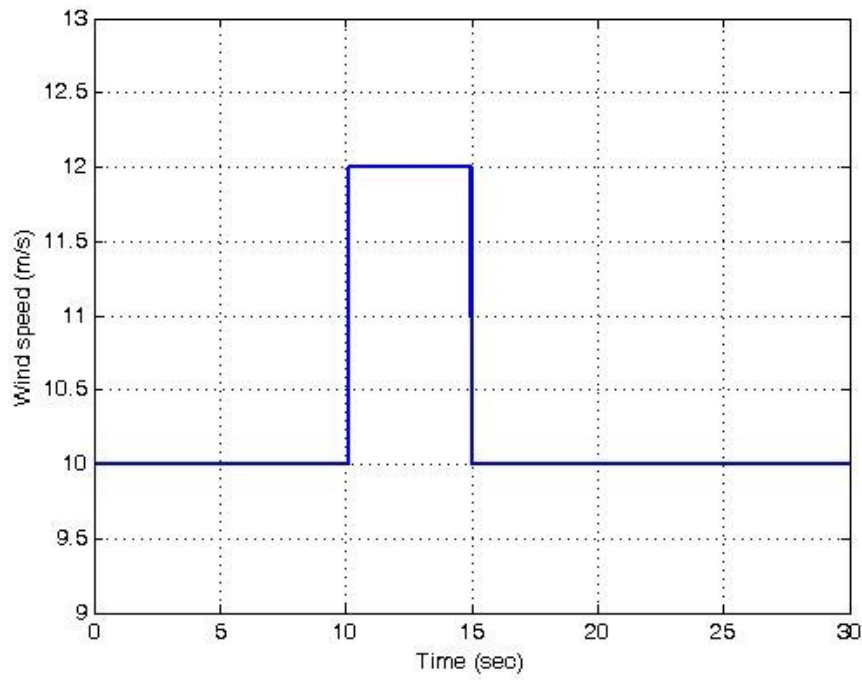
Figure 4.10 Input wind speed
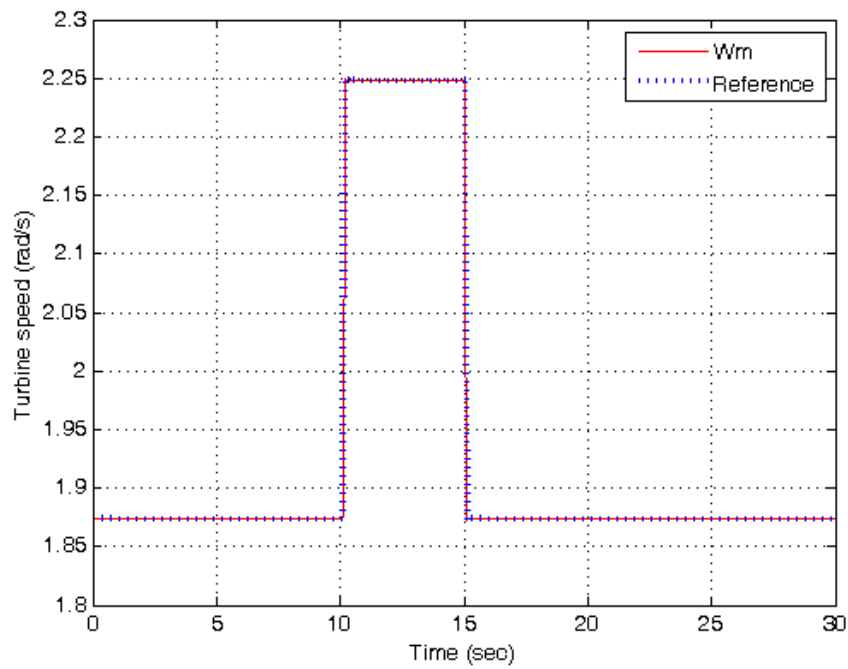
Figure 4.11 Wind turbine speed against reference
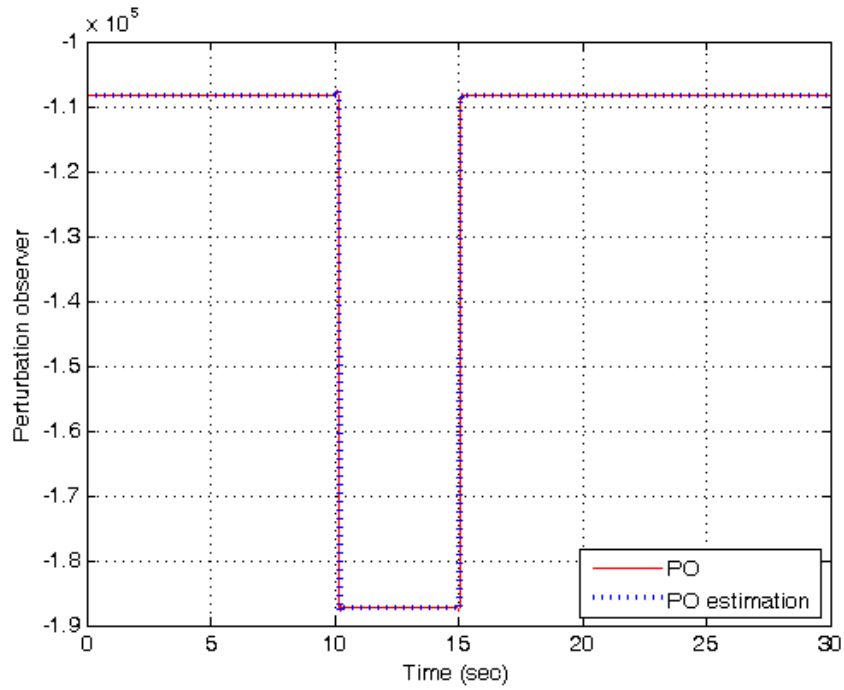
Figure 4.12 Perturbation observer against estimation
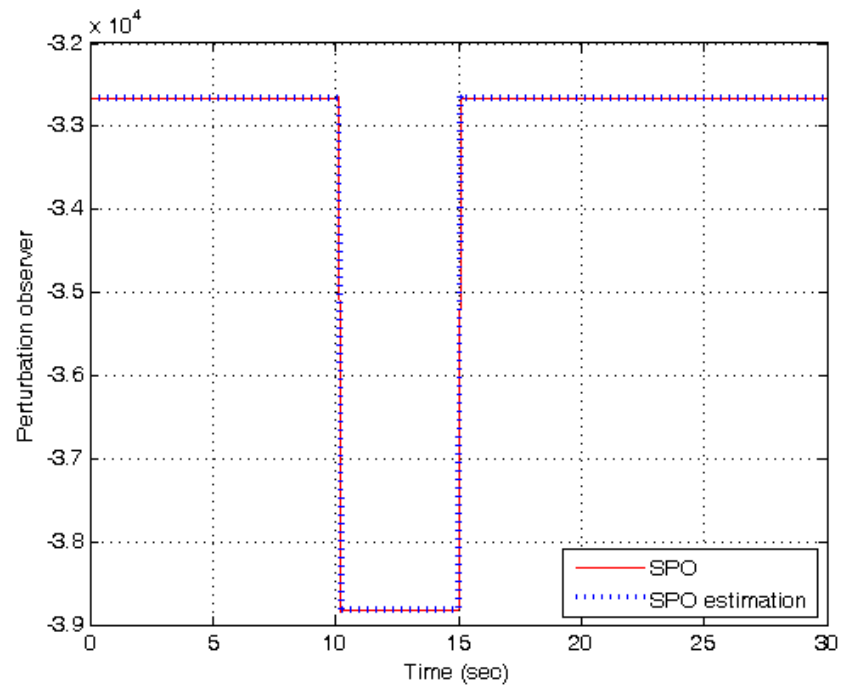
Figure 4.13 State and perturbation observer against estimation
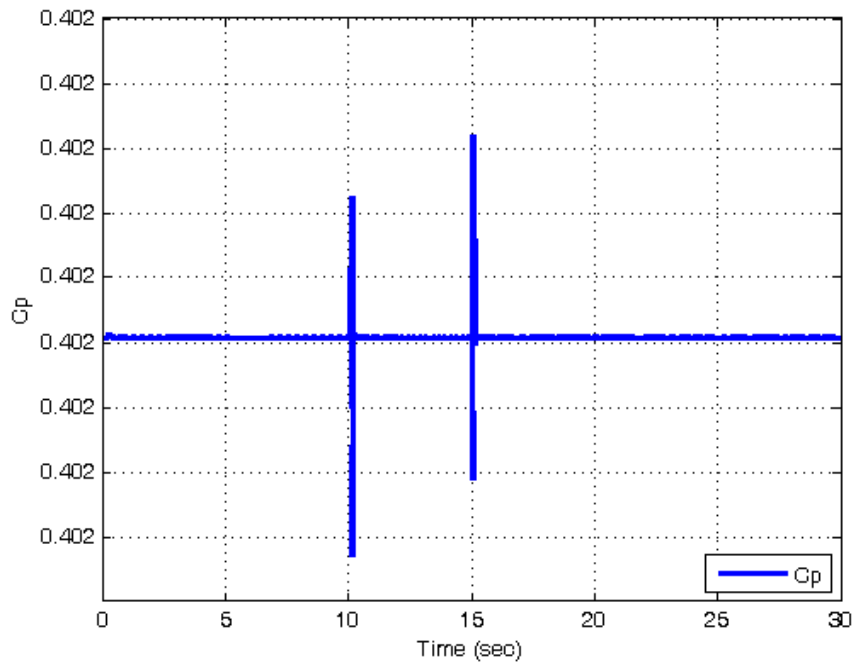
Figure 4.14 Power coefficient
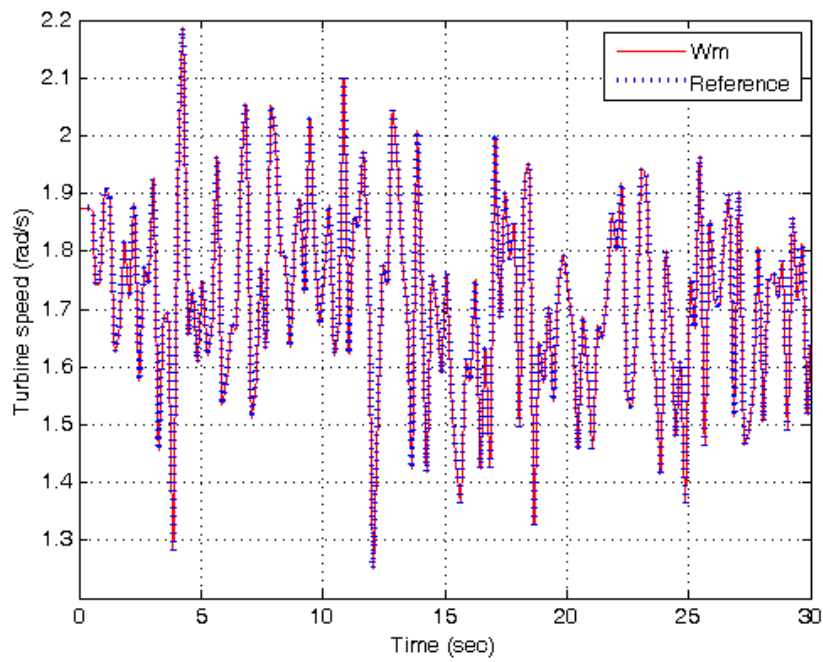
Figure 4.15 Wind turbine speed against reference

96
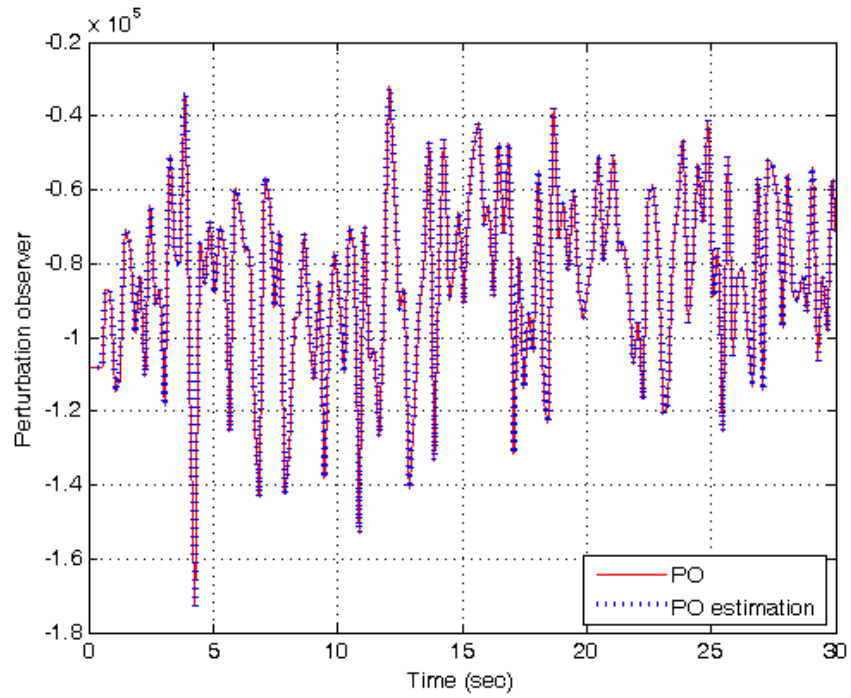
Figure 4.16 Perturbation observer against estimation
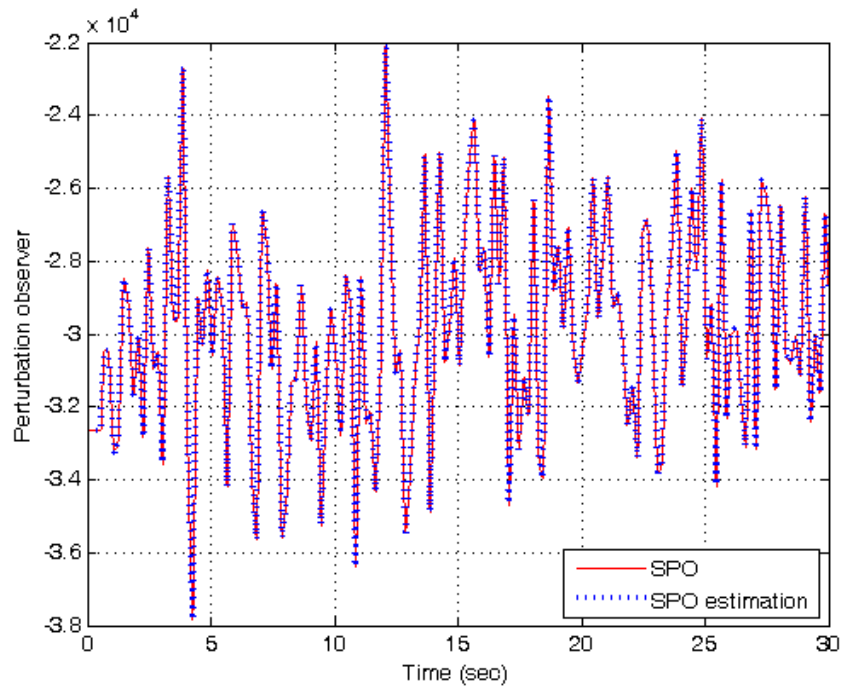
Figure 4.17 State and perturbation against estimation

97
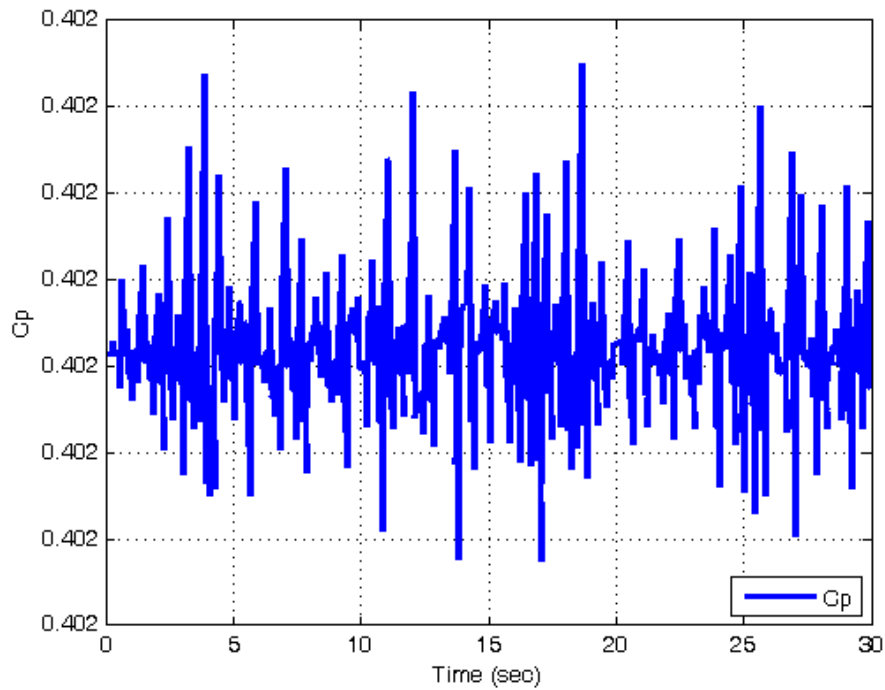
Figure 4.18 Power coefficient

4.5 Summary

Two nonlinear controllers for wind turbine MPPT were introduced in this chapter. The nonlinear feedback control cancels out the system nonlinear perturbations and uses linear control method to design the controllers. Nonlinear adaptive controller uses observers to adapt the varying and uncertain parameters that improve the system robustness. The results show that both nonlinear feedback and adaptive control could handle the nonlinear problem very well.

Different from the conventional controller that directly works on the control plant by modifying the current and voltage, nonlinear controller includes more mathematical transformation and it is able to predict the system disturbance based on the existing system status. The addition of these applied mathematics problems makes the nonlinear controller more sophisticated and robustness to handle the outside disturbance that this system may meet during operation. Nevertheless, it is hard to judge which control strategy is better than the other, both conventional controller and

nonlinear controller has advantages and its drawbacks. The study in the chapter just gives some try to the other possible control strategies for wind turbine MPPT.

Although using the comprehensive nonlinear controller to handle the system nonlinearities of wind turbines shows good results, this nonlinear control method is difficult to apply in the real wind turbine system. The conventional PI controller has higher simplicity and is more convenient to embed into a microcontroller. It is true that the PI controller only controls the objective at one operation point, but industries believe it is more reliable. Therefore, in the real case, a set of operation points and the corresponding control parameters were prepared in advance, and the sensed operation conditions was compared with this pre-evaluated conditions. They are used to control wind turbines by parameters mapping.

Chapter 5 Magnetic Equivalent Circuit Modelling of a Permanent Magnet Synchronous Machine

5.1 Introduction

The last two chapters have introduced the wind turbine MPPT control by regulating the speed of a PMSG. However, no matter using conventional or nonlinear control strategy, they are both only effect on the linear region of electrical generator power speed range. Under some conditions such as stator winding isolation break down, power electric fault, and sudden high wind speed, the electrical generator may subject to magnetic saturation. When the magnetic saturation happens, the flux linkage will change and thus further affect the other machine operating characteristics, i.e. inductance, torque, speed. Since these parameters change, the designed controller may not be able to continually control the electrical machine. Therefore, a model that is able to work out these parameters will be helpful and support the controllers continually control the electrical machine. One possible approach to build such model is by using magnetic equivalent circuit method.

Magnetic equivalent circuit (MEC) is a useful tool in electrical machine analysis. A significant advantage of MEC analysis is that it requires less computational time with relatively high degree of accuracy. The MEC model can be solved by electric circuit nodal analysis method or by classical direct nonlinear iterative method. The magnetic flux solved by MEC is verified by finite element method (FEM) analysis. The result

shows that this MEC model has reasonable accuracy with much less computational time.

Permanent magnet synchronous machines (PMSM) have advantages in robustness and high power density. It has become very popular in renewable energy industry. In wind power industry, seven mega-watt PMSM wind turbine has been successfully installed and there is still a trend in developing higher power ratings. In hybrid and electric vehicle industry, nearly all their products use PMSM as traction machine.

Finite element method (FEM) is a sophisticated approach in electrical machine design and analysis. It is powerful and provides high degree of accuracy in predicting electrical machine performance. The drawback of using FEM is the long computational time. Magnetic equivalent circuit (MEC) is another useful tool in electrical machine design and analysis. It has prominent attribute of fast computation time compared to FEM [25]. However, MEC approach does not give as high an accuracy as FEM [29]. Improving the accuracy of MEC has attracted great interests as can be seen from the research literatures. In electrical machines, air-gap is a very sensitive area since it stores the most of magnetic energy and the MEC here interconnects machine rotor and stator. Therefore the degree of detail in modelling of flux flow in the air-gap determines the accuracy of the entire MEC model. An MEC model of a fractional-slot interior permanent magnet machine using progressive air-gap modelling is described in [28]. In [26], the cross-coupling saturation effects are considered in MEC modelling for an interior permanent magnet synchronous machine (IPMSM) with three layers of flux barriers in the rotor. A surface mounted PMSM MEC model having a variety of flux leakages is given in [27]. In [42], an MEC model for mutually coupled switch-reluctance machine is introduced. In [43], a comparison of mesh- and nodal- based methods is presented in terms of computational speed and accuracy.

This chapter proposes an MEC model of an interior permanent magnetic

synchronous machine with double layer stator winding. The general approach for MEC modelling is given in section 5.2. Section 5.3 describes the direct non-linear iterative approach and the electric circuit nodal analysis approach which can be used to solve the MEC. In section 5.4, flux computed by MEC and FEM are compared.
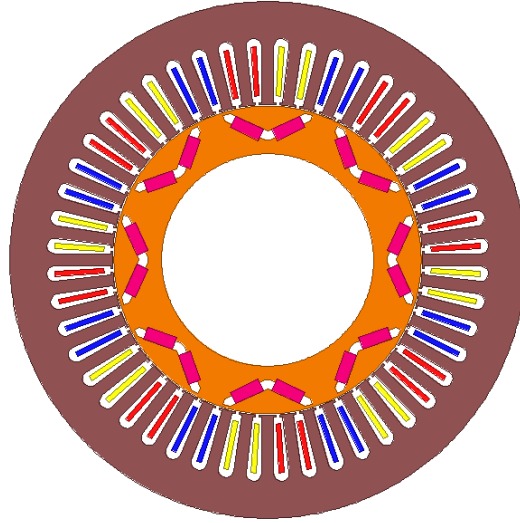
Figure 5.1 Layout of permanent magnet synchronous generator

5.2 Magnetic Equivalent Circuit

Magnetic equivalent circuit contains two parts, an equivalent passive permeance and an active source. Flux flow can be computed by analyzing and solving the MEC. The fundamental equation to calculate flux is in equation 5.1.

$$\varphi = G * F \tag{5.1}$$

where φ is the magnetic flux, G is the permeance, and F is the magneto-motive force (MMF).

Permeance, in general, represents the capacity of a certain amount of material to allow flux flow through it. It is determined by geometrical size and material permeability. In electromagnetic devices, permeance is usually regarded as a permeance tube, as it is more intuitive and easy to calculate. The permeance of a

permeance tube is defined by:

$$G = \frac{\mu A}{L} \tag{5.2}$$

where μ is permeability of the material, A is the area perpendicular to flux lines, L is the length of the path that flux will pass. The common shapes of permeance tubes that appear in electromagnetic devices are shown in Figure 5.2, which also provides their respective permeance equations.

Sometimes for convenience in analysis, the inverse of permeance is used, which is called reluctance. The property of reluctance is thus opposite to that of permeance and is given by,

$$R = \frac{L}{\mu A} \tag{5.3}$$

Magnetic flux flow is represented by flux lines. Though flux line does not exist in real world, it intuitively depicts the direction of flux flow; at the same time density of flux lines is used to represent magnetic field strength. To develop the magnetic equivalent circuit of an electromagnetic device, a good approximation of flux flow is essential. A concept that magnetic flux always seeks the path with higher permeance to pass through is the basic idea to predict the flux flow.

To facilitate the approximation of the path of flux, it is convenient to break up the path into a number of permeance tubes. The permeance of these tubes includes geometrical characteristic and material properties. All the tubes together will form an element network. This network is called magnetic equivalent circuit which is able to represent various peculiarities of this electromagnetic device. The number of elements required to reflect an electromagnetic device depends on the device size and the required accuracy. Theoretically, the number of elements can be as much as is possible since it increases the accuracy of the MEC model. However, too many elements will unnecessarily slow down the computation without a corresponding significant contribution in accuracy. Hence there is always a trade-off between computational time and the degree of accuracy in MEC model [29].

The inset type of permanent magnet electrical machine for our study uses the v-shape magnet orientation and each alternating magnet has opposite polarity. In magnetic equivalent circuit modelling, permanent magnet is regarded as an active source represented by a non-saturating resistance and a voltage source connected in series. Equivalent permeance of rotor iron is determined according to Figure 5.2. The resulting MEC for one magnetic pole pair is shown in Figure 5.3.

The stator uses double layer chorded winding configuration. Two groups of coil carrying different currents share each slot. Thus it is more appropriate to represent coils by two different sources in the MEC, one source located at the back equals to the sum of magneto-motive force from each layer and the other equals to bottom layer coil magneto-motive force.

Stator back joint area is divided into link-part and main-part. For easy permeance calculation, link-part is represented by T-shape element which is further divided into three rectangular tubes. The main-part iron is represented as a rectangular flux tube and the stator tooth is represented by two vertical trapezoidal flux tubes.

Stator tooth to tooth leakage flux is represented by non-saturating permeance tubes at the slot area. Tooth end is represented by three permeance tubes in parallel. The tube in the middle is main flux which flow from tooth to airgap and two tubes at side are fringing flux which leak from the tooth. Partial stator MEC is depicted in Figure 5.4.

$$G = \mu l \frac{h}{w1 - w2} \ln\left(\frac{w1}{w2}\right)$$

(a)

$$G = \mu l \frac{w1 - w2}{h} \frac{1}{\ln\left(\frac{w1}{w2}\right)}$$

(b)

$$G = \frac{\mu A}{L}$$

(c)

$$G = \frac{4\mu A}{(r1 - r2)}$$

(d)
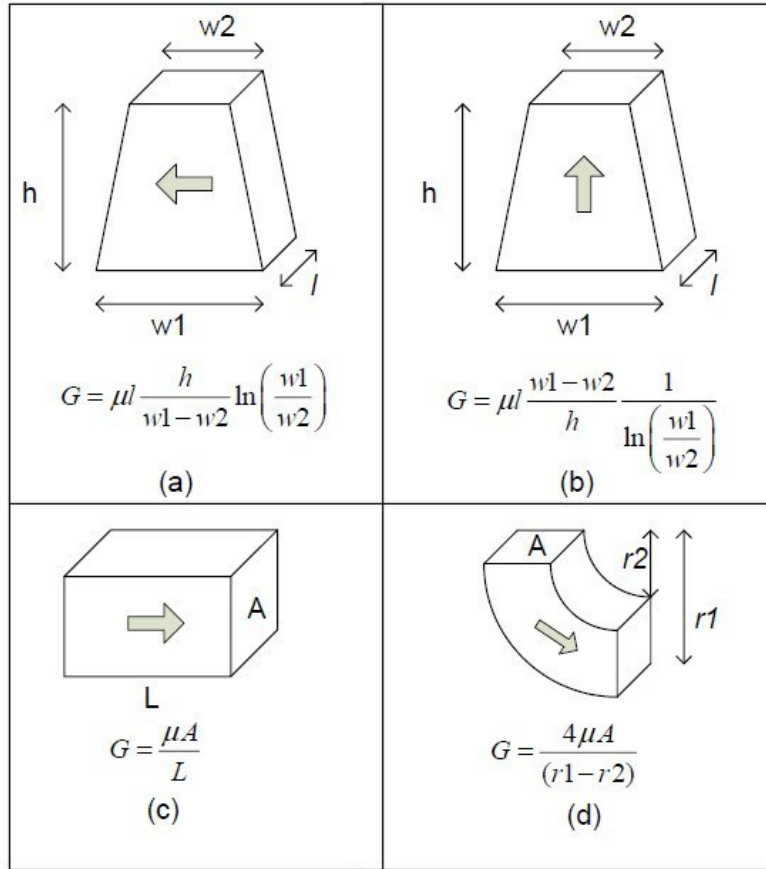
Figure 5.2 Common shapes of permeance in electrical machines
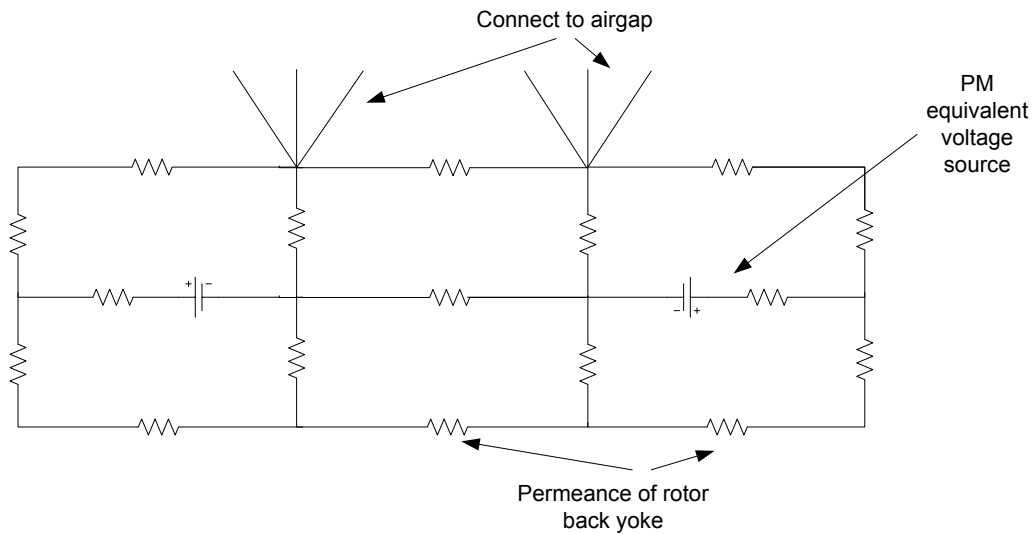
Figure 5.3 MEC of machine rotor
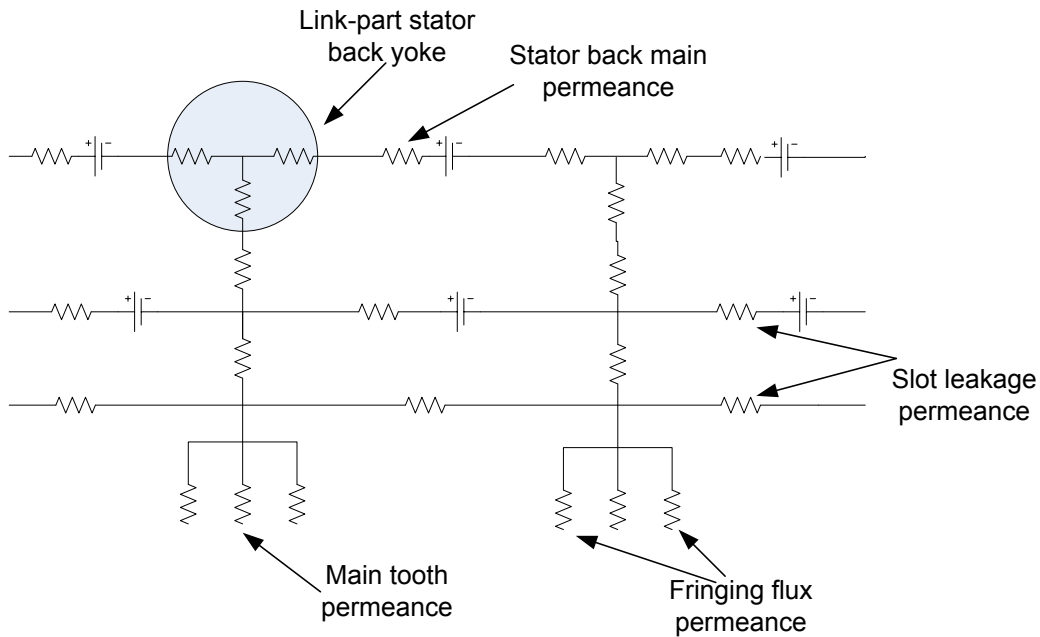
Figure 5.4 MEC of machine stator

Electrical machine airgap is a very sensitive part for MEC modelling. Airgap is a relatively small area with high flux density gradient that interconnects rotor and stator permeance elements [28]. In order to achieve a good accuracy for MEC model, it is necessary to maintain a certain degree of element density in this area.

The quantity of elements is increased by putting additional layers of permeance elements between the airgap. This method is shown in Figure 5.5. A boundary is drawn first between rotor and stator circumferential elements as shown in figure 5.5(a). By connecting the intersection of each permeance element and boundary line, a rectangular horizontal permeance can be created between the nodes as in figure 5.5(b), and then a vertical permeance is created accordingly at the node as seen in figure 5.5(c). In figure 5.5(d), a new layer of created elements is evolved. More layers in the airgap area can be created by repeating the same approach if higher element density is required.

5.3 Model Solution

Magnetic equivalent circuit is analogous to resistive electric circuit. Some of the techniques that are suitable to solve electric circuit problem is also applicable to solve magnetic equivalent circuit. The classic approach to solve magnetic equivalent circuit is by using Kirchhoff's Voltage Law (KVL) and Kirchhoff's Current Low (KCL).

Though the same approach of solving resistive electric circuit can be used, the main difference between them is that in MEC the permeance elements of ferromagnetic material is non-linear variables, while electric circuit resistance is usually considered as constant value. Therefore non-linear iteration method is necessarily applied in solving MEC.

5.3.1 MEC Solution Algorithm

In order to more conveniently apply KVL and KCL approach, magnetic reluctance is used instead of permeance. It is not a new concept, but just to make the meaning of components of MEC consistent with the meaning of components in electric circuit. The magnitude of reluctance is the inverse of associated permeance as represented by equation 5.4. A partial MEC network is depicted in Figure 5.6. The steps to find the flux in each path is illustrated here, and the same approach can be applied to whole model.

The flux flows in the thirty paths are corresponding to thirty unknowns. Thus thirty equations are required to solve it. According to KVL, the sum of the potential drop equals to the relative potential source. Since there are twelve closed-loops, twelve equations are formulated as follows.

$$(R_1 \times \varphi_1) + (R_7 \times \varphi_7) + (R_{13} \times \varphi_{13}) + (R_8 \times \varphi_8) = b_1$$
$$(R_2 \times \varphi_2) + (R_8 \times \varphi_8) + (R_{14} \times \varphi_{14}) + (R_9 \times \varphi_9) = b_2$$
$$\vdots \qquad\qquad\qquad\qquad\qquad\qquad\qquad (5.4)$$
$$(R_{18} \times \varphi_{18}) + (R_{24} \times \varphi_{24}) + (R_{30} \times \varphi_{30}) + (R_{19} \times \varphi_{19}) = b_{12}$$
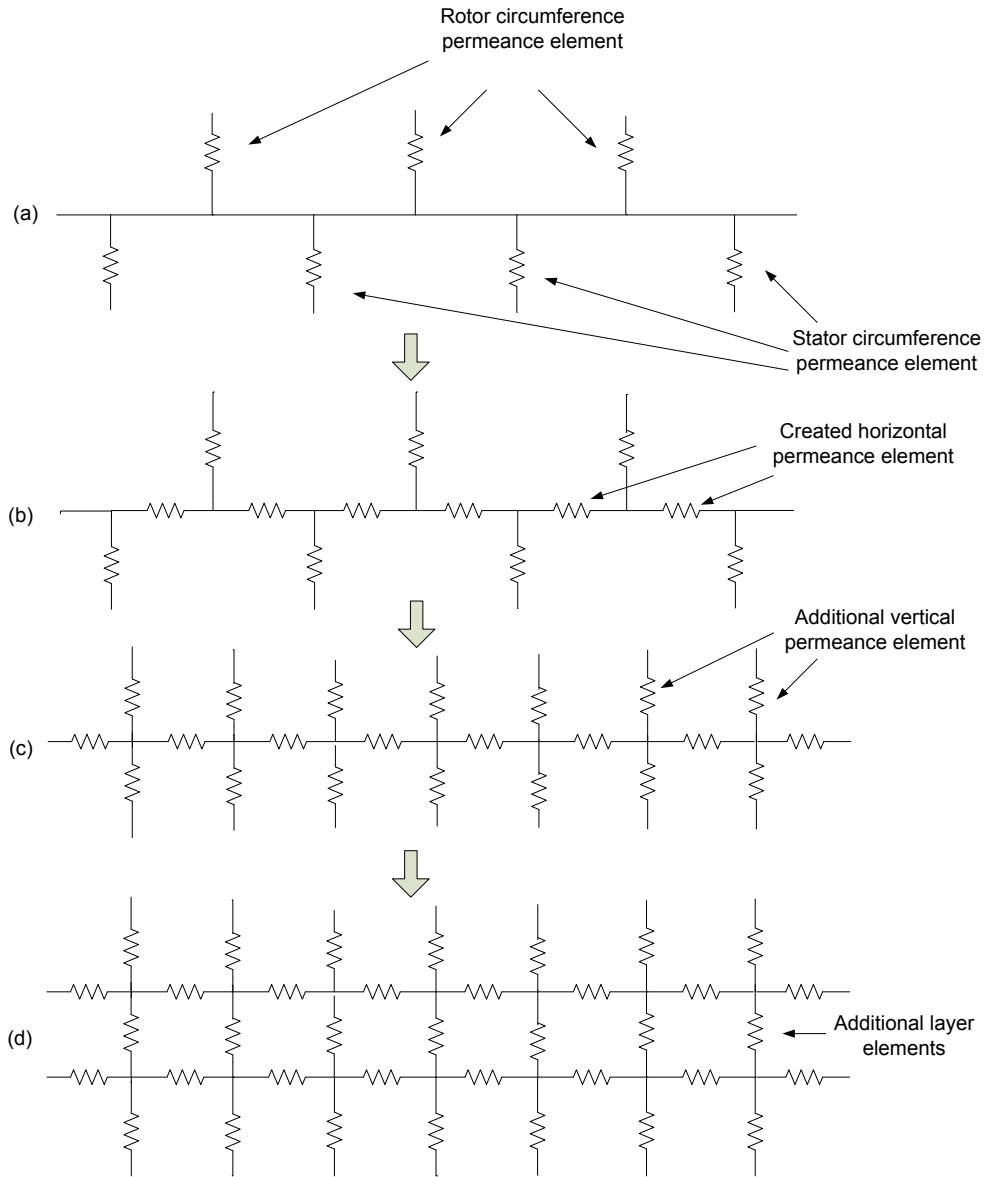
Figure 5.5 Airgap elements network
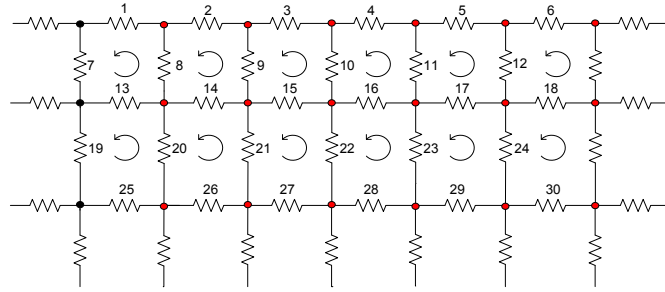
Figure 5.6 Partial of stator MEC network

According to KCL, the total flux flow into the node equals to the total flux flow out of it. Since there are eighteen nodes (red dots in figure 5.6) corresponding to twelve loops, the other eighteen equations are found. As the left and right boundaries are in symmetrical, only one node will be included.

$$
\begin{aligned}
(\varphi_1 \times R_1) + (\varphi_2 \times R_2) + (\varphi_8 \times R_8) &= 0 \\
(\varphi_2 \times R_2) + (\varphi_3 \times R_3) + (\varphi_9 \times R_9) &= 0 \\
&\vdots \\
(\varphi_{30} \times R_{30}) + (\varphi_{19} \times R_{19}) + (\varphi_{25} \times R_{25}) &= 0
\end{aligned}
\tag{5.5}
$$

These thirty equations are composed into one matrix as in equation 5.6. In the reluctance matrix $A_{1,1} = R_1$; $A_{1,8} = R_8$; $A_{1,7} = R_7$; $A_{1,13} = R_{13}$, b_1 equals to the relative equivalent MMF source of the closed-loop. The same procedure is repeated for the rest of closed- loops and the matrix elements are filled up accordingly. Flux at each path is obtained by solving the matrix.

$$
\begin{bmatrix}
A_{1,1} & A_{1,2} & \cdots & \\
A_{2,1} & A_{2,2} & & A_{2,30} \\
\vdots & & \ddots & \\
A_{30,1} & A_{30,2} & & A_{30,30}
\end{bmatrix}
\begin{bmatrix}
\varphi_1 \\
\varphi_2 \\
\vdots \\
\varphi_{30}
\end{bmatrix}
=
\begin{bmatrix}
b_1 \\
b_2 \\
\vdots \\
b_{30}
\end{bmatrix}
\tag{5.6}
$$

5.3.2 Nonlinear Iterative Approach

The permeance for saturating element is non-linear variable in solving MEC model. Depending on the flux field strength, permeability of ferromagnetic material varies non-linearly. The relation between magnetic field and permeability is shown by B-H curve in figure 5.7, where slope of the curve is permeability μ.

The permeability at different flux density level is calculated by iteration approach. Flux density is computed at each flux path based on initial permeance, and new permeability is computed by interpolating flux density B from the B-H curve. New flux density is then computed by using the updated permeability. Permeance for non-saturating elements such as the ones in the air-gap is fixed at constant values. Iteration stops when the convergence criteria is satisfied. The flowchart in figure 5.8 shows the non-linear iteration steps to solve an MEC model.
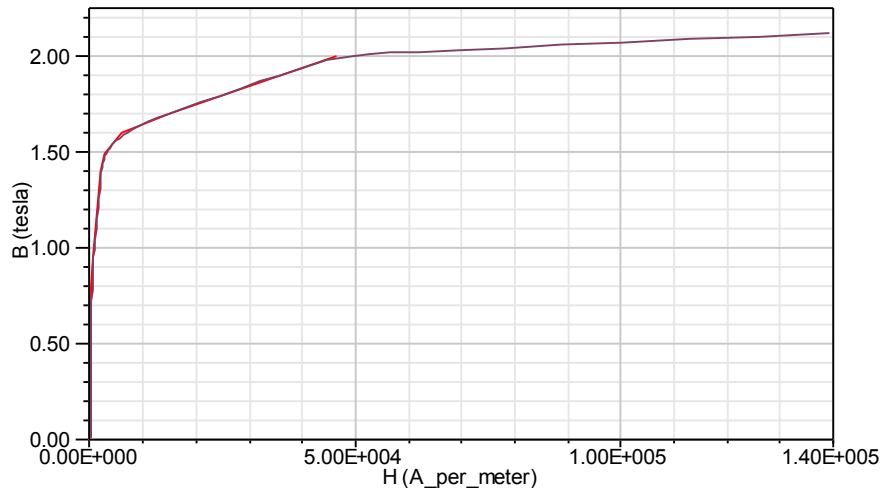
Figure 5.7 B-H curve

The new permeability of any saturating element is determined using a weighted average method given by equations 5.7 and 5.8.

$$\mu_{updated} = (\mu_{new} \times G_{new}) + (\mu_{old} \times G_{old}) \tag{5.7}$$

$$G_{new} + G_{old} = 1 \tag{5.8}$$

where G_{new} and G_{old} is weighted average gain for new and old permeability, respectively. MEC model Simulation and verification

Since MEC model is analogous to electric circuit model, an alternative way to simulate the MEC model is by using electric circuit nodal analysis type of simulation instead of solving the MEC model directly. FEM analysis can then be used to verify MEC model.

5.3.3 Electric Circuit Nodal Analysis Approach

To apply the electric circuit nodal analysis to solve the MEC model, components that are used to represent magnetic network elements have to be converted into its equivalent electric component. The permeance element is converted into equivalent resistor and MMF source is converted into equivalent voltage source. For non-linear permeance element, equivalent non-linear resistor created by the same non-linear iteration computation approach introduced in the last section has to be applied. The equivalent electric circuit is solved by Matlab/SimPowerSystem toolbox. This toolbox is a tool commonly used in analyzing electric circuits for power engineering.

Part of the equivalent circuit model of the interior PM machine is shown in figure 5.9. The blue and red elements represent non-linear elements which contain iteration computation while the yellow elements represent constant permeance which belong to slot and airgap areas. Current flow in the electric circuit is equivalent to flux flow of the MEC model. The simulation results obtained by nodal analysis is shown and compared to those obtained by solving MEC model directly in figure 5.10 for flux densities at the back area of each tooth. The left hand side graphs is by solving MEC model directly, while the right hand side graphs are the result from electric circuit nodal analysis. Since these two approaches are not exactly the same, the transient performances are not expected to be matching. Only steady state values are thus compared and these are found to be exactly the same.

```
┌─────────────────────────────┐
│  Initialization of permeability, │
│  permeance tube area and width │
└─────────────────────────────┘
              │
              ▼
┌─────────────────────────────┐
│  Calculate permeance; Fix the │
│  permeance for non-saturating │
│  elements                     │
└─────────────────────────────┘
              │
              ▼
┌─────────────────────────────┐
│  Compute flux and flux density │◄──────┐
│  at each path;                 │       │
└─────────────────────────────┘       │
              │                          │
              ▼                          │
┌─────────────────────────────┐       │
│  Interpolation method to find  │       │
│  relative field intensity H with│   Replace saturating elements
│  flux densign B. Find the      │       │
│  corresponding permeability u  │       │
└─────────────────────────────┘       │
              │                          │
              ▼                          │
┌─────────────────────────────┐       │
│  Update permeance              │       │
└─────────────────────────────┘       │
              │                          │
              ▼                          │
┌─────────────────────────────┐   No   │
│  Converged?                    │───────┘
└─────────────────────────────┘
              │ Yes
              ▼
┌─────────────────────────────┐
│  Display required parameters:  │
│  flux, flux density            │
└─────────────────────────────┘
```

Figure 5.8 Nonlinear iteration flow chart
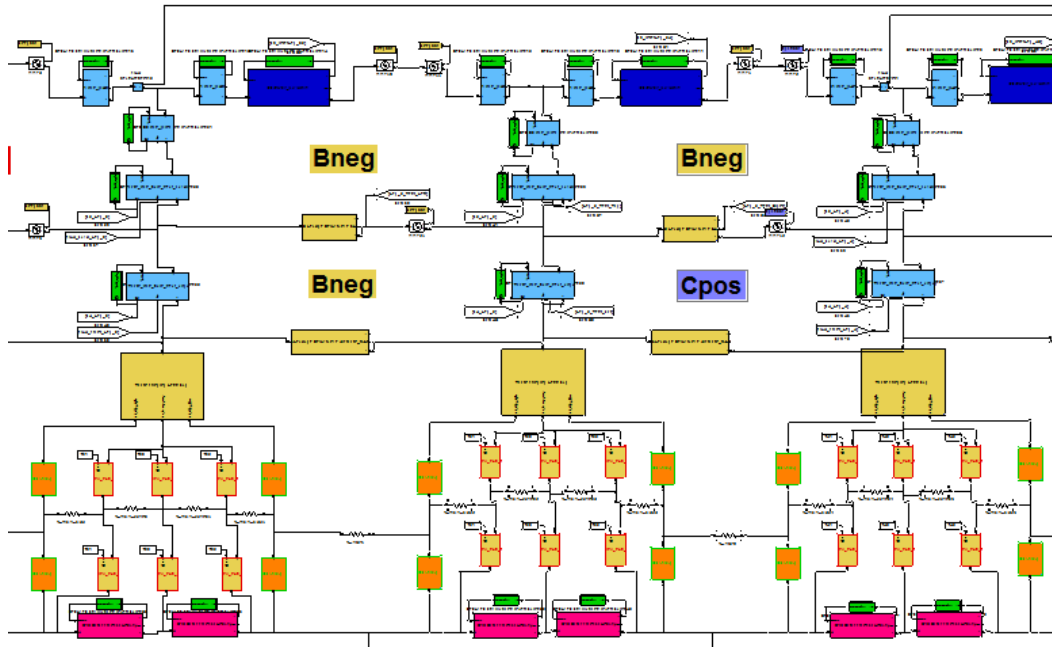
Figure 5.9 Equivalent electric circuit model
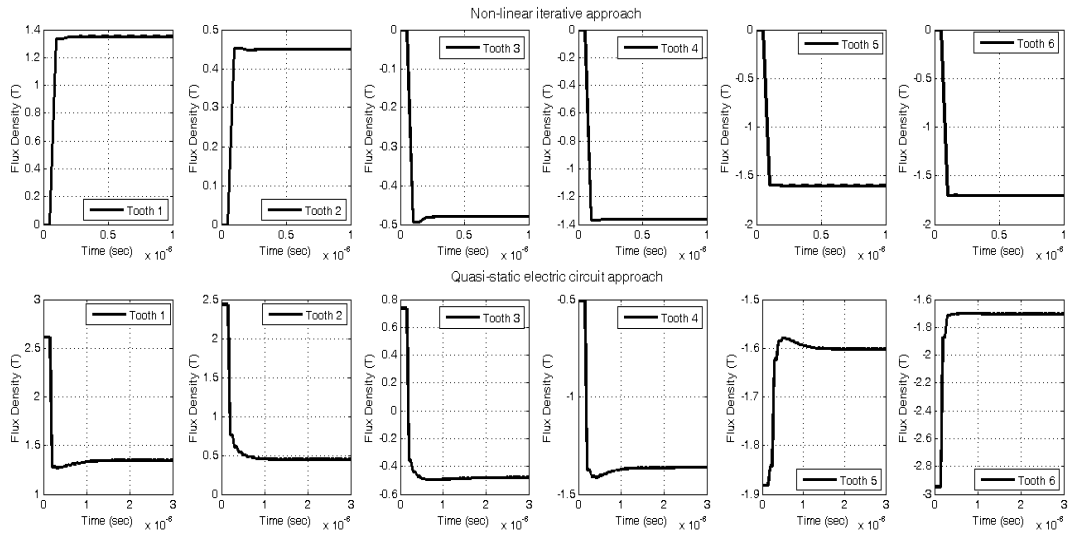
Figure 5.10 Flux comparison at each stator back tooth

5.4 Model Verification

Finite element method has been effectively used to analyse electromagnetic problems in general. It is known to generate very accurate results if complete characteristics of magnetic material can be provided [29]. The drawback by using this method is that it

requires long computational time. There are many commercially available finite element software packages to solve electromagnetic problems. The evaluation time by using FEM is sixty-nine seconds using the same workstation compared to that for MEC which is thirteen seconds. For two dimensional problems, flux can be calculated from average surface magnetic potential by equation 5.9. According to Stoke's theorem, magnetic flux can be found from average magnetic potentials by equation 5.10.

$$A_s = \left(\frac{\int\limits_S A_z dS}{S} \right) \tag{5.9}$$

$$\varphi = \left(\frac{\int\limits_S A_{z|coil\_1} dS_1}{S_1} \right) - \left(\frac{\int\limits_S A_{z|coil\_2} dS_2}{S_2} \right) \tag{5.10}$$

where A_z is z axis component of magnetic vector potential, S is surface area, φ is the flux passing in-between the two coils.

Flux evaluated by FEM that pass through stator tooth is compared to the flux associated with the same area evaluated by MEC model. The stator winding configuration is shown in Figure 5.11. Table 5.1 shows the comparison of back and front flux from leg 1 to leg 6, respectively. From the results, the percentage error corresponding to leg 2 and leg 3 is large because of the high relative error in this area. It can be found that only minority of flux pass through leg 2 and 3. Errors for other tooth legs are less than ten percent.
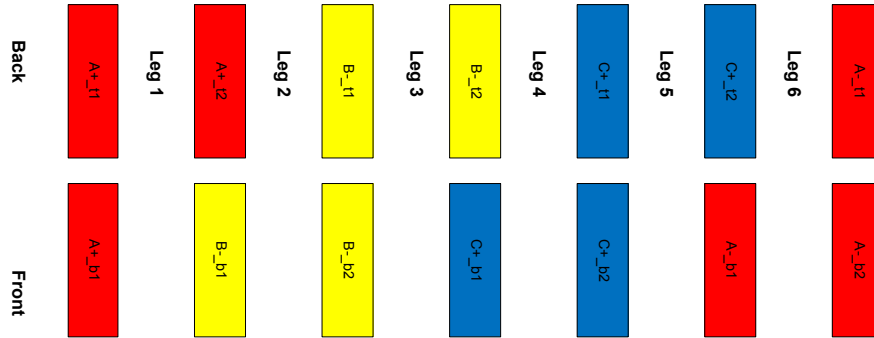
Figure 5.11. Stator winding configuration

	FEM SOFTWARE		MEC MODEL		PERCENTAGE ERROR %	
LEG	BACK	FRONT	BACK	FRONT	BACK	FRONT
1	-0.031	-0.0301	-0.0318	-0.03	1.65	0.33
2	-0.009	-0.0066	-0.0105	-0.004	12.67	39.4
3	0.014	0.0155	0.0121	0.015	16.42	3.19
4	0.035	0.0351	0.0322	0.033	9.41	6.08
5	0.039	0.0398	0.0381	0.037	4.56	7.00
6	0.039	0.0365	0.0401	0.036	1.34	1.82

Table 5.1 Comparison of FEM and MEC

This chapter presents the MEC design and solving approach for a PMSM with double layer stator winding. This MEC model can be solved either using an electric circuit nodal analysis method, or using classical iteration solving approach. The flux solved by MEC method has also been compared to flux evaluated by FEM. The error between these two methods is about 10% and computational time of MEC is found to be five times faster than FEM.

115

5.5 Summary

The magnetic equivalent circuit has been wildly used for electrical machine design due to the fast computation speed. It has the analogous relation with electric circuit and the technique to solve electric circuit is usually compatible to solve magnetic equivalent circuit. The fundamental element to compose magnetic equivalent circuit is flux tube which acting as the carrier of magnetic flux. The characteristic of flux tubes is represented by reluctance or permeance which is the function of the material permeability and geometrical shape. Although flux tube is equivalent to resistor in electric circuit, unlike the linear relation between resistance and current, the relation between reluctance and magnetic flux can be either linear or nonlinear depends on the material properties. An interior type permanent magnet synchronous machine is studied and the corresponding magnetic equivalent circuit model is presented in this chapter.

One of the main features of the model in the present study that is different from other models presented in the literature is the double layer chorded stator winding configuration and V-shape magnet orientation. Some researcher have presented magnetic equivalent circuit model for permanent magnet machines, but none of them have double layer winding and V-shape magnet orientation. The studies of leakage flux for electrical machines are also included in the presented MEC model.

The overall magnetic equivalent circuit model contains one hundred and thirty seven states of variable which can be solved by the linear nodal and potential approach. Because these variables are mixed with linear and nonlinear elements, an iterative approach is used to solve nonlinear items as shown in figure 5.8. Although all of the flux paths of the MEC model are solved, the fluxes contribute to stator phasor flux linkage attracts more attention since machine performance such as back EMF, torque, and inductance can be derived from it. The accuracy of the MEC model is verified by a commercial software packages based on finite element method. Finite element method is popular to determine electrical machine behavior attributes to its high accuracy. However, due to the drawback in long computational time, it still cannot

replace magnetic equivalent circuit method as a powerful tool in quickly evaluating machine performance. By comparing the flux calculated by MEC model and FEM, it can be concluded that the MEC model for interior permanent magnet synchronous machine is five times faster but including ten percent error.

The MEC model only evaluates machine performance statistically since the interconnections (airgap elements) between rotor and stator flux tubes continuously change due to the rotor motion. Therefore, in order to derive machine behavior, a series MEC for different rotor position have to be solved. This becomes the main difficulty in coupling the MEC model for electrical machine control.

Chapter 6 Conclusion and Future Work

6.1 Overview of the Thesis

Wind energy is a dominant renewable energy resource. Most of time, power generated from wind farms is cheaper and more reliable compared to the rest of the renewable energy resources. In this thesis, a brief introduction of wind power generation was included in Chapter 1, which include the typical configuration of horizontal and vertical axis wind turbine, the induction generator wind turbine and permanent magnet synchronous generator wind turbine, as well as the literature review of maximum power point tracking control of wind power generation. From the literature review, it has shown that the wind turbine MPPT control strategy usually adopt conventional vector control method, this method uses gain-scheduled PI controllers which only controls the plant at one operation point and thus has limited control range. Hence to use a set of PI parameters incorporating with a mapping technic are essential to control the wind turbine properly. Different from the conventional PI control strategy, nonlinear control method provide global trajectory tracking, this method had been used to control electrical machines but hardly can be seen to carry out wind turbine MPPT control. Therefore, the study of this project is trying to propose the nonlinear control strategy for wind turbine MPPT.

In Chapter 2, the corresponding wind turbine mathematical models, the a-b-c to d-q transformation, and some study of power electronics are presented. The models introduced are used to simulate wind power generation in the computer. The a-b-c to d-q transformation is the fundamental tool to analyse three phase balanced operating

electrical machines, which convert this three AC quantities to two DC quantities and simplify the problem. The power electronics are the essential devices to achieve maximum power point control strategy, and all the control strategies are implemented by these devices to control the electrical machine. However, the MPPT controller design in this project does not consider the effect of power electronics, and the relative studies will be left for future works.

In chapter 3, the conventional vector control strategy for wind turbine MPPT is introduced. Wherein, the machine d-axis current is controller to zero, and gives full control capability to regulate machine q-axis current which determines machine speed. The computer simulation shows very promising results, indicating that the actual wind turbine speed follows the reference speed with ignorable damping. Even through, it has to be emphasized that this simulation only gives the ideal result. In the real case, the machine d-axis can be hardly regulated to zero. There must be a trade-off between machine d-q axis current, otherwise the energy dissipation is unbalanced. Also, the controller PI parameters are limited by the switching capability of power converter, the zero damping is almost impossible.

In chapter 4, a different nonlinear control strategy is represented. This study begins with a feedback linearization controller, which is used to regulate machine q-axis current and two PI controllers are eliminated. Based on the feedback linearization, the nonlinear adaptive controller (NAC) which relies on perturbation observers is designed. The perturbation observer is used to estimate the system perturbation and feed to the adaptive controller, and thus this controller uses the estimated system properties instead of actual system properties, which improves the system robustness. The NAC uses a second order and a third order perturbation observer to estimate electrical machine flux and speed. The simulation results also show zero damping of system dynamics. This is also the ideal situation that does not consider the limitation of power converters.

Since the aim of this study is to propose a nonlinear control strategy for wind turbine

MPPT control that differs the gain-scheduled conventional controller, the simulation in both chapter 3 and chapter 4 have neglected the constrains of power converter and show the ideal system response when the system is subjected to the step input change. In the real case, the controller design and implementation should consider the characteristics of power converters, including power rating, protective circuit, thermal dissipation, operation environment, etc.

Lastly, in chapter 5, the permanent magnet synchronous machine was analyzed. A double layer permanent magnet synchronous machine was modelled by magnetic equivalent circuit which is a method popular in electrical machine design. It gives an approximation of machine magnetic field and enables the designers to derive machine properties such as flux linkage and inductance even under magnetic saturated or partial saturated condition. These conditions usually happen when machine experiences fault or overloading. Hence, if the MEC model has fast computation speed, it may be helpful to provide the updated operation properties for control purpose. This proposed MEC model is gauged by comparing the flux pass through stator teeth with the solution given by finite element method, and the results are promising shows that MEC model gives error less ten percent and computation speed at least five times faster. Nevertheless, this study so far only give preliminary results and much more work should be done in the future.

6.2 Future Work

Although the modelling of the prospective controller has shown good results for wind turbine maximum power point tracking, in the real case it cannot be worked as expected since sometimes there is always a gap between computer modelling and practical experiment. Therefore, it is necessary to prototype the prospective nonlinear controllers and use experiments to verify the prospective advantages compared to conventional controller. Nevertheless, the cost to carry out this experiment may be very high and it will be also time consuming. In order to reduce the cost and time taken, we would like to conduct a hardware-in-loop experiment by using the dSpace

system. This system contains digital to analogue ports and a digital signal processor that enables fast prototyping. Controllers will be programmed automatically by the dSpace system and the corresponding digital signals can be converted to analogue signals, and thus to control the permanent magnet synchronous machine through the power converter.

Since the electrical machine flux linkage can be worked out by magnetic equivalent circuit mode, we would like to observe the back electro-motive force (EMF) and compute inductance in the future. If these parameters can be calculated in a very short time, these values may be used for real time machine control. However, it will be a big challenge as there is still a ten percent error compared to the finite element method. This accuracy may not be acceptable for online controlling. The anticipate goal for the online control purpose is to reduce the error to less than five percent, this is the experience values from some machine control system designers In order to improve the model accuracy, the three dimensional magnetic equivalent circuit model may be used and the airgap flux leakage has be specified more precisely. However, by doing this may bring up the other problem which is the longer computational time. Therefore, tradeoffs between computation speed and accuracy have to be found.

References

[1]   T. Ackermann, *Wind power in power systems*. Chichester: John Wiley & Sons, 2005.

[2]   *Kyoto Protocol to the United Nations Framework Convention on Climate Change*: [Geneva : U.N., 1998].

[3]   J. Pipe, *Wind power : is it reliable?* London: Aladdin/Watts, 2010.

[4]   H. B. Hendriks, *Application of an advanced cost model in the different design phases of an offshore wind turbine*. Petten: Netherlands Energy Research Foundation, 2001.

[5]   M. G. Simo\es and F. A. Farret, *Renewable energy systems : design and analysis with induction generators*. Boca Raton, Fla. ; London: CRC, 2004.

[6]   G. A. Moberg, *AC and DC motor control*. New York ; Chichester: Wiley, 1987.

[7]   J. F. Gieras and M. Wing, *Permanent magnet motor technology : design and applications*, 2nd ed. ed. New York: Marcel Dekker, 2002.

[8]   J. Pyrhonen, T. Jokinen, and V. Hrabovcova, *Design of rotating electrical machines*. Chichester: John Wiley & Sons, 2008.

[9]   A. J. G. Westlake, J. R. Bumby, and E. Spooner, "Damping the power-angle oscillations of a permanent-magnet synchronous generator with particular reference to wind turbine applications," *Iee Proceedings-Electric Power Applications,* vol. 143, pp. 269-280, May 1996.

[10]   M. Yin, G. Y. Li, M. Zhou, and C. Y. Zhao, "Modeling of the wind turbine with a permanent magnet synchronous generator for integration," *2007 IEEE Power Engineering Society General Meeting, Vols 1-10,* pp. 3164-3169, 2007.

[11]   J. S. Thongam, P. Bouchard, H. Ezzaidi, and M. Ouhrouche, "Wind Speed Sensorless Maximum Power Point Tracking Control of Variable Speed Wind Energy Conversion Systems," *2009 IEEE International Electric Machines & Drives Conference, Vols 1-3,* pp. 1826-1831, 2009.

[12]   S. Morimoto, T. Nakamura, and Y. Takeda, "Power maximization control of variable-speed wind generation system using permanent magnet synchronous generator," *Electrical Engineering in Japan,* vol. 150, pp. 11-19, Jan 30 2005.

[13]   I. Boldea and S. A. Nasar, *Vector control of AC drives*. Boca Raton: CRC Press, 1992.

[14]   A. D. Hansen and G. Michalke, "Modelling and Control of Variable-speed Multi-pole Permanent Magnet Synchronous Generator Wind Turbine," *Wind Energy,* vol. 11, pp. 537-554, Sep-Oct 2008.

[15]   A. D. Hansen and G. Michalke, "Multi-pole permanent magnet synchronous generator wind turbines' grid support capability in uninterrupted operation during grid faults," *Iet Renewable Power Generation,* vol. 3, pp. 333-348, Sep 2009.

[16]   J. J. E. Slotine and W. Li, *Applied nonlinear control*. London: Prentice Hall, 1991.

[17]   M. Bodson, J. N. Chiasson, R. T. Novotnak, and R. B. Rekowski, "High-Performance Nonlinear Feedback-Control of a Permanent-Magnet Stepper Motor," *First IEEE Conference on Control Applications, Proceedings, Vols 1 and 2,* pp. 510-515, 1992.

[18]   J. Solsona, M. I. Valla, and C. Muravchik, "Nonlinear control of a permanent magnet synchronous motor with disturbance torque estimation," *IEEE Transactions on Energy Conversion,* vol. 15, pp. 163-168, Jun 2000.

[19]   H. Rasmussen, "A new observer for speed sensorless field oriented control of an induction motor," *Iecon-2002: Proceedings of the 2002 28th Annual Conference of the IEEE Industrial Electronics Society, Vols 1-4,* pp. 420-425, 2002.

[20]   M. Pahlevaninezhad, S. Eren, A. Bakhshai, and P. Jain, "Maximum Power Point Tracking of a Wind Energy Conversion System Using Adaptive Nonlinear Approach," *2010 Twenty-Fifth Annual IEEE Applied Power Electronics Conference and Exposition (Apec),* pp. 149-154, 2010.

[21]   S. D. Sudhoff, B. T. Kuhn, D. C. Aliprantis, and P. L. Chapman, "An advanced induction machine model for predicting inverter-machine interaction," *Pesc 2001: 32nd Annual Power Electronics Specialists Conference, Vols 1-4, Conference Proceedings,* pp. 2043-2052, 2001.

[22]   S. D. Sudhoff, B. T. Kuhn, K. A. Corzine, and B. T. Branecky, "Magnetic equivalent circuit modeling of induction motors," *IEEE Transactions on Energy Conversion,* vol. 22, pp. 259-270, Jun 2007.

[23]   S. Touati, R. Ibtiouen, O. Touhami, and A. Djerdir, "Experimental Investigation and Optimization of Permanent Magnet Motor Based on Coupling Boundary Element Method with Permeances Network," *Progress in Electromagnetics Research-Pier,* vol. 111, pp. 71-90, 2011.

[24]   S. Touati, R. Ibtiouen, A. Djerdir, J. A. Farooq, A. Miraoui, and O. Touhami, "Hybrid Boundary Element with Permeances Network Methods for Modeling Permanent Magnet Motors in Automotive Applications," *International Review of Electrical Engineering-Iree,* vol. 3, pp. 900-905, Sep-Oct 2008.

[25]   V. Ostovic, *Dynamics of saturated electric machines*. New York, N.Y.: Springer, 1989.

[26]   S. H. Han, T. A. Jahns, and W. L. Soong, "A magnetic circuit model for an IPM synchronous machine incorporating moving airgap and cross-coupled saturation effects," *IEEE IEMDC 2007: Proceedings of the International Electric Machines and Drives Conference, Vols 1 and 2,* pp. 21-26, 2007.

[27]   Y. Kano, T. Kosaka, and N. Matsui, "Simple nonlinear magnetic analysis for permanent-magnet motors," *IEEE Transactions on Industry Applications,* vol. 41, pp. 1205-1214, Sep-Oct 2005.

[28]   J. K. Tangudu, T. M. Jahns, A. EL-Refaie, and Z. Q. Zhu, "Lumped Parameter Magnetic Circuit Model for Fractional-Slot Concentrated-Winding Interior Permanent Magnet Machines," *2009 IEEE Energy Conversion Congress and Exposition, Vols 1-6,* pp. 3110-3117, 2009.

[29]   M. Yilmaz and P. T. Krein, "Capabilities of Finite Element Analysis and Magnetic Equivalent Circuits for Electrical Machine Analysis and Design," *2008 IEEE Power Electronics Specialists Conference, Vols 1-10,* pp. 4027-4033, 2008.

[30]   Z. Q. Zhu, Y. Pang, D. Howe, S. Iwasaki, R. Deodhar, and A. Pride, "Analysis of electromagnetic performance of flux-switching permanent-magnet machines by nonlinear adaptive lumped parameter magnetic circuit model," *IEEE Transactions on Magnetics,* vol. 41, pp. 4277-4287, Nov 2005.

[31]   A. R. Tariq, C. E. Nino-Baron, and E. G. Strangas, "Iron and Magnet Losses and Torque Calculation of Interior Permanent Magnet Synchronous Machines Using Magnetic Equivalent Circuit," *IEEE Transactions on Magnetics,* vol. 46, pp. 4073-4080, Dec 2010.

[32]   B. Asghari and V. Dinavahi, "Experimental Validation of a Geometrical Nonlinear Permeance Network Based Real-Time Induction Machine Model," *IEEE Transactions on Industrial Electronics,* vol. 59, pp. 4049-4062, Nov 2012.

[33]   G. M. Masters, *Renewable and efficient electric power systems*. Hoboken, N.J.: Wiley-Interscience ; [Chichester : John Wiley], 2004.

[34]   O. Anaya-Lara, *Wind energy generation : modelling and control*. Oxford: Wiley, 2009.

[35]   (2012). *MATLAB & SIMULINK [electronic resource] : student version (R2012a. ed.)*.

[36] D. W. Novotny and T. A. Lipo, *Vector control and dynamics of AC drives*. Oxford: Clarendon, 1996.

[37] C.-M. Ong, *Dynamic simulation of electric machinery : using MATLAB/SIMULINK*. Upper Saddle River, N.J.: Prentice Hall PTR ; London : Prentice-Hall International, 1998.

[38] B. K. Bose, *Modern power electronics and AC drives*. Upper Saddle River, NJ: Prentice Hall PTR, 2001.

[39] S. S. Ang, *Power-switching converters*. New York: Dekker, 1995.

[40] Y. C. Chen, P. Pillay, and A. Khan, "PM wind generator comparison of different topologies," *Conference Record of the 2004 IEEE Industry Applications Conference, Vols 1-4,* pp. 1405-1412, 2004.

[41] H. S. Ko, H. W. Kim, and S. S. Kim, "Modeling and control of PMSG-based variable-speed wind turbine," *Electric Power Systems Research,* vol. 80, pp. 46-52, Jan 2010.

[42] J. M. Kokernak and D. A. Torrey, "Magnetic circuit model for the mutually coupled switched-reluctance machine," *IEEE Transactions on Magnetics,* vol. 36, pp. 500-507, Mar 2000.

[43] H. W. Derbas, J. M. Williams, A. C. Koenig, and S. D. Pekarek, "A Comparison of Nodal- and Mesh-Based Magnetic Equivalent Circuit Models," *IEEE Transactions on Energy Conversion,* vol. 24, pp. 388-396, Jun 2009.